ISOLATION OF NOVEL NATURAL PRODUCTS WITH DISTINCT ANTI-MITOTIC ACTIVITIES FROM THE CANADIAN PLANT *ARNICA CORDIFOLIA*

TANNER LOCKWOOD
B.Sc. Biochemistry, University of Lethbridge, 2022

A thesis submitted
in partial fulfilment of the requirements for the degree of

MASTER OF SCIENCE

in

BIOLOGICAL SCIENCES

Department of Biological Sciences
University of Lethbridge
LETHBRIDGE, ALBERTA, CANADA

ISOLATION OF NOVEL NATURAL PRODUCTS WITH DISTINCT ANTI-MITOTIC ACTIVITIES FROM THE CANADIAN PLANT *ARNICA CORDIFOLIA*

TANNER LOCKWOOD

Date of defence: July 29, 2024

Dr. Roy Golsteyn Thesis Supervisor	Professor	Ph.D.
Dr. Trushar Patel Thesis Examination Committee Member	Professor	Ph.D.
Dr. Dmytro Yevtushenko Thesis Examination Committee Member	Associate Professor	Ph.D.
Dr. Theresa Burg Chair, Thesis Examination Committee	Professor	Ph.D.

ABSTRACT

This thesis investigates anti-mitotic natural products isolated from *Arnica cordifolia* (heartleaf arnica), a Canadian plant species. Extracts prepared from *A. cordifolia* induced mitotic arrest without affecting mitotic spindle morphology, a phenotype unlike that of any mitotic inhibitor previously identified by our laboratory. By investigating this unique phenotype, we identified five anti-mitotic sesquiterpene lactones from *A. cordifolia* using biology-guided fractionation: three novel structures, and the known compounds aromaticin and pulchellin-2α-*O*-isovalerate. These compounds induced mitotic arrest with distinct effects on mitotic spindle morphology. Investigation into potential target pathways revealed that aromaticin treatment induced ubiquitin foci formation in cancer cells, suggesting that it may affect the ubiquitin-proteasome pathway. This is the first report of three novel mitotic inhibitors, of the anti-mitotic effects of pulchellin-2α-*O*-isovalerate, and of the anti-mitotic and ubiquitin-altering effects of aromaticin. Differences in the structures and biological activities of these anti-mitotic sesquiterpene lactones suggest they act by distinct cellular targets and mechanisms of action. The discovery of mitotic inhibitors from Canadian plant species and other underexplored sources of natural products expands our understanding of mitosis, and these compounds may have applications in research or therapy.

ACKNOWLEDGEMENTS

I am very grateful to my supervisor Dr. Roy Golsteyn for the opportunity to grow as a student and as a researcher in his laboratory. Since joining the Natural Product Laboratory as an undergraduate student and throughout the entirety of my M.Sc. program, he has provided me with the guidance, direction, and research opportunities to succeed as a scientist. I deeply appreciate your continued support and belief in my future as a scientist.

I am thankful for the counsel given by my supervisory committee members Dr. Trushar Patel and Dr. Dmytro Yevtushenko, and their assistance throughout my graduate studies. I would like to thank the current and past members of the Natural Product Laboratory Shannon Healy Knibb, Larissa Smith, David Witten, Brinnley Zanewich, Haley Allard, Nadia Hand, and Araba Sagoe-Wagner for their help and advice throughout this research project. I also thank Dr. Raymond Andersen, Dr. David Williams, and Benjamin Yeremy for their expertise during the collaboration to purify and identify the natural products described in this thesis.

I am most thankful to my family for their steadfast support of my education. To my parents Davin and Gwen, my brother Nathan, and my grandparents, thank you all for always emphasizing the importance of doing my best, for being interested in all my schoolwork and research, and for supporting me every step of the way.

TABLE OF CONTENTS

THESIS EXAMINATION COMMITTEE …… ii

ABSTRACT …….. iii

ACKNOWLEDGEMENTS …….. iv

LIST OF TABLES ……. ix

LIST OF FIGURES …… x

LIST OF ABBREVIATIONS …….. xii

CHAPTER 1: General Introduction …… 1

1.1. Natural Products …… 2

1.2. Canadian Plants as a Source of Natural Products …….. 4

1.2.1. Ecological zones of Southern Alberta, Canada ……. 4

1.2.2. Natural products isolated from Canadian plants ……... 5

1.3. Sesquiterpene Lactones ……. 7

1.4. Natural Products as Mitotic Inhibitors ……..... 11

1.4.1. Inhibitors targeting microtubules …… 13

1.4.2. Inhibitors targeting mitotic regulatory components …… 15

1.4.3. Anti-mitotic sesquiterpene lactones …… 16

1.4.4. Identification and purification of anti-mitotic natural products …….. 19

1.5. The Cell Cycle and Mitosis …….. 20

1.5.1. Overview of the cell cycle ……... 21

1.5.2. Mitosis …… 22

1.6. Investigation of *Arnica cordifolia*, a Canadian Plant Species …….. 24

1.7. Hypothesis and Objectives ……... 26

CHAPTER 2: Identification and characterization of five anti-mitotic sesquiterpene lactones from the Canadian plant species *Arnica cordifolia* 27

2.1. Introduction 27

2.2. Materials and Methods 28

2.2.1. Collection of plant material 28

2.2.2. Preparation of plant extracts 28

2.2.3. UV-visible spectroscopy 29

2.2.4. Cell culture 29

2.2.5. Light microscopy 30

2.2.6. Cell viability assay 30

2.2.7. Flow cytometry 31

2.2.8. β-mercaptoethanol reduction assay 32

2.2.9. Immunofluorescence microscopy 32

2.2.10. Bioassay-guided fractionation 33

2.2.11. Statistical analysis 34

2.3. Results 35

2.3.1. Extracts prepared from *Arnica cordifolia* induce mitotic arrest in cancer cells 35

2.3.2. Isolation and anti-mitotic activity of five sesquiterpene lactones from *Arnica cordifolia* 54

2.4. Discussion 68

2.4.1. Multiple anti-mitotic compounds isolated from *Arnica cordifolia* 70

2.4.2. Aromaticin treatment affects ubiquitin staining in cancer cells 75

CHAPTER 3: Partial separation of *Arnica cordifolia* leaf extract by column chromatography …… 79

3.1. Introduction …… 79

3.2. Materials and Methods …… 80

3.2.1. Collection of plant material …… 80

3.2.2. Preparation of plant extracts …… 80

3.2.3. Fractionation of plant extracts …… 81

3.2.4. UV-visible spectroscopy …… 81

3.2.5. Cell culture …… 82

3.2.6. Light microscopy …… 82

3.2.7. Immunofluorescence microscopy …… 83

3.3. Results and Discussion …… 84

CHAPTER 4: Investigation of potential cellular targets of *Arnica cordifolia* leaf extract …… 91

4.1. Introduction …… 91

4.2. Materials and Methods …… 91

4.2.1. Collection of plant material …… 91

4.2.2. Preparation of plant extracts …… 92

4.2.3. Cell culture …… 92

4.2.4. Immunofluorescence microscopy …… 93

4.3. Results …… 94

4.3.1. *Arnica cordifolia* leaf extract treatment damages DNA in some but not all mitotic cells …… 94

4.3.2. *Arnica cordifolia* leaf extract treatment does not impact CENP-E or BubR1 localization ……. 96

4.4. Discussion ……. 100

CHAPTER 5: Future Directions ……. 103

REFERENCES ……... 105

APPENDIX I: Supplementary Materials for Chapter 2 ……... 118

LIST OF TABLES

Table 2.1. Comparison of the structural features and cytotoxicity of anti-mitotic sesquiterpene lactones isolated from *A. cordifolia* …… 60
Table 2.2. Comparison of the biological activities of sesquiterpene lactones isolated from *A. cordifolia* on HT-29 cells …….. 61

LIST OF FIGURES

Figure 1.1. Major subclasses of sesquiterpene lactones 10
Figure 1.2. The α-methylene-γ-butyrolactone moieties of sesquiterpene lactones alkylate exposed thiol groups on biomolecules by hetero-Michael addition reactions 10
Figure 1.3. Chemical structures of natural product mitotic inhibitors 12
Figure 1.4. Chemical structures of anti-mitotic sesquiterpene lactones 18
Figure 2.1. Ethanolic and dichloromethane extracts prepared from *A. cordifolia* are spectrophotometrically distinct 42
Figure 2.2. Dichloromethane extract prepared from *A. cordifolia* is cytotoxic to HT-29 cells 42
Figure 2.3. *A. cordifolia* extracts induce a rounded morphology in HT-29 cells 43
Figure 2.4. *A. cordifolia* extracts induce a rounded morphology in U2OS cells 45
Figure 2.5. Extracts prepared from *A. cordifolia* plants collected in two different years induce cell rounding 46
Figure 2.6. Extracts prepared from *A. cordifolia* leaves, flowers and stems induce cell rounding 47
Figure 2.7. *A. cordifolia* extracts induce G2/M phase arrest 48
Figure 2.8. Cells treated with *A. cordifolia* extracts contain phosphorylated histone H3, but these extracts have differing effects on the mitotic spindle 49
Figure 2.9. β-mercaptoethanol inhibits the anti-mitotic activity of *A. cordifolia* extracts 51
Figure 2.10. Anti-mitotic activity of *A. cordifolia* extracts is retained after treated cells are washed with untreated media 53
Figure 2.11. Chemical structures of five sesquiterpene lactones isolated from *A. cordifolia* leaf material 59
Figure 2.12. Isolated sesquiterpene lactones are cytotoxic to HT-29 cells 60
Figure 2.13. Isolated sesquiterpene lactones induce a rounded morphology in HT-29 cells 62
Figure 2.14. β-mercaptoethanol inhibits the anti-mitotic activity of isolated sesquiterpene lactones 63
Figure 2.15. Cells treated with isolated sesquiterpene lactones contain phosphorylated histone H3, but these compounds have differing effects on the mitotic spindle 65
Figure 2.16. Cells treated with RA-312 show punctate ubiquitin staining 67
Figure 2.17. Chemical structures of aromaticin (RA-312) and two sesquiterpene lactones previously isolated from *A. cordifolia*, graveolide and 2,3-dihydroaromaticin 75
Figure 2.18. Chemical structures of the epoxide-containing sesquiterpene lactones RA-315 and parthenolide 75
Figure 3.1. Anti-mitotic of *A. cordifolia* leaf extract is retained after column chromatography 88
Figure 3.2. Cytotoxic *A. cordifolia* leaf extract fractions induce cell rounding at lower concentrations 89
Figure 3.3. Cells treated with *A. cordifolia* leaf extract fractions contain phosphorylated histone H3 and undistorted mitotic spindles 90
Figure 4.1. Treatment with *A. cordifolia* leaf extract damages DNA in some mitotic cells, but not in interphase cells 95

Figure 4.2. Treatment with *A. cordifolia* leaf extract does not affect CENP-E localization in mitotic cells ……... 98
Figure 4.3. Treatment with *A. cordifolia* leaf extract does not affect BubR1 localization in mitotic cells ……... 99

Supplemental Figure 2.1. Anti-mitotic activity of *A. cordifolia* leaf extract is retained after fractionation ……... 119
Supplemental Figure 2.2. Subfractions of *A. cordifolia* leaf extract fractions show anti-mitotic activity …… 120
Supplemental Figure 2.3. RA-298 and RA-299 are the most potent anti-mitotic subfractions …… 121

LIST OF ABBREVIATIONS

β-TRCP	beta-transducin repeat containing E3 ubiquitin protein ligase
γH2AX	γ-histone H2AX
ANOVA	one-way analysis of variance
APC/C	anaphase promoting complex/cyclosome
ATCC	American Type Culture Collection
ATP	adenosine triphosphate
BME	beta-mercaptoethanol
BSA	bovine serum albumin
Bub3	budding uninhibited by benzimidazole protein 3
BubR1	budding uninhibited by benzimidazole-related protein 1
Cdc20	cell division cycle protein 20
Cdk	cyclin-dependent kinase
CENP-E	centrosome-associated protein E
CGI	chemical-genetic interaction
CKI	cyclin-dependent kinase inhibitor
Cul1	cullin 1
DAPI	4′,6-diamidino-2-phenylindole
DHPO	2α,6α-diacetoxy-4β-hydroxy-11(13)-pseudoguaien-12,8α-olide
DMEM	Dulbecco's modified Eagle medium
DMSO	dimethyl sulfoxide
DNA	deoxyribonucleic acid
EDTA	ethylenediaminetetraacetic acid
F12	nutrient mixture F12
FBS	fetal bovine serum
FE	flower extract
G0 phase	resting phase
G1 phase	gap 1 phase
G2 phase	gap 2 phase
GTP	guanosine triphosphate
h	hour
HEPES	4-(2-hydroxyethyl)-1-piperazineethanesulfonic acid
HPLC	high-performance liquid chromatography
HT-29	human colorectal adenocarcinoma cell line
IC50	half-maximal inhibitory concentration
IgG	immunoglobulin G
LE	leaf extract
M phase	mitotic phase
Mad2	mitotic arrest deficient 2
MCC	mitotic checkpoint complex
MEM	minimum essential media
MTOC	microtubule organizing centre
MTT	(3-(4,5-dimethylthiazol-2-yl)-2,5-diphenyltetrazolium bromide
NF-κB	nuclear factor kappa-light-chain-enhancer of activated B cells
NIPA	nuclear-interacting partner of ALK

NMR	nuclear magnetic resonance
NT	not-treated
PBS	phosphate buffered saline
PH3	phospho-histone H3
Plk1	polo-like kinase 1
RNA	ribonucleic acid
S phase	DNA synthesis phase
SAC	spindle assembly checkpoint
SCF	Skp1-Cul1-F-box
SE	stem extract
Skp1	S-phase kinase-associated protein 1
Skp2	S-phase kinase-associated protein 2
U2OS	human osteosarcoma cell line
UbcH5	ubiquitin-conjugating enzyme H5
USP7	ubiquitin-specific-processing protease 7
UV	ultraviolet
v	volume
w	weight

CHAPTER 1

General Introduction

This thesis is about the isolation of anti-mitotic natural products from the Canadian plant *Arnica cordifolia* (heartleaf arnica). Through the Prairie to Pharmacy Program, our laboratory has studied natural products from Canadian plant species to understand biological connections in cells and for applications in research and human health. This work has largely focused on members of the Asteraceae family, which are characterized by the production of sesquiterpene lactones. Our laboratory has previously discovered two anti-mitotic sesquiterpene lactones from native Asteraceae species: pulchelloid A from *Gaillardia aristata* (great blanketflower) (Bosco et al., 2021), and hymenoratin from *Hymenoxys richardsonii* (pingue rubberweed) (Molina et al., 2021). These compounds induce mitotic arrest with distortion of the mitotic spindle. Interestingly, a previous screen performed by our laboratory discovered that extracts prepared from *A. cordifolia* induced mitotic arrest without affecting mitotic spindle morphology (Molina, 2018). This observation prompted further investigation into the natural products of *A. cordifolia*, as described in this thesis.

Pursuit of this unique mitotic arrest phenotype led to the identification of five anti-mitotic sesquiterpene lactones from *A. cordifolia*: three novel structures, and the known compounds aromaticin and pulchellin-2α-*O*-isovalerate. Aromaticin and one of the novel compounds induced mitotic arrest without distortion of the mitotic spindle, whereas the other three compounds induced mitotic arrest with spindle distortion reminiscent of arrests induced by other anti-mitotic sesquiterpene lactones. Investigation into potential target

pathways revealed that aromaticin treatment induced ubiquitin foci formation in cancer cells, suggesting that it may affect the ubiquitin-proteasome pathway. This is the first report of three novel mitotic inhibitors, of the anti-mitotic effects of pulchellin-2α-*O*-isovalerate, and of the anti-mitotic and ubiquitin-altering effects of aromaticin. Differences in the structures and biological activities of these anti-mitotic sesquiterpene lactones suggest that they possess different cellular targets and mechanisms of action from both one another and previously described mitotic inhibitors. This thesis contributes to a growing body of evidence that Canadian plant species are an underexplored source of mitotic inhibitors. Novel mitotic inhibitors expand our understanding of mitosis and have the potential for therapeutic use.

1.1. Natural Products

Natural products are compounds produced by living organisms. The diversity of life is reflected in the diversity of natural products produced, with over 300 000 different natural products having been isolated from plants, fungi, marine life, microbes, and other organisms (Sorokina and Steinbeck, 2020). Natural products are typically classified as either primary metabolites, which are involved in essential life processes like growth and reproduction, or secondary metabolites, which are involved in other non-essential, yet beneficial processes (Elshafie et al., 2023). Secondary metabolites typically help the organisms that produce them to adapt to their environments, defend against herbivory or predation, or compete with other organisms (Dias et al., 2012). Due to these biological

activities, several natural products have therapeutic and research applications: approximately 65% of therapeutic agents approved since 1981 are natural products, mimics or derivatives of natural products, or synthetic drugs based on natural product pharmacophores (Newman and Cragg, 2020). Plants are a particularly valuable source of useful natural products, making their investigation critical for drug discovery. Many medicines have been developed from plant-derived natural products, including the anti-cancer drug paclitaxel (Taxol®), isolated from *Taxus brevifolia* (Pacific yew) (Cragg, 1999), and the anti-malarial drug artemisinin, isolated from *Artemisia annua* (Sweet wormwood) (Su and Miller, 2015). However, since less than 15% of known plant species have been investigated for biological activity, it is expected that many more useful natural products remain to be discovered (Cragg and Newman, 2005).

Plant-derived natural products have a long and storied history in medicine. Medicinal herbs have been used by humanity for millennia, with the oldest written recipes for herbal remedies dating back approximately 5000 years (Petrovska, 2012). Traditional medicines remain in use today, with up to 80% of the world's population relying on herbal medicine as a primary healthcare source (Ekor, 2013). Additionally, when comparing natural product medicines to the plants they were isolated from, the majority show related or identical therapeutic uses and ethnomedical uses (Fabricant and Farnsworth, 2001). Outside of known medicinal herbs, bioactive natural products continue to be discovered through the screening of both individual plants and extract libraries (Newman, 2017). Evidently, continued research into the natural products of plants is likely to uncover additional compounds with benefits to human health and wellness. Contributing to this

research, this thesis describes the investigation of natural products from a Canadian plant and their biological activities in human cancer cells.

1.2. Canadian Plants as a Source of Natural Products

1.2.1. Ecological zones of Southern Alberta, Canada

Canada is divided into fifteen ecological zones that differ widely in biotic and abiotic features, leading to a corresponding variety in flora. Within the southern regions of Alberta, two ecozones are present: prairies and montane cordillera. The prairie ecozone spans from near the western border of Alberta to the eastern border of Manitoba and is characterized by a subhumid to semiarid climate (Sauchyn et al., 2002). It features limited precipitation, high winds, long daytime exposure, and extreme temperature variations between seasons, leading to frequent and severe drought (McGinn, 2010). These extreme conditions, alongside pressure from herbivory, may contribute to the production of secondary metabolites by prairie plant species to adapt and survive (Alokam et al., 2002; Akula and Ravishankar, 2011; Molina et al., 2022).

These conditions contrast with those of the montane cordillera ecozone, which ranges from the mountainous western border of Alberta to the interior of British Columbia. Spanning the Rocky Mountains, the montane cordillera features both alpine and forested regions with a mild climate (Chiarle et al., 2021). The ecozone also contains approximately 15 000 glaciers, about 1 000 of which are located within Alberta (Clague et al., 2011). Due

to the geologically recent retreat of glaciation in this ecozone, the flora consists of both ancient alpine species and newly established postglacial species (Harris, 2007). These distinctions between the environments of the montane cordillera and prairie ecozones suggest a similar distinction in secondary metabolites between their flora.

1.2.2. Natural products isolated from Canadian plants

The plants of the Canadian prairie and montane cordillera ecozones are promising candidates for the discovery of novel natural products (Molina et al., 2022). The most notable Canadian natural product is the breast cancer chemotherapy medication paclitaxel (Taxol®), isolated from *Taxus brevifolia* (Pacific yew) which grows in the montane cordillera and Pacific maritime ecozones (Cragg, 1999). The prairie and montane cordillera ecozones also contain several plants used in First Nation Traditional medicine, further indicating that natural products with useful bioactivities can be isolated from Canadian plants. Kindscher (1992) described the medicinal uses of 203 plants native to the prairies, with 172 species used in Traditional medicine. In the montane cordillera, multiple Traditional medicinal plants have been detailed in interviews with elders and herbalists from the Carrier people of central British Columbia (Ritch-Krc et al., 1996). Evidently, Canadian plants have remarkable potential as sources of medicinally relevant natural products.

Despite these bioactivities, plants from these Canadian ecozones are currently underexplored in natural product science. Historically, natural product science has focused

on species from tropical rainforests and other regions of extreme biodiversity (Joffe and Thomas, 1989; Newman, 1994). This is reflected by the United States National Cancer Institute's Natural Product Repository, the world's largest natural product library, which lacks plant collections from the Canadian prairie and montane cordillera ecozones (Thornburg et al., 2018). However, current models of plant biodiversity report that whereas overall species richness is greatest in the tropics and other equatorial areas, the rates of speciation and diversification are highest in higher and lower latitude areas such as Canada (Tietje et al., 2022; Dimitrov et al., 2023). High phylogenetic diversity has been correlated with phytochemical diversity (Defossez et al., 2021), supporting the concept that Canadian plants are an attractive source of novel natural products.

To investigate Canadian plants for natural products with potential research or therapeutic applications, we established the Prairie to Pharmacy Program. Through this program, we have identified several natural products from Canadian prairie and montane cordillera plant species. Extracts prepared from *Symphoricarpos occidentalis* (snowberry) induce perinuclear vacuolation in response to light exposure (Tuescher et al., 2021). Luteolin, isolated from *Thermopsis rhombifolia* (buffalo bean), inhibits cyclin-dependent kinase 9 and induces cell cycle arrest at G1 phase (Kernéis et al., 2015; Tuescher et al., 2020). Pulchelloid A, isolated from *Gaillardia aristata* (great blanket flower) (Bosco et al., 2021), and hymenoratin, isolated from *Hymenoxys richardsonii* (pingue rubberweed) (Molina et al., 2021), are two sesquiterpene lactones that induce mitotic arrest in human cancer cells with distortion of the mitotic spindle. Similar mitotic arrest phenotypes have been reported after treatment with the butenolide anemonin, isolated from *Pulsatilla*

nuttalliana (prairie crocus) (Healy Knibb, 2024), and the sugar ester (+)-6-tuliposide A, isolated from *Erythronium grandiflorum* (glacier lily) (Healy Knibb, 2024). This thesis contributes five natural products isolated from *Arnica cordifolia*, a Canadian plant native to the montane cordillera ecozone. These results contribute to a growing body of research on the natural products of Canadian plants and their bioactivities.

1.3. Sesquiterpene Lactones

Sesquiterpene lactones are a broad group of secondary metabolites with several important biological uses. Over 6000 sesquiterpene lactones have been discovered from plants and marine organisms, with substantial chemical diversity existing between sesquiterpene lactones (Adekenov, 2017; Amorim et al., 2013). Plants are the primary source of sesquiterpene lactones. They are found in approximately 16 plant families and are near-ubiquitous in Asteraceae, while also appearing in some members of families including Apiaceae and Magnoliaceae (Amorim et al., 2013). Sesquiterpene lactones are primarily found in the flowerheads and leaves of Asteraceae species, with glandular trichomes serving as sites of both sesquiterpene lactone biosynthesis and storage (Padilla-Gonzalez et al., 2016). Sesquiterpene lactones have also been found in the shoots and roots of some plants.

As terpenoids, sesquiterpene lactones are predominantly colourless lipophilic compounds (Chadwick et al., 2013). Like other sesquiterpenes, sesquiterpene lactones have a 15-carbon backbone generated from three isoprene units. Sesquiterpene lactones are

unique among sesquiterpenes due to a lactone ring at the C6/C7 or C8/C7 positions of the skeleton, typically in the form of a highly reactive α-methylene-γ-lactone (Schmidt, 2006). The carbon backbone is cyclized, with over 30 different skeletal structures of sesquiterpene lactones having been reported (Schmidt, 2006). These skeletal structures can be described by their particular cyclizations and positions of substituents attached to the backbone, with the largest subclasses being the eudesmanolides (C6 bicyclic), guaianolides (C5/C7 bicyclic), pseudoguaianolides (C5/C7 bicyclic), germacranolides (C10 monocyclic), and xanthanolides (C7 monocyclic) (Figure 1.1). Guaianolides and pseudoguaianolides are the most common sesquiterpene lactone structures, and differ solely by the position of a methyl group at either C4 (guaianolides) or C5 (pseudoguianolides) (Barbero and Prandi, 2018).

Sesquiterpene lactones have many important ecological roles. They are principally used in chemical defense by plants against herbivory and infectious microorganisms (Padilla-Gonzalez et al., 2016; Ivie et al., 1975; Harmatha and Nawrot, 1984; Bennett et al., 1994), and can be used by plants to inhibit the growth of competitors (allelopathy) (Macías et al., 1992; Callaway and Ridenour, 2004). Within these interspecies interactions, it is found that sesquiterpene lactones have inhibitory activities including anti-inflammatory (Lyss et al., 1998; García-Piñeres et al., 2001), anti-tumour (Zhang et al., 2005; Ghantous et al., 2010; Kreuger et al., 2012; Bosco and Golsteyn, 2017), and anti-protozoal effects (Schmidt et al., 2009). As a result of these bioactivities, several sesquiterpene lactones are being investigated in laboratory and clinical settings for beneficial effects on human health. Important examples include the anti-inflammatory compounds parthenolide (isolated from *Tanacetum parthenium* (feverfew)) (Freund et al.,

2020) and helenalin (isolated from *Arnica montana* (Arnica)) (Lyss et al., 1998), the anti-malarial agent artemisinin (isolated from *Artemisia annua* (Qinghao)) (Miller and Su, 2011), and the calcium pump inhibitor thapsigargin (isolated from *Thapsia garganica* (deadly carrot)) (Thastrup et al., 1990).

The majority of beneficial sesquiterpene lactone activities and cytotoxic effects have been attributed to the α-methylene-γ-lactone moiety (Jackson et al., 2017). Found in approximately 3% of all known natural products and 70% of sesquiterpene lactones, the α-methylene-γ-lactone acts as a Michael acceptor to bond covalently with nucleophiles (Schmidt, 2006; Kitson et al., 2009). Additionally, approximately half of all sesquiterpene lactones contain one or more additional α,β-unsaturated carbonyl structures, such as cyclopentenone groups, which serve as additional reactive centers (Schmidt, 2006). Through a hetero-Michael addition reaction, these functionalities primarily alkylate exposed thiol groups on biomolecules (Jackson et al., 2017); alkylation of stronger non-thiol nucleophiles is possible but uncommon in accordance with Pearson's hard-soft acid-base principle (Schmidt, 2006). Thus, the main targets for covalent adduct formation are exposed cysteine side chains on proteins and other thiol-containing molecules such as glutathione (Figure 1.2). The formation of covalent adducts can disrupt the structure and function of these targets, leading to biological activity. Though cysteine is the least surface-exposed amino acid (Poole, 2015), approximately 70% of protein thiol groups remain solvent-exposed meaning that sesquiterpene lactones–especially those with multiple reactive centers–have a vast number of potential alkylation targets (Requejo et al., 2010; Poole, 2015). Despite this general bioactivity contributing to cytotoxicity at higher dosages,

a degree of target specificity is conferred by the structures of the sesquiterpene lactone and target due to steric effects and non-covalent stabilizing interactions (Takahashi et al., 2024; Schmidt, 2006).

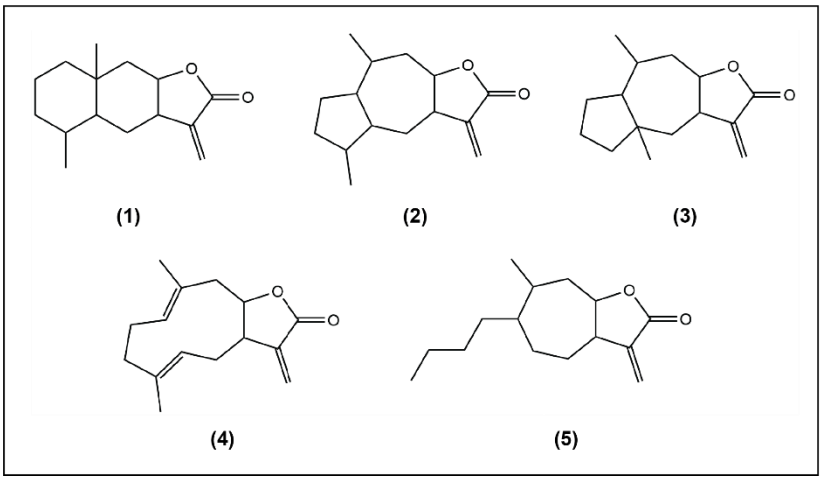

Figure 1.1. Major subclasses of sesquiterpene lactones. Eudesmanolide **(1)**, guaianolide **(2)**, pseudoguaianolide **(3)**, germacranolide **(4)**, xanthanolide **(5)**.

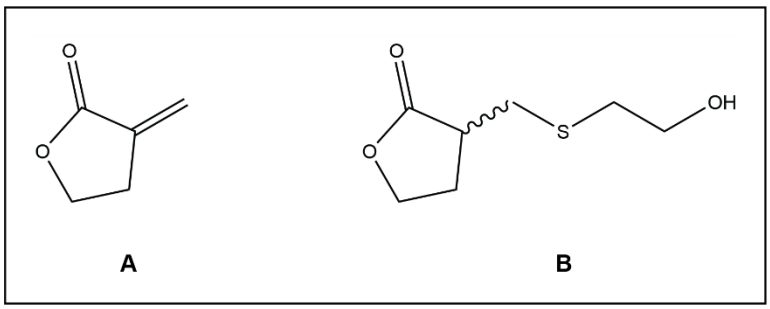

Figure 1.2. The α-methylene-γ-butyrolactone moieties of sesquiterpene lactones alkylate exposed thiol groups on biomolecules by hetero-Michael addition reactions. **A.** Chemical structure of α-methylene-γ-butyrolactone. **B.** Reaction product of α-methylene-γ-butyrolactone with the thiol group of β-mercaptoethanol. Similar reactions are possible with other thiol groups.

1.4. Natural Products as Mitotic Inhibitors

There is great interest in understanding how human cells undergo mitosis, and natural products, such as paclitaxel, are amongst the best mitotic inhibitors known in medicine. Mitosis is a fundamental process for all eukaryotes, and remarkable fidelity is required to ensure that the genome is correctly copied and transferred during cell division. When cell division fails, cells may die or undergo genomic change, which can lead to diseases such as cancer (Hayashi and Karlseder, 2013). To study cell division in greater detail, chemical inhibitors are often used to stop normal mitotic processes (Hung et al., 1996). Arresting cells in mitosis allows researchers to observe the mitotic machinery more easily and investigate the molecular mechanisms of the cell cycle. In addition to their roles in cell cycle research, several mitotic inhibitors are also used in the treatment of cancer to inhibit tumour growth (Dickson and Schwartz, 2009; Chan et al., 2012). Acquiring additional knowledge about mitosis and potentially finding new therapeutic agents requires the discovery of novel mitotic inhibitors.

Natural products are a major source of new mitotic inhibitors. Nearly two-thirds of approved anti-cancer drugs are natural products or synthetic derivations thereof, including many of the most widely used mitotic inhibitors such as paclitaxel (Taxol®), vinblastine, and their derivatives (Newman and Cragg, 2020). This chapter provides examples of natural product mitotic inhibitors and their mechanisms of action (Figure 1.3), helping to better position the discoveries of novel anti-mitotic natural products.

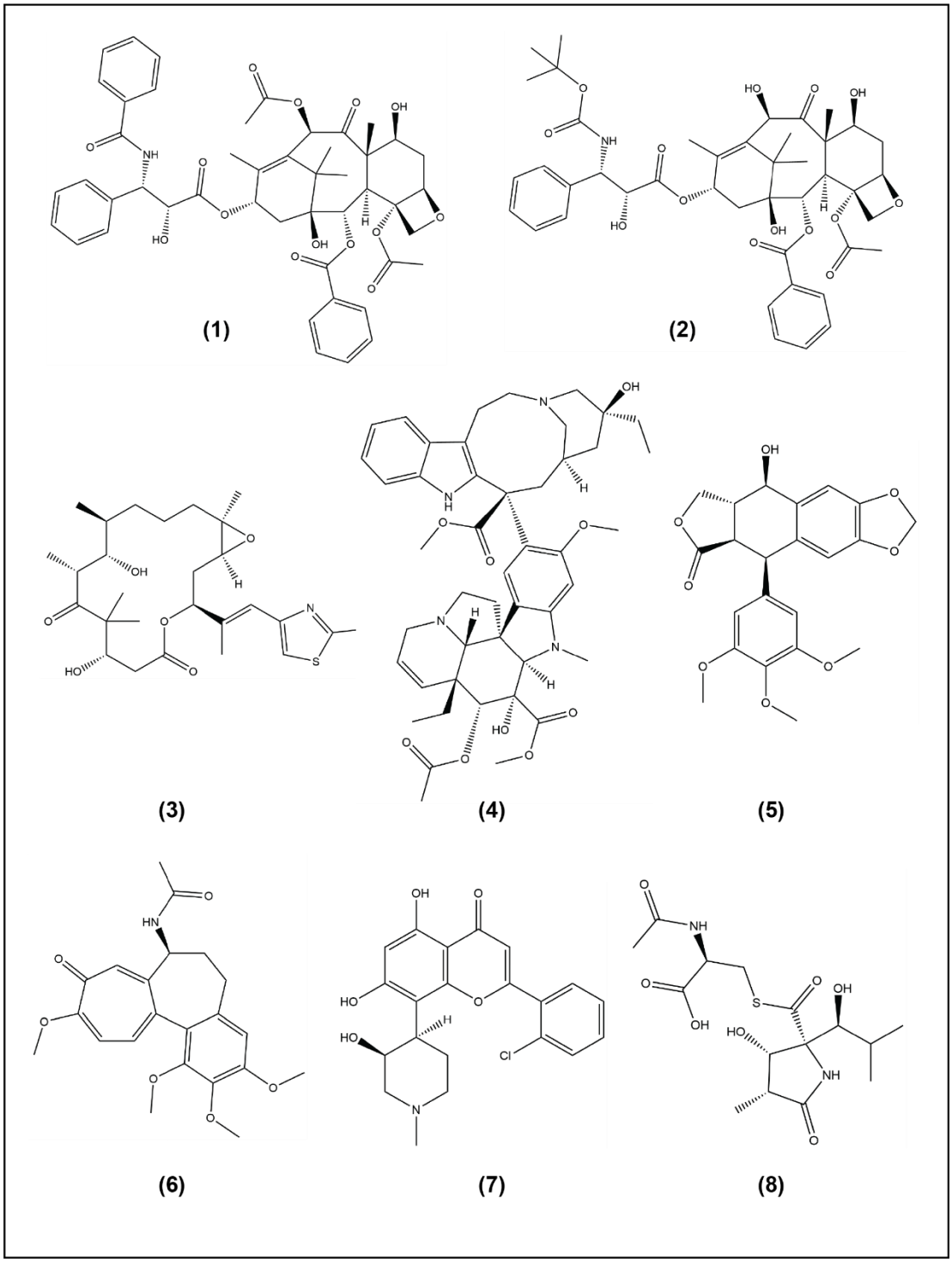

Figure 1.3. Chemical structures of natural product mitotic inhibitors. Paclitaxel **(1)**, docetaxel **(2)**, epothilone B **(3)**, vinblastine **(4)**, colchicine **(5)**, podophyllotoxin **(6)**, flavopiridol **(7)**, lactacystin **(8)**.

1.4.1. Inhibitors targeting microtubules

Many mitotic inhibitors act by directly targeting microtubules (Perez, 2009; Bhat and Setaluri, 2007; Jordan and Wilson, 1998). Microtubules are cytoskeletal elements with important functions in intracellular transport, cell shape, polarity, motility, and mitosis (Goodson and Jonasson, 2018). A microtubule is formed from α- and β-tubulin heterodimers arranged into hollow filaments, with the minus end attached to microtubule-associated proteins at a microtubule organizing centre (MTOC). In mitosis, microtubules form the mitotic spindle that transports chromosomes to separate poles of the dividing cell. Disruption of spindle formation or microtubule dynamics can lead to activation of the spindle assembly checkpoint, as kinetochores will fail to attach to the spindle (Matson and Stukenberg, 2011). This critical role in mitosis makes microtubules an attractive target for anti-cancer drugs. Inhibitors that directly target microtubules can be divided into two groups: microtubule-stabilizing agents and microtubule-destabilizing agents.

Microtubule-stabilizing agents are compounds that promote tubulin polymerization and stabilize microtubules once assembled (Perez, 2009; Bhat and Setaluri, 2007; Jordan and Wilson, 1998). Examples of microtubule-stabilizing agents include taxanes and epothilones. Paclitaxel (Taxol®), a natural product isolated from *Taxus brevifolia* (Pacific yew), is a taxane microtubule-stabilizing agent used in the treatment of multiple cancer types (Cragg, 1999). Paclitaxel and other taxanes bind to a site on β-tubulin on the interior of microtubules, promoting tubulin polymerization and microtubule stabilization that ultimately leads to mitotic arrest (Snyder et al., 2001). Interestingly, though this binding site is shared by epothilones, the structural differences between epothilones and taxanes

permit unique molecular interactions with the residues of β-tubulin (Bode et al., 2002; Akbari et al., 2011). Due to these unique interactions, epothilones have been shown to retain activity against some paclitaxel-resistant cancer cell lines (Kowalski et al., 1997). This slight difference in activity showcases the value of discovering novel mitotic inhibitors. This value is further exemplified in the comparison of paclitaxel and docetaxel (Taxotere®), another clinically relevant taxane derived from the related species *Taxus baccata* (English yew). Differences in the potency of microtubule stabilization and structures of polymerized tubulin induced by these taxanes lead to distinct use cases and safety profiles, despite their shared binding site and similar chemical structures (Verweij et al., 1994; Lai et al., 2022). Evidently, the discovery of both novel classes of mitotic inhibitors and novel mitotic inhibitors in known classes can provide additional options for precision medicine.

A similar pattern can be observed in microtubule-destabilizing agents. Natural products such as vinca alkaloids, colchicines, and podophyllotoxins work oppositely to microtubule-stabilizing agents by depolymerizing microtubules and inhibiting tubulin polymerization (Perez, 2009; Bhat and Setaluri, 2007; Jordan and Wilson, 1998). Vinca alkaloids, such as vinblastine, bind to a site near the GTP-binding site of β-tubulin and inhibit tubulin exchange (Himes, 1991; Perez, 2009), whereas colchicines and podophyllotoxins bind to a different site on β-tubulin that sterically hinders α-tubulin to inhibit microtubule assembly (Ravelli et al., 2004; Lu et al., 2012). The differences in binding sites and mechanisms of action of these microtubule-destabilizing agents, as well

as more subtle differences between inhibitors that share a common binding site (Lu et al., 2012), further emphasize the value of discovering novel mitotic inhibitors.

1.4.2. Inhibitors targeting mitotic regulatory components

Mitotic inhibitors may also target components required for the regulation of mitosis. By targeting mitosis-specific kinases and other proteins instead of microtubules that have uses outside of mitosis, these inhibitors offer increased therapeutic efficacy and fewer side effects (Marzo and Naval, 2013). Examples of such inhibitors include cyclin-dependent kinase (Cdk) inhibitors that block transitions between phases of the cell cycle and mitotic progression, Aurora kinase A and B inhibitors that interfere with mitotic entry and spindle assembly, and motor protein inhibitors that affect spindle assembly and chromosome transport (Marzo and Naval, 2013; Zhang et al., 2021; Bavetsias and Linardopoulos, 2015). Several natural product kinase inhibitors have been discovered and derivatized for clinical use (Bailon-Moscoso et al., 2017).

An example of a natural product kinase inhibitor is the flavone flavopiridol (alvocidib). Flavopiridol is a Cdk inhibitor used in the treatment of myeloid leukemia and was the first Cdk inhibitor to reach clinical trials (Zeidner and Karp, 2015; Zhai et al., 2002). Flavopiridol is a semi-synthetic derivative of the natural product rohitukine, first isolated from the Indian medicinal plant *Aphanamixis polystachya* (previously *Amoora rohituka*) (Harmon et al., 1979; Zhai et al., 2002). Flavopiridol inhibits Cdks by binding to the ATP-binding cleft, preventing Cdk-driven protein phosphorylation and blocking cell

cycle progression at the G1/S or G2/M phase boundaries (De Azevedo Jr. et al., 1996; Canduri et al., 2004).

Other mitotic inhibitors indirectly affect mitotic regulatory components. The first non-peptidic proteasome inhibitor to be discovered was lactacystin, a natural product isolated from *Streptomyces lactacystinaeus* (Tomoda and Omura, 2000). Lactacystin specifically and irreversibly binds to several catalytic subunits of the 20S proteasome, inhibiting multiple peptidase activities of the proteasome complex (Fenteany et al., 1995). By inhibiting the ubiquitin-proteasome pathway, lactacystin prevents the degradation of mitotic proteins such as cyclin B leading to cell cycle arrest (Brandeis and Hunt, 1996). Interestingly, when compared to peptidic proteasome inhibitors, lactacystin is highly specific for the proteasome and does not inhibit other proteases (Omura and Crump, 2019). This gives lactacystin an important role in cancer therapy and research, and emphasizes the value of natural product inhibitors in these areas (Omura and Crump, 2019). As seen through these examples, natural products can be of direct therapeutic use or serve as scaffolds for the development of novel mitotic inhibitors.

1.4.3. Anti-mitotic sesquiterpene lactones

A small subset of sesquiterpene lactones induce mitotic arrest in cancer cells, with activities dependent on the α-methylene-γ-lactone moiety and other α,β-unsaturated carbonyl groups (Figure 1.4) (Bosco and Golsteyn, 2017). Costunolide, a sesquiterpene lactone related to parthenolide, induces cell cycle arrest at metaphase (Liu et al., 2011).

Costunolide causes tubulin polymerization resulting in microtubule aggregation and bundling, suggesting the arrest may be linked to altered microtubule dynamics (Bocca et al., 2004). Parthenolide and coronopilin both bind directly to cysteine-rich tubulin, thus interfering with microtubule dynamics (Cotugno et al., 2012; Hotta et al., 2021). It is currently unknown if a similar mechanism is responsible for the anti-mitotic activity of costunolide. Mitotic spindle distortion has been reported in mitotically-arrested cells after treatment with a small but growing number of sesquiterpene lactones, including pulchelloid A (Bosco et al., 2021), hymenoratin (Molina et al., 2021), 6-*O*-angeloylplenolin (Liu et al., 2011), melampodin-A acetate (Robles et al., 2015), and psilostachyins A and C (Sturgeon et al., 2005). Interestingly, 6-*O*-angeloylplenolin and psilostachyins A and C induce mitotic arrest with aberrant spindle morphology without affecting microtubule polymerization or dynamics, suggesting that there may be several mechanisms that produce a mitotic arrest with spindle distortion (Liu et al., 2015; Sturgeon et al., 2005). 6-*O*-angeloylplenolin is suggested to target Skp1 (S-phase kinase associated protein 1), inhibiting the Skp1-Cul1-F-box (SCF) complex and preventing the degradation of proteins involved in mitotic progression (Liu et al., 2015). However, apart from 6-*O*-angeloylplenolin, the mechanisms leading to these mitotic arrests are unknown. Additional research is required to elucidate the mechanisms of these anti-mitotic sesquiterpene lactones.

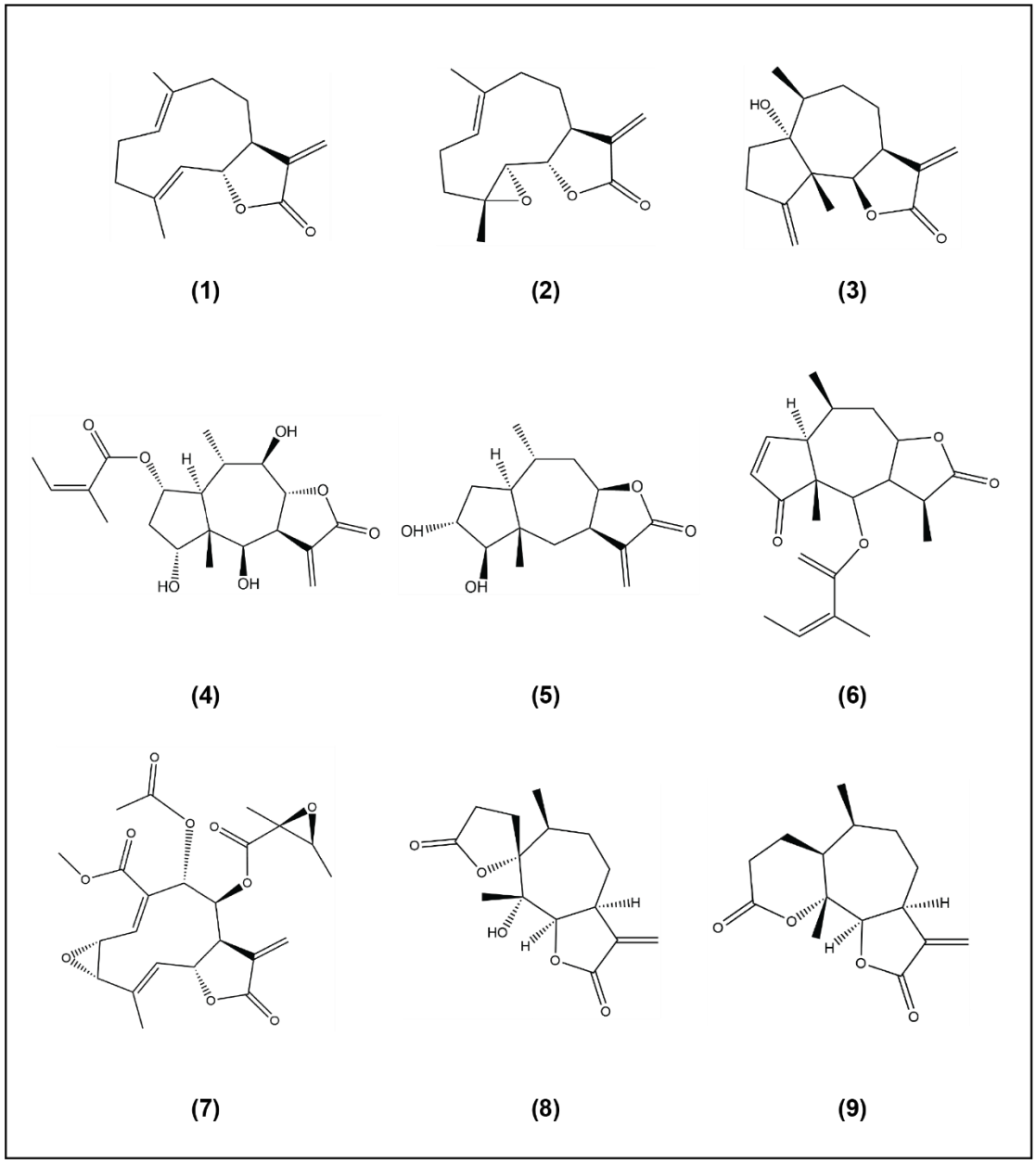

Figure 1.4. Chemical structures of anti-mitotic sesquiterpene lactones. Costunolide **(1)**, parthenolide **(2)**, coronopilin **(3)**, pulchelloid A **(4)**, hymenoratin **(5)**, 6-*O*-angeloylplenolin **(6)**, melampodin-A acetate **(7)**, psilostachyin A **(8)**, psilostachyin C **(9)**.

1.4.4. Identification and purification of anti-mitotic natural products

The complexity of the many pathways required for mitosis and the perspective that most natural products remain to be discovered supported the rationale to discover new mitotic inhibitors. This goal led us to consider how best to conduct this screening. Libraries of crude extracts or fractions are typically screened either for activity against a predetermined mitotic target, or for general inhibition of cell proliferation (Atanasov et al., 2021; Wilson et al., 2020). However, the nature of target-based screening requires that natural products with other promising activities are not detected. Conversely, inhibitors of cell proliferation require additional investigation to identify the mechanism of action, such as distinguishing between cytotoxic and anti-mitotic compounds.

Phenotypic assays, in contrast to targeted assays, are a powerful method to find inhibitors to many mitotic targets. Mitosis is particularly suited to phenotypic screens because of the unique rounded morphology of mitotic cells (Kubara et al., 2012). Phenotypic assays have been used to discover several natural products with anti-mitotic activities, including paclitaxel (Cragg, 1999), and are of vital importance in the modern drug discovery process (Swinney and Anthony, 2011; Vincent et al., 2022). This study employs a phenotypic assay that detects a mitosis-dependent morphology change in HT-29 human colorectal adenocarcinoma cells (Kubara et al., 2012), a cell line capable of remaining in prolonged mitotic arrest (Gascoigne and Taylor, 2008). As a rounded cell morphology is indicative of mitosis, monitoring for the accumulation of rounded cells after treatment screens for any compound that induces mitotic arrest. To confirm that the rounded cells are arrested in mitosis, the DNA content of treated cells is evaluated by flow

cytometry, and cells are examined for the mitotic marker phospho-histone H3 (PH3) by immunofluorescence microscopy.

After confirmation of the extract's biological activity, we use biology-guided fractionation to purify progressively the active compounds. During biology-guided fractionation, phenotypic assays are used to identify active fractions over the course of multiple chromatographic separations. This allows for the biological activity to be followed throughout successive fractionations until pure compounds are isolated. Target-specific studies are then performed to determine the cellular targets and mechanisms of action of the pure compounds. Our approach has been successful in the isolation of several mitotic inhibitors from plant extracts, including pulchelloid A (Bosco et al., 2021) and hymenoratin (Molina et al., 2021). This thesis describes the isolation of five anti-mitotic natural products from the Canadian plant *Arnica cordifolia* by use of this approach.

1.5. The Cell Cycle and Mitosis

The cell cycle is the ubiquitous process by which cells grow, replicate their DNA, and divide into daughter cells. This complex process uses cyclins, cyclin-dependent kinases (Cdks), and numerous regulatory proteins to direct the cell through a specific series of events, ultimately leading to mitosis. The cell cycle can be divided into interphase, which encompasses G1 (gap 1), S (synthesis), and G2 (gap 2) phases, and mitosis (M phase), which consists of prophase, prometaphase, metaphase, anaphase, and telophase. Understanding these phases and the proteins involved in their progression is necessary as

these proteins are typically the targets of mitotic inhibitors. The following sections will describe these phases and the transitions between them in greater detail, with particular focus on the events of mitosis.

1.5.1. Overview of the cell cycle

The cell cycle consists of two major phases, S phase and M phase, that are separated by two gap phases, G1 and G2. In G1, cells grow larger, synthesizing the RNA and proteins required to continue the cell cycle. Progression to S phase is regulated by the G1/S checkpoint, the first of three main checkpoints in the cell cycle. At the G1/S checkpoint, intra- and extracellular conditions are assessed to determine if it is favourable for the cell to continue with division. Cells that pass the G1/S checkpoint become committed to division and enter S phase, whereas those that do not do so will enter G0, an additional gap phase. In S phase, cells duplicate their genome by DNA synthesis. Once duplicated, the cells progress into G2 where they prepare to enter mitosis by synthesizing required mitotic proteins. This preparation is verified by the G2/M checkpoint, which assesses the duplicated genome for damaged DNA to ensure faithful replication. If no damage is detected, the cell proceeds to M phase. Otherwise, the cell will arrest at the checkpoint to allow for DNA repair if possible, or to undergo cell death or checkpoint adaptation (Swift and Golsteyn, 2014). The final checkpoint, termed the M checkpoint or spindle assembly checkpoint (SAC), ensures that all chromosomes are correctly aligned and separated during mitosis. The progression of the cell cycle through these checkpoints is controlled by Cdks,

which must first be activated by binding to cyclically produced proteins called cyclins (Hochegger et al., 2008). Once activated, cyclin-Cdk complexes phosphorylate other mitotic proteins to drive cell cycle progression. The levels of each cyclin vary between cell cycle phases due to changes in both protein synthesis and degradation by the ubiquitin-proteasome pathway, allowing Cdk activity to be regulated in each phase.

1.5.2. Mitosis

Mitosis is initiated by activation of the cyclin B-Cdk1 complex. This complex, along with the cyclin A-Cdk1 complex, triggers a phosphorylation cascade that phosphorylates over 1000 proteins (Crncec and Hochegger, 2019). The mitotic kinases Aurora kinase A, Aurora kinase B, and polo-like kinase 1 (Plk1) are activated downstream or simultaneously of the cyclin B-Cdk1 complex and phosphorylate additional proteins (Van Horn et al. 2010; Willems et al., 2018; Golsteyn et al., 1995). One critical protein phosphorylation event is the phosphorylation of histone H3 on the serine 10 residue by Aurora B kinase, which triggers chromatin condensation into chromosomes and marks the beginning of prophase (Prigent and Dimitrov, 2003). Also in prophase, the nucleolus disappears, the two centrosomes move to opposite poles of the cell, and the cytoskeleton is disassembled giving the cell a distinctive round shape. Prophase is followed by prometaphase, in which the cyclin B-Cdk1 complex phosphorylates nuclear lamins to cause the breakdown of the nuclear membrane. Without the nuclear membrane, spindle microtubules from the centrosomes are able to grow outwards and connect to the

kinetochore of each chromosome, forming a bipolar mitotic spindle. Stable kinetochore-microtubule attachment is facilitated by the motor protein CENP-E, which is localized to kinetochores by Aurora kinase B and BubR1 (Vigneron et al., 2004). Cyclin A is degraded by the 26S proteasome in prometaphase, indicating that Cdk1 activity relies entirely on cyclin B in the following stages of mitosis.

In metaphase, the chromosomes align along the cell equator, forming a metaphase plate. This alignment is primarily performed by the mitotic spindle, where balanced spindle tension leads to chromosomes positioned at the equator. Chromosome alignment is assisted by the kinetochore-localized motor proteins dynein and CENP-E (Schaar et al., 1997). Premature progression to anaphase is prevented by the SAC, which monitors the attachment of kinetochores to microtubules and generation of spindle tension. Unattached kinetochores and kinetochores lacking tension activate the checkpoint and prompt the assembly of the mitotic checkpoint complex (MCC). The MCC is a complex of four proteins–BubR1, Bub3, Cdc20, and Mad2–that inhibits the anaphase-promoting complex/cyclosome (APC/C), an E3 ubiquitin ligase whose function is required for mitotic progression. This inhibition results from Cdc20 being the activating component of the APC/C. Successful attachment of all kinetochores silences the SAC and releases Cdc20 from MCC sequestration, allowing for activation of the APC/C. Once activated, the APC/C ubiquitinates cyclin B and securin to cause their degradation by the proteasome. Cyclin B degradation ends Cdk1 activity, and securin degradation marks the start of anaphase.

In anaphase, the sister chromatids are separated and moved to the two spindle poles. The degradation of securin frees separase from sequestration, allowing separase to

enzymatically degrade the cohesin rings joining sister chromatids. The separated chromatids are then transported to the spindle poles by the mitotic spindle, which disassembles afterward. In telophase, new nuclear envelopes are formed around each group of chromatids. Finally, the two daughter cells are separated through cytokinesis. Successful completion of mitosis is essential for the growth of organisms. Aberrant cell cycling or errors in mitosis can lead to cancer and other diseases. Mitotic inhibitors serve as tools to study cell division and treat cell cycle-related diseases, giving their discovery both research and therapeutic value.

1.6. Investigation of *Arnica cordifolia*, a Canadian Plant Species

This thesis analyzes natural products isolated from *Arnica cordifolia,* a botanical species native to the montane cordillera ecological zone of Alberta, Canada. Also known as heartleaf arnica, *A. cordifolia* belongs to the Asteraceae family and is one of 18 Arnica species native to Canada (Brouillet et al., 2024). Found throughout North America, *A. cordifolia* is one of the most widely distributed Arnica species with a range spanning from Alaska to New Mexico, USA (Maguire, 1943). *A. cordifolia* is a herbaceous perennial with cordate and dentate leaves arranged oppositely along simple erect stems (Wolf and Denford, 1984). It features yellow ray and disc flowers characteristic of Asteraceae species.

Other members of this genus, particularly the European species *A. montana*, have been used in traditional medicine to treat inflammation, pain, and bruising (Kriplani et al., 2017). *A. montana* flower extracts continue to be used as herbal remedies, and have seen

success in clinical trials for the treatment of pain and inflammation (Jeffrey and Belcher, 2002; Kneusel et al., 2002). These activities are attributed to pseudoguaianolide sesquiterpene lactones in *A. montana*, principally helenalin and dihydrohelenalin esters (Lyss et al., 1998). Helenalin has been demonstrated to inhibit the NF-κB pathway (Lyss et al., 1998) and induce apoptosis in cancer cells (Kriplani and Guarve, 2020).

By contrast, little research has been done on the related North American species *A. cordifolia* and its chemical constituents. A chemical analysis of 16 *Arnica* species found that unlike *A. montana*, *A. cordifolia* did not contain helenalin, dihydrohelenalin, or their derivatives (Ekenäs et al., 2009). A previous investigation of sesquiterpene lactones from *A. cordifolia* reported the presence of three other pseudoguaianolides: carabrone, graveolide, and 2,3-dihydroaromaticin (Merfort and Wendisch, 1993). Though these three compounds are cytotoxic to several cancer cell lines, none have been reported to induce mitotic arrest (Lee et al., 2002; Zheng et al., 2013).

Our laboratory previously observed that extracts prepared from *A. cordifolia* harboured anti-mitotic activity (Molina, 2018). Treatment of human cancer cells with *A. cordifolia* extracts induced mitotic arrest seemingly without distortion of the mitotic spindle, a phenotype unlike any mitotic inhibitor or anti-mitotic extract in the Prairie to Pharmacy Program's library. This observation prompted further investigation into *A. cordifolia* with an approach focused on the characterization of the outlier phenotype. In this thesis we report the isolation of the anti-mitotic compounds of *A. cordifolia* and characterize the distinct mitotic arrest phenotypes they induce.

1.7. Hypothesis and Objectives

The observation that *A. cordifolia* extracts induced a distinct mitotic arrest phenotype in human cancer cells as compared to other anti-mitotic natural products in our laboratory posed an interesting scientific question as to how these activities would be reconciled at the chemical level. We hypothesize that *A. cordifolia* contains an anti-mitotic sesquiterpene lactone with a different structure and cellular target than previously described anti-mitotic sesquiterpene lactones. To test this hypothesis, this thesis addresses the following objectives:

- Characterize the anti-mitotic effects of *A. cordifolia* extracts in cancer cell lines.
- Isolate and identify the active compound(s) from *A. cordifolia* through biology-guided fractionation.

By acting on these objectives, this study is the first to report the structures and anti-mitotic activities of three novel natural products from *A. cordifolia*. Additionally, this is the first report of the anti-mitotic activities of aromaticin and pulchellin-2α-*O*-isovalerate, and of the effects of aromaticin on ubiquitination. The distinguishable mitotic arrest phenotypes induced by these compounds suggest that they act upon different cellular targets.

CHAPTER 2

Identification and characterization of five anti-mitotic sesquiterpene lactones from the Canadian plant species *Arnica cordifolia*

2.1. Introduction

Arnica cordifolia is a botanical species from the Asteraceae family native to the montane cordillera ecological zone of Alberta, Canada. A previous screen of *A. cordifolia* in our laboratory reported anti-mitotic activity on human cancer cell lines. This activity was independently replicated, as cells treated with *A. cordifolia* extracts acquired a rounded morphology and were positive for the mitotic indicator protein phospho-histone H3. Further investigation revealed that cells treated with leaf extract exhibited undistorted bipolar mitotic spindles, whereas cells treated with whole plant and flower extracts exhibited both distorted and undistorted spindles. The observation of multiple distinct mitotic arrest phenotypes suggested the presence of more than one anti-mitotic compound. In collaboration with Dr. Raymond Andersen from the University of British Columbia, biology-guided fractionation was utilized to isolate five active compounds from *A. cordifolia* leaves. Three novel sesquiterpene lactones were discovered, as well as the known compounds aromaticin and pulchellin-2α-*O*-isovalerate. These compounds induced mitotic arrest with distinct effects on the mitotic spindle. Investigation into potential cellular targets revealed that aromaticin treatment produced ubiquitin foci, suggesting possible inhibition of the ubiquitin-proteasome pathway. This is the first report of three novel sesquiterpene lactones and their anti-mitotic activities. Furthermore, this is the first

study to attribute anti-mitotic activities to aromaticin and pulchellin-2α-*O*-isovalerate, and to report the effects of aromaticin on ubiquitin.

2.2. Materials and Methods

2.2.1. Collection of plant material

Aerial parts of flowering *A. cordifolia* plants were collected sustainably in the Porcupine Hills, Alberta, Canada at 49° 58' 15" N and 114° 5' 13" W, elevation approximately 1700 m during 2022 and 2023. Permits from the local and provincial governments were obtained prior to collection. *A. cordifolia* taxonomy was confirmed to species level, and voucher specimens were submitted to the University of Lethbridge Herbarium as Golsteyn #420. After collection, plants were dried at 40 °C then stored at room temperature and protected from light.

2.2.2. Preparation of plant extracts

Extracts were prepared from either total or separated plant parts (leaves, flowers, stems) ground into a fine powder. The powdered material was suspended to 10% (w/v) in either 75% (v/v) ethanol (Greenfield Global; P016EAAN) in water or 100% dichloromethane (Fisher Chemical; D37-4). Suspensions were placed on a shaker overnight at room temperature and protected from light. Suspensions were then filtered by Grade 1 Whatman paper and the solvent was evaporated at room temperature. Extracts

were dissolved in methanol (Fisher Chemical; A452-4) to 50 mg/mL and stored at -20 °C for use in subsequent experiments.

2.2.3. UV-visible spectroscopy

Extracts were diluted to 1 mg/mL in methanol, then 75 µL of each extract was loaded into separate wells of a 96-well plate. A control well was loaded with 75 µL of methanol. The absorbance of each sample was measured from 300 to 700 nm using a Biotek Epoch microplate spectrophotometer using Gen5 software (Agilent Technologies), with a step of 2 nm between reads. Absorbance data were blanked to the methanol control.

2.2.4. Cell culture

The human cell lines HT-29 (ATCC HTB-38) and U2OS (ATCC HTB-96) were obtained from the American Type Culture Collection (ATCC). HT-29 cells were cultured in RPMI 1640 media (Gibco; 21870-092) supplemented with 10% (v/v) FBS (Gibco; 12484-028) and 1% (v/v) GlutaMAX (Gibco; 35050-061), and incubated at 37 °C in 5% CO_2. Cells were split and the media were changed every three to four days. HT-29 cells were plated at a density of 2.0×10^5 cells/well in 6-well culture plates or 2.0×10^4 cells/well in 12-well culture plates and incubated at 37 °C for 48-72 h prior to treatment.

U2OS cells were cultured in DMEM / F12 (1:1) media (Gibco; 11320-033) supplemented with 10% (v/v) FBS, 1% (v/v) GlutaMAX, 1% (v/v) MEM Non-Essential

Amino Acids Solution (Gibco; 11140-050), and 1.5% (v/v) HEPES (Gibco; 15630-080), and incubated at 37 °C in 5% CO_2. Cells were split and the media were changed every three to four days. U2OS cells were plated at the same densities as HT-29 cells and incubated at 37 °C for 24-48 h prior to treatment.

The compounds nocodazole (Sigma-Aldrich; M1404), paclitaxel (Sigma-Aldrich; T7402), pulchelloid A, and MG132 (Sigma-Aldrich; M7449-1ML) were dissolved in DMSO (Sigma-Aldrich; D2438), stored at -20 °C, and used at concentrations of 500 nM, 100 nM, 5 μM, and 300 nM respectively. In not-treated cells, 0.4% (v/v) methanol or DMSO was added as a solvent vehicle control.

2.2.5. Light microscopy

Images were captured with an Infinity 1 camera with Infinity Capture imaging software (Lumenera Corporation) on an Olympus CKX41 inverted microscope. Images were processed using Adobe Photoshop (CC 25.6.0). Cells were manually scored for rounded or flat morphology and counted with ImageJ software (IJ 1.54i). At least 200 HT-29 cells or 85 U2OS cells were counted for each treatment.

2.2.6. Cell viability assay

The cytotoxicity of plant extracts and purified compounds was measured by MTT ((3-(4,5-dimethylthiazol-2-yl)-2,5-diphenyltetrazolium bromide) assay (Sigma-Aldrich;

M2128-1G). HT-29 cells were plated at a density of 4.8 x 10^5 cells/96-well culture plate and cultured at 37 °C for 48 h prior to treatment. All treatments were tested in triplicate and independent experiments were conducted at least three times. After 72 h of treatment, 20 µL of MTT solution (5 mg/mL MTT in PBS (137 mM NaCl, 3 mM KCl, 100 mM Na_2HPO_4, 18 mM KH_2PO_4)) was added to each well and incubated at 37 °C for 3.5 h. The media were then removed and 150 µL of MTT solvent (4 mM HCl, 0.1% (v/v) octylphenoxypolyethoxyethanol, in isopropanol) was added to each well. Plates were placed on a shaker in the dark until all formazan crystals had dissolved, then absorbance was measured at 590 nm using a Cytation™ 5 Cell Imaging Multi-Mode Reader with Gen5 software (Agilent Technologies) and blanked against a control well not seeded with cells.

The concentrations of each plant extract or compound were plotted against normalized percent absorbance using GraphPad Prism software. The normalized percent absorbance was calculated as:

Normalized percent absorbance = (absorbance / DMSO absorbance) x 100

Where DMSO absorbance refers to the absorbance of 0.1% (v/v) DMSO-treated cells from a control well. IC_{50} values were determined through non-linear regression (inhibitor concentration versus normalized response) using GraphPad Prism software.

2.2.7. Flow cytometry

HT-29 cells were seeded at a density of 0.3 x 10^5 cells/25 cm^2 flask and incubated at 37 °C for 48 prior to treatment. After 18 h treatment, cells were collected by

trypsinization and centrifuged at 300 x g for five minutes. Cells were washed with warm PBS with 0.8% (v/v) FBS and 1 mM EDTA (Caledon Laboratories; 3460-1), then resuspended to a concentration of 2.0 x 10^6 cells/mL in cold PBS with 0.8% (v/v) FBS and 1 mM EDTA. From each suspension, 500 µL was added dropwise to 500 µL of cold 70% ethanol in water then stored at -20 °C overnight. Cells were then resuspended and 200 µL aliquots were transferred to 1.5 mL microfuge tubes. Each aliquot was centrifuged at 300 x g for five minutes, washed with PBS, centrifuged again, then resuspended in 200 µL of Muse™ Cell Cycle Staining Reagent for 30 minutes in the dark. Cells were then analyzed for DNA content using a Muse™ Cell Analyzer. Flow cytometry assays were performed three times.

2.2.8. β-mercaptoethanol reduction assay

HT-29 cells were plated at a density of 2.0 x 10^4 cells/well in 12-well culture plates and incubated at 37 °C for 48-72 h prior to treatment. Treatments were incubated at 37 °C for 2 h with or without 100 µM β-mercaptoethanol (MP BioMedical, 02194705-CF) prior to addition to cells. After 18 h treatment, light microscopy images were taken as described above.

2.2.9. Immunofluorescence microscopy

HT-29 cells were plated at a density of 2.0 x 10^5 cells/well in 6-well culture plates or 2.0 x 10^4 cells/well in 12-well culture plates and incubated at 37 °C for 48-72 h prior to

treatment. After 18 h treatment, the media were aspirated and cells were fixed with 3% (v/v) paraformaldehyde (Ted Pella; 18505) in PBS for 20 minutes at room temperature. Fixation was then quenched with 50 mM NH_4Cl (Sigma-Aldrich; A4514) in PBS for 10 minutes. Cells were permeabilized with 0.2% (v/v) Triton X-100 (Millipore; EM-9410) in PBS for 5 minutes, followed by blocking with 3% (w/v) BSA (MP Biomedicals; 810551) in PBS-T (0.1% (v/v) Tween-20 (VWR Life Science; EM-9480) in PBS) for 30 minutes. Cells were then incubated overnight at 4 °C with anti-phospho-Ser10 histone H3 (Millipore; 06-570; 1:1000), anti-α-tubulin (Santa Cruz Biotechnology; sc-53030; 1:300), or anti-ubiquitin (Cell Signalling; 58395; 1:300) primary antibodies. The following day, cells were washed with PBS-T, then incubated at room temperature for 45 minutes with secondary antibodies Alexa Fluor™ 594 AffiniPure™ goat anti-rabbit IgG (Jackson ImmunoResearch; 111-585-003; 1:400) and Alexa Fluor™ 488 goat anti-rat IgG (Invitrogen; A11006; 1:200). DNA was stained with 300 nM DAPI (4′,6-diamidino-2-phenylindole) (Invitrogen; D1306) in PBS-T for 15 minutes at room temperature. Cells were then imaged with a Cytation™ 5 Cell Imaging Multi-Mode Reader using Gen5 software (Agilent Technologies). A minimum of 200 total cells were counted for each treatment using ImageJ software, and three independent experiments were conducted.

2.2.10. Bioassay-guided fractionation

Extraction of material, fractionation of extracts, and identification of compounds were carried out by Dr. Raymond Andersen (University of British Columbia), Dr. David Williams (University of British Columbia), and Benjamin Yeremy (University of British

Columbia). Approximately 100 g of dried and powdered *A. cordifolia* leaf material was extracted and partitioned either between water and butanol, or water and ethyl acetate. The ethyl acetate extract was further fractionated, yielding six subfractions. These fractions were labelled as RA-288 through RA-296 and evaluated for activity by the cell rounding assay. The active ethyl acetate subfractions RA-293 and RA-294 were further fractionated, yielding RA-297 through RA-303, and RA-304 through RA-307, respectively. The active subfractions RA-298 and RA-299 were purified by HPLC, yielding 2.0 mg of aromaticin (RA-312), 1.9 mg of novel compound RA-313, 2.3 mg of RA-314 (an approximately 1:1 mixture of pulchellin-2α-*O*-isovalerate (RA-314-1) and novel compound RA-314-2), and 4.3 mg of novel compound RA-315. Chemical structures were determined by NMR and mass spectrometry.

2.2.11. Statistical analysis

Data were analyzed using Microsoft Excel 365 and GraphPad Prism 10 software. Data were plotted as means of three independent experiments ± standard error of the means. One-way analysis of variance (ANOVA) with Tukey's or Dunnett's post hoc tests were used to determine statistical significance in bar graphs with the exception of β-mercaptoethanol reduction assays, where two-way ANOVA was used. Differences were considered significant when $p < 0.05$.

2.3. Results

2.3.1. Extracts prepared from Arnica cordifolia induce mitotic arrest in cancer cells

Arnica cordifolia is a prominent botanical species from the Asteraceae family that grows in the montane cordillera ecological zone of Alberta, Canada. It displays heart-shaped opposite leaves, erect stems, and the characteristic features of Asteraceae species with ray and disc flowers (Figure 2.1A). It is taxonomically related to the widely used medicinal plant *Arnica montana*.

We collected whole aerial parts of *A. cordifolia* in-bloom and extracted the dried material with either 75% (v/v) ethanol in water (PP-1910A) or 100% dichloromethane (PP-1910B). These two extracts were spectrophotometrically distinct when analyzed by UV-visible absorbance. PP-1910A absorbed relatively strongly at 350 nm, whereas PP-1910B had relatively stronger absorbance from 380-480 nm, indicating that the extracts were likely composed of different compounds (Figure 2.1B).

We then examined the two extracts for cytotoxicity on HT-29 cells by MTT assay (Figure 2.2). HT-29 cells were either not-treated or treated with varied concentrations of camptothecin, a positive control with anti-proliferative effects, or with *A. cordifolia* extracts. After 72 h treatment, the half-maximal inhibitory concentration (IC_{50}) of each treatment was determined. Camptothecin had an IC_{50} of 36 ± 8 nM, as expected (not shown). PP-1910A treatment had no effect on cell viability at any tested concentration, whereas PP-1910B treatment at 300 μg/mL, the highest concentration tested, decreased

cell viability to 40%. These data revealed that neither extract was particularly toxic, and enabled us to select concentrations for phenotypic assays.

A prior phenotypic screen in the laboratory suggested that *A. cordifolia* extracts induce cell rounding, a feature of mitosis (Molina, 2018; Kubara et al., 2012). This result was unexpected, as the related species *A. montana* had not been reported to harbour anti-mitotic activity. To confirm the cell rounding activity of *A. cordifolia* extracts, we tested PP-1910A and PP-1910B on HT-29 cells by phenotypic assay. Cells were either not-treated or treated with the tubulin depolymerizing agent nocodazole as a positive control or with varied concentrations of PP-1910A or PP-1910B (Figures 2.3 and 2.4). After 18 h treatment, the percentage of cells with rounded morphology was determined (Figures 2.3C and 2.4B). In not-treated cells, 3 ± 1% exhibited a rounded morphology, whereas 82 ± 2% of nocodazole-treated cells were rounded, as expected. Treatment with PP-1910A induced 15 ± 1% cell rounding at 500 µg/mL, but did not induce cell rounding at lower concentrations. PP-1910B induced 14 ± 1% cell rounding at 500 µg/mL and 20 ± 1% cell rounding at 150 µg/mL. Additionally, we tested a dichloromethane extract prepared from *A. cordifolia* material collected at the same site the following year (Figure 2.5). The percentages of rounded cells induced after treatment with the two dichloromethane extracts were not significantly different. These data showed that the cell rounding activity of *A. cordifolia* extracts had been independently replicated.

We then tested the cell rounding activity of *A. cordifolia* extracts in a second cell line to determine whether this activity was unique to HT-29 cells or broadly applicable as a cell rounding agent. U2OS cells were either not-treated or treated with nocodazole or

varied concentrations of PP-1910A or PP-1910B. After 18 h treatment, the percentage of cells with rounded morphology was determined (Figures 2.3C and 2.4B). Not-treated cells exhibited little rounding, whereas 39 ± 3% of nocodazole-treated cells were rounded. PP-1910A induced 24 ± 4% cell rounding at 500 μg/mL but did not induce cell rounding at lower concentrations. PP-1910B was again more potent, being toxic at 500 μg/mL and inducing 31 ± 4% cell rounding at 150 μg/mL. Knowing that the cell rounding activity of the dichloromethane extract PP-1910B was replicable and the most potent in two cell lines, we selected it for further investigation.

To determine whether a particular plant organ contained the active compounds that induced cell rounding, we separated *A. cordifolia* plants into leaves, flowers, and stems and prepared 100% dichloromethane extracts from each organ. (Figure 2.6). HT-29 cells were either not-treated or treated with nocodazole, whole plant extract PP-1910B, or varied concentrations of leaf extract (LE), flower extract (FE), or stem extract (SE) for 18 h. Not-treated cells exhibited little rounding, whereas 91 ± 1% of nocodazole-treated cells were rounded. LE and FE both induced cell rounding at 50 μg/mL (LE: 18 ± 1%, FE: 16 ± 1%) and 150 μg/mL (LE: 42 ± 2%, FE: 41 ± 3%) concentrations. SE was less potent, inducing only 11 ± 1% cell rounding at 50 μg/mL and 31 ± 3% cell rounding at 150 μg/mL, which was similar to values induced by the whole plant extract's 29 ± 2% cell rounding at a concentration of 150 μg/mL. LE, FE, and SE were all toxic at 500 μg/mL. These data suggest that *A. cordifolia* aerial parts, particularly leaves and flowers, contain compounds that induce cell rounding.

Since a rounded cell morphology can be indicative of mitosis, we used flow cytometry to determine whether *A. cordifolia* extract treatment resulted in a cell cycle arrest. HT-29 cells were not-treated, or treated with nocodazole or *A. cordifolia* extracts PP-1910B, LE, or FE and examined for DNA content (Figure 2.7). Not-treated cells had a phase distribution of 50 ± 2% in G1, 19 ± 1% in S, and 30 ± 1% in G2/M phases, whereas 96 ± 1% of nocodazole-treated cells were in G2/M phase. The phase distributions of cells treated with *A. cordifolia* extracts were 36 ± 5% of PP-1910B-treated cells in G1, 11 ± 2% in S, and 53 ± 8% in G2/M phases. LE and FE phase distributions were not significantly different from those of PP-1910B. These data indicate that cell populations treated with *A. cordifolia* extracts had a higher number of cells in G2/M phase than non-treated populations.

To determine whether these cells had been arrested in G2 or M phase, we used phospho-Ser10 histone H3 (PH3) and α-tubulin antibody staining and observed cells by immunofluorescence microscopy (Figure 2.8A). Cells were either not-treated or treated with the tubulin depolymerizing agent nocodazole, the tubulin stabilizing agent paclitaxel (Taxol®), or *A. cordifolia* extracts PP-1910B, LE, or FE. After 18 h, cells were fixed and stained with anti-PH3 and anti-α-tubulin antibodies to reveal mitotic cells and mitotic spindles, respectively. The mean percentages of PH3-positive cells were 4 ± 1% for not-treated cells, 69 ± 3% for nocodazole-treated cells and 68 ± 4% for paclitaxel-treated cells, which confirmed the accumulation of mitotic cells after nocodazole or paclitaxel treatment relative to not-treated cells (Figure 2.8B). Cells treated with PP-1910B had 10 ± 2% PH3-positive cells, whereas 22 ± 4% of cells treated with LE and 22 ± 4% of cells treated with

FE were PH3-positive. These data confirmed that the cell rounding observed after *A. cordifolia* extract treatment represented cells arrested in mitosis.

We next compared the organization of α-tubulin in not-treated cells, cells treated by known tubulin toxins, and cells treated by *A. cordifolia* extracts (Figure 2.8A). Not-treated mitotic cells displayed the normal range of mitotic tubulin structures, including bipolar mitotic spindles. Nocodazole-treated cells displayed little staining, as nocodazole prevents tubulin polymerization that is required for mitotic spindle formation. Paclitaxel-treated cells showed intensely stained and distorted spindle structures, consistent with paclitaxel-stabilized microtubules. In cells treated with PP-1910B or FE, 27 ± 6% and 20 ± 5% of mitotic cells respectively showed distorted mitotic spindle structures that were distinguishable from those of paclitaxel-treated cells (Figure 2.8B). Strikingly, only 9 ± 1% of LE-treated cells showed a distorted mitotic spindle; this was not significantly different from the percentage of distorted spindles detected in not-treated cells (5 ± 4%). The presence of both mitotic cells with distorted spindles and mitotic cells with undistorted spindles after PP-1910B or FE treatment suggests that *A. cordifolia* aerial parts may contain multiple anti-mitotic compounds that induce mitotic arrest by distinct mechanisms. In particular, the compounds that induce mitotic arrest without distortion of the mitotic spindle appeared to be localized primarily in leaves.

By comparing the staining of PH3 and α-tubulin in treated cells, we were able to observe the arrangement of chromosomes relative to the mitotic spindle. Not-treated cells showed typical mitotic chromosome arrangements with undistorted spindles. Nocodazole and paclitaxel treatments both resulted in the condensation of chromosomes, with

chromosomes distributed throughout nocodazole-treated cells and concentrated around the distorted spindles of paclitaxel-treated cells. Strikingly, after treatment with any of the *A. cordifolia* extracts, cells with bipolar spindle structures had chromosome arrangements reminiscent of cells in prometaphase or metaphase. Extract-treated cells without bipolar spindles instead had chromosomes disorganized throughout their distorted spindle structures.

Previous work in our laboratory has shown that several anti-mitotic compounds that induce mitotic arrest with distorted mitotic spindles, such as pulchelloid A, can be inactivated by treatment with the reducing agent β-mercaptoethanol (BME) (Healy Knibb, 2024). As both distorted and undistorted spindles were observed after treatment with PP-1910B and FE, we used a chemical test with BME to determine if the cell rounding activity of each extract could be inhibited by BME treatment. Extracts were incubated for 2 h with or without 100 μM BME before their addition to HT-29 cells. To serve as controls, the same incubations were done with untreated media, nocodazole (unaffected by BME reduction), and pulchelloid A (inactivated by BME reduction) (Healy Knibb, 2024). Cells were observed by light microscopy after 18 h treatment (Figure 2.9). Not-treated cells showed no significant difference in cell rounding in the presence or absence of BME. Similarly, BME incubation did not reduce the number of round cells after nocodazole treatment. Pulchelloid A, as expected, showed a significant reduction in cell rounding activity after BME incubation. Strikingly, PP-1910B, LE, and FE treatments all had fewer rounded cells after BME incubation. This result revealed that the *A. cordifolia* leaf extracts were unlike any that we or others had reported: though the chemistry of the active

compounds may be similar to that of pulchelloid A, their effects on the mitotic spindle are biologically distinct.

Since the anti-mitotic activities of *A. cordifolia* extracts were inhibited by BME reduction, we suspected that the active compounds may act by forming covalent bonds to cellular targets (Jackson et al., 2017). To investigate this, HT-29 cells were either not-treated or treated with nocodazole, pulchelloid A, LE, or FE, then washed with untreated media after 6 h of treatment (Figure 2.10). Cells were imaged by light microscopy after an additional 12 h. Not-treated cells showed no significant difference in cell rounding when the cells were washed when compared to unwashed cells. Nocodazole, a reversible inhibitor of mitosis, induced significantly less cell rounding when it was removed by changing the media. By contrast, the suspected covalent inhibitor pulchelloid A did not show a significant change in cell rounding between washed and unwashed cells. Similarly, significant changes in cell rounding were not observed between washed and unwashed cells after treatment with either LE or FE. This suggests that the active compounds may be covalent inhibitors of mitosis, and further supports that these compounds may be chemically similar to pulchelloid A.

Since the distinct anti-mitotic activities of *A. cordifolia* extracts suggested that these extracts contained multiple active compounds, we selected leaf material as the source for bioassay-guided fractionation. Leaves were chosen because of the novel biological and chemical properties of LE. Due to the similar responses of LE and FE treatments in the BME and washoff assays, we suspected that these active compounds would be chemically similar but would have distinct effects on the mitotic spindle.

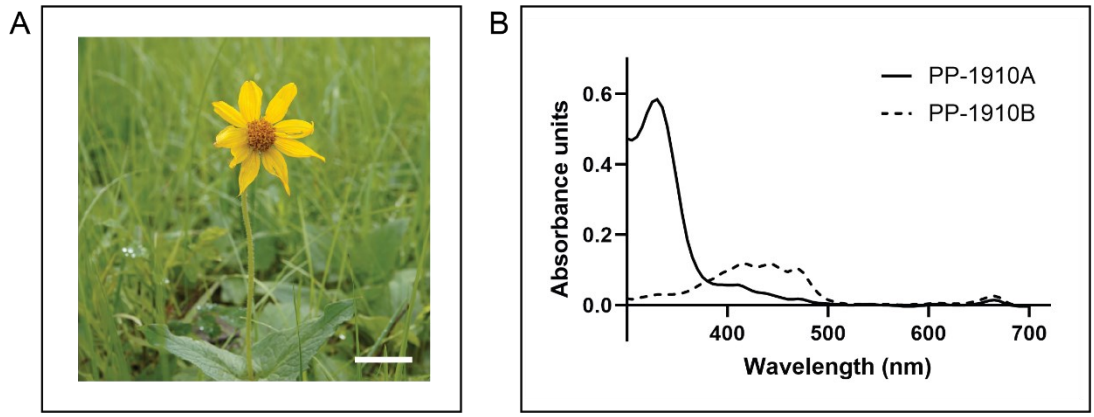

Figure 2.1. Ethanolic and dichloromethane extracts prepared from *A. cordifolia* are spectrophotometrically distinct. **A.** *A. cordifolia*. Scale bar represents 5 cm. **B.** UV/visible absorbance spectra of 75% (v/v) ethanol in water (PP-1910A) and 100% dichloromethane (PP-1910B) extracts prepared from *A. cordifolia* aerial plant material. Extracts were diluted to 1 mg/mL in methanol, then absorbance was read from 300 to 700 nm on a Biotek Epoch microplate spectrophotometer.

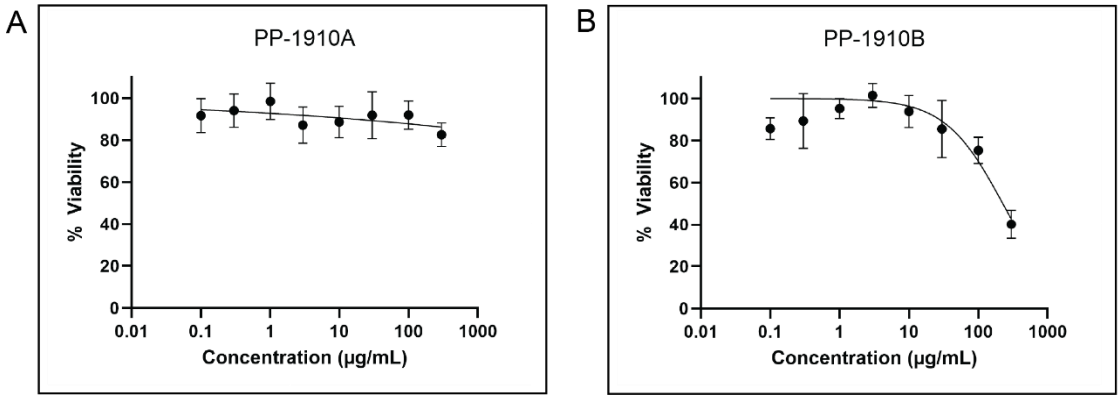

Figure 2.2. Dichloromethane extract prepared from *A. cordifolia* is cytotoxic to HT-29 cells. HT-29 cells were treated with varying concentrations of PP-1910A (**A**) or PP-1910B (**B**) for 72 h, then cell viability was determined by MTT assay. Standard errors of the means are shown.

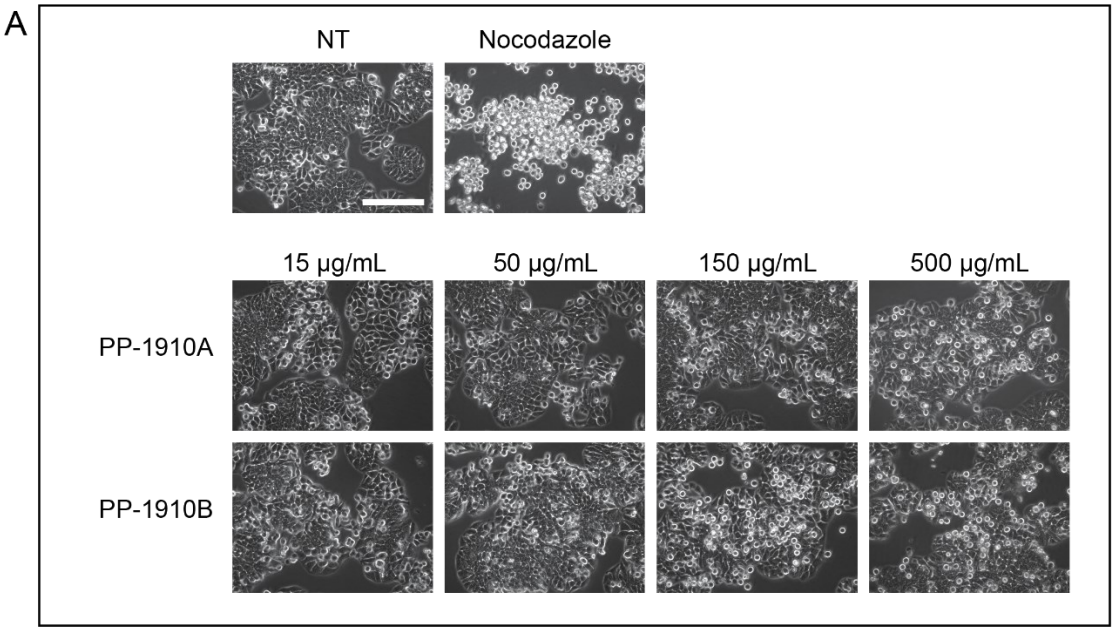
A
NT
Nocodazole
15 µg/mL
50 µg/mL
150 µg/mL
500 µg/mL
PP-1910A
PP-1910B

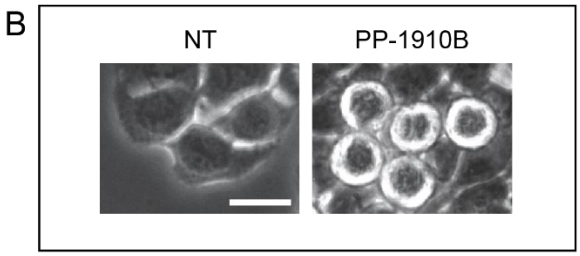
B
NT
PP-1910B

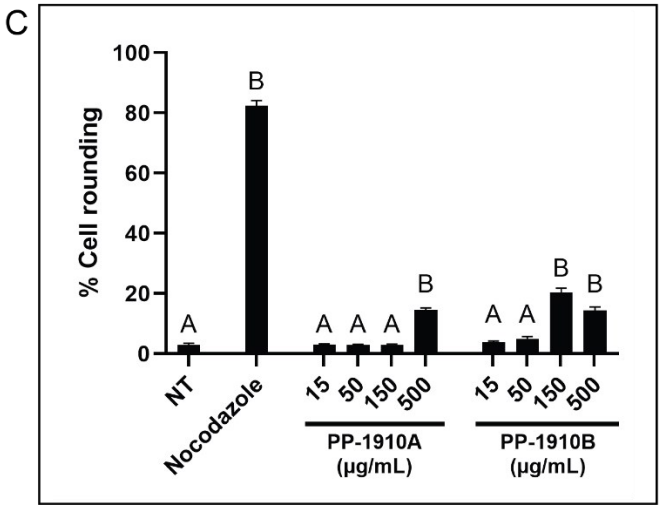
C
% Cell rounding
100
80
60
40
20
0
A
B
A A A
B
A A
B
B
NT
Nocodazole
15 50 150 500
PP-1910A (µg/mL)
15 50 150 500
PP-1910B (µg/mL)

Figure 2.3. *A. cordifolia* extracts induce a rounded morphology in HT-29 cells. **A.** HT-29 cells were either not-treated (NT) or treated with nocodazole or various concentrations of PP-1910A or PP-1910B for 18 h and observed by light microscopy. Scale bar represents 50 μm. **B.** Zoomed images of not-treated cells and cells treated with 150 μg/mL PP-1910B show a rounded morphology indicative of mitosis. Scale bar represents 10 μm. **C.** The mean percentages of rounded cells after each treatment described in **A** were determined by counting cells and manually scoring them for rounded morphology. The standard errors of the means are shown and treatments that were significantly different from not-treated cells are shown by letters ($p < 0.05$).

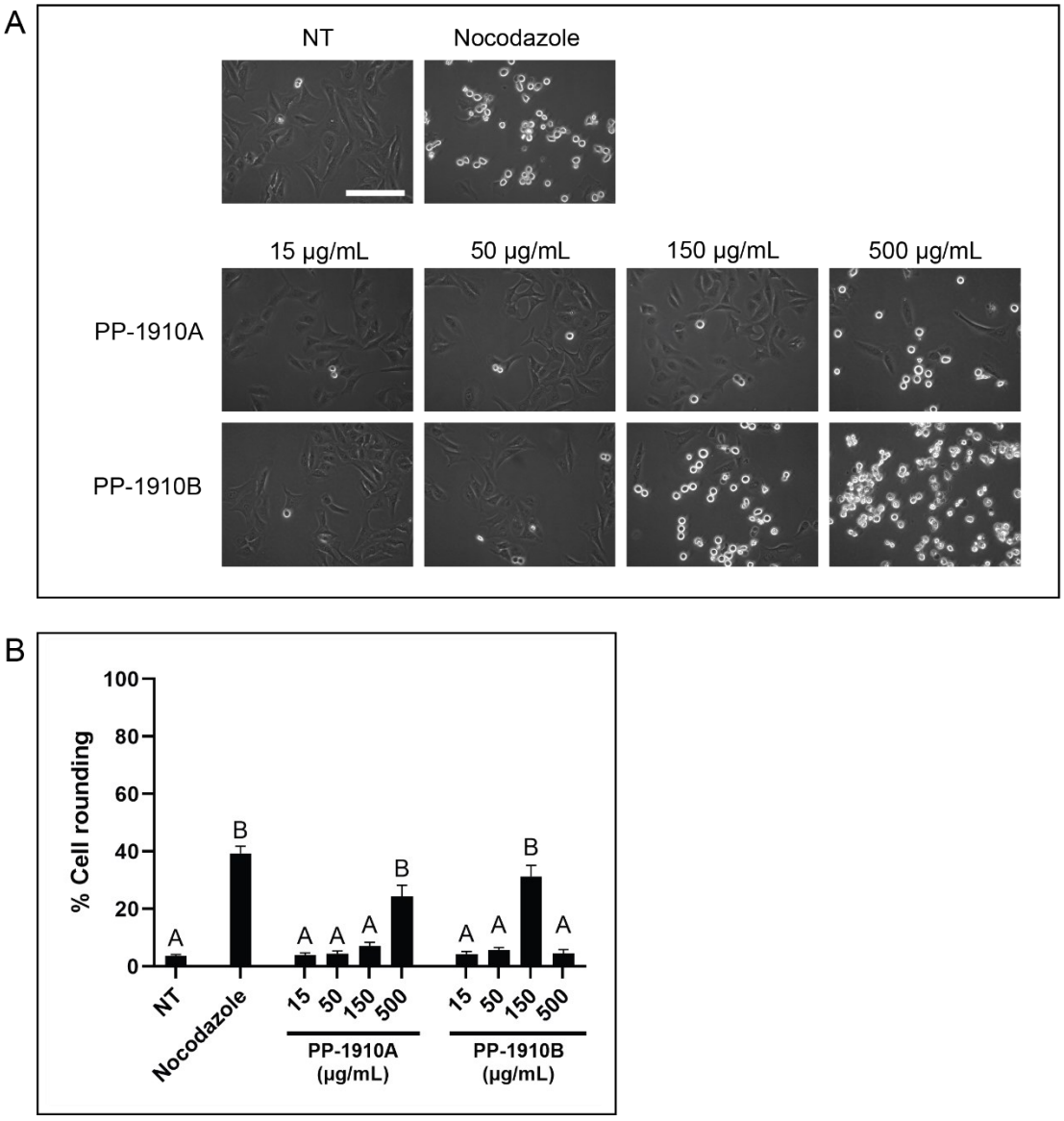

Figure 2.4. *A. cordifolia* extracts induce a rounded morphology in U2OS cells. **A.** U2OS cells were either not-treated (NT) or treated with nocodazole or various concentrations of PP-1910A or PP-1910B for 18 h and observed by light microscopy. Scale bar represents 50 µm. **B.** The mean percentages of rounded cells after each treatment described in **A** were determined. The standard errors of the means are shown and treatments that were significantly different from not-treated cells are shown by letters ($p < 0.05$).

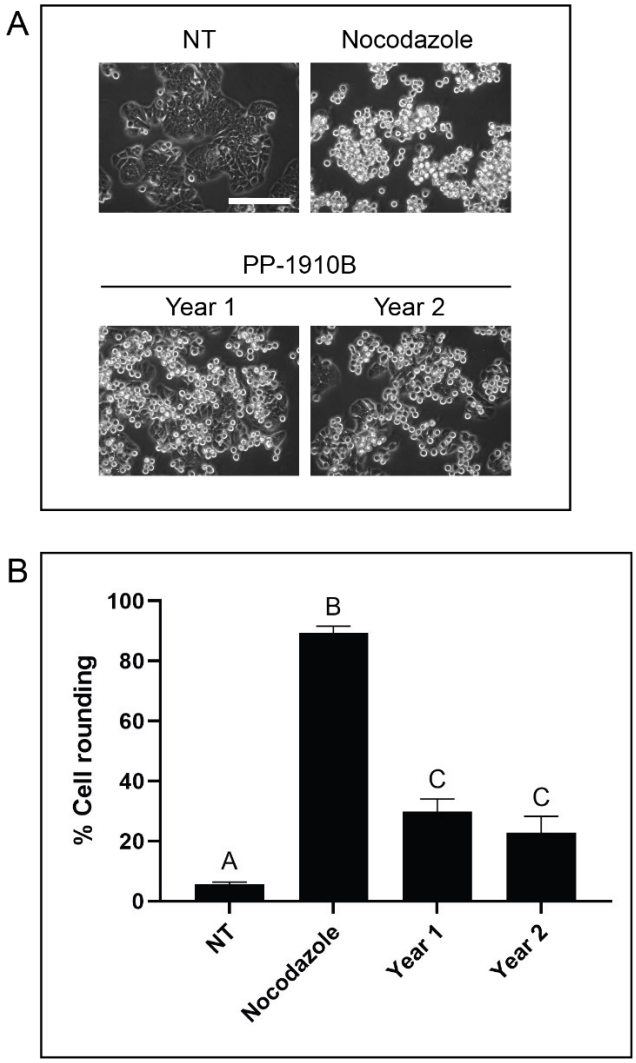

Figure 2.5. Extracts prepared from *A. cordifolia* plants collected in two different years induce cell rounding. **A.** HT-29 cells were either not-treated (NT) or treated with nocodazole or dichloromethane extracts of *A. cordifolia* (PP-1910B) collected in either 2022 (Year 1) or 2023 (Year 2) for 18 h and observed by light microscopy. Scale bar represents 50 µm. **B.** The mean percentages of rounded cells after each treatment described in **A** were determined. The standard errors of the means are shown and treatments that were significantly different from not-treated cells are shown by letters ($p < 0.05$).

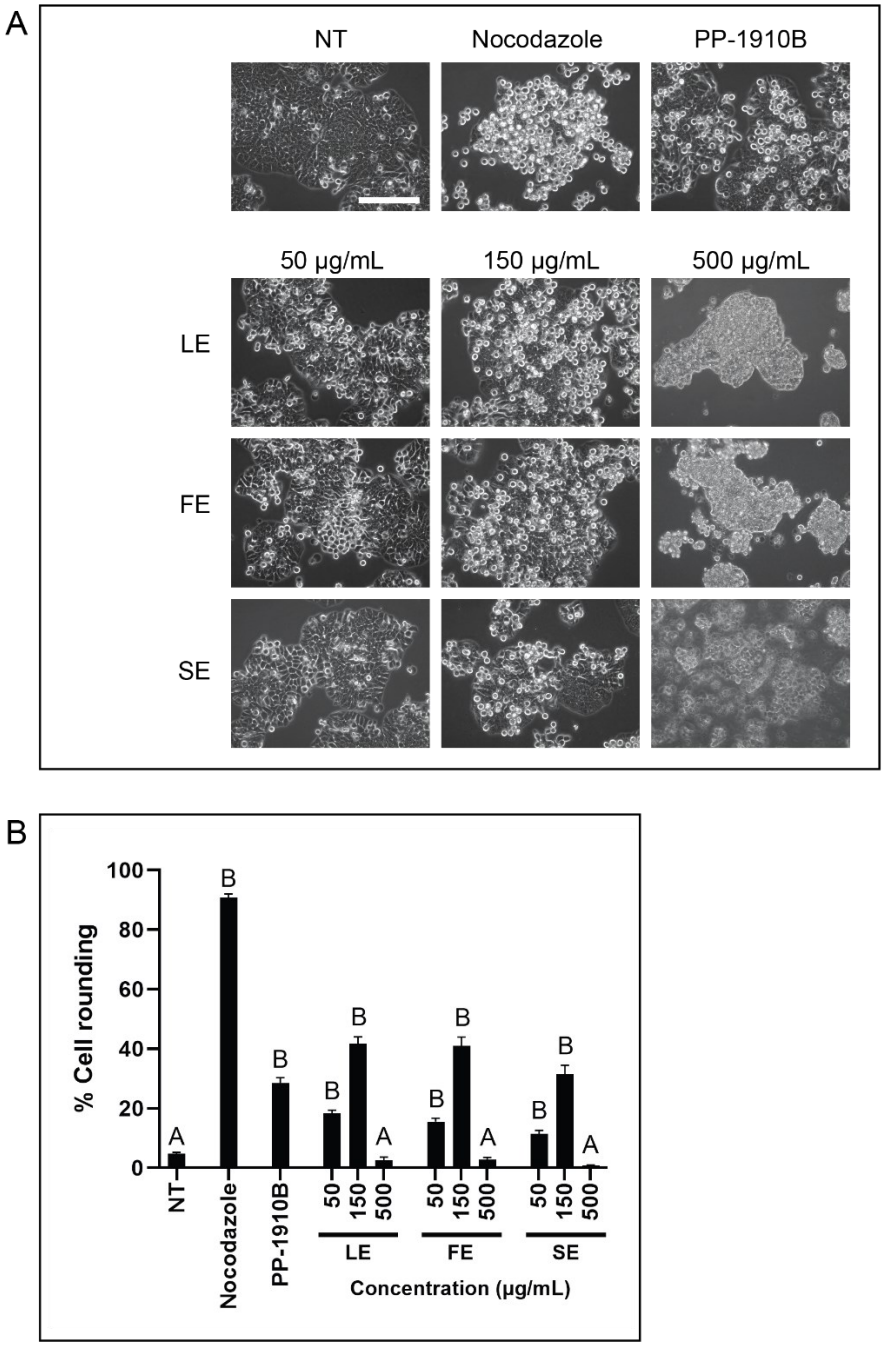

Figure 2.6. Extracts prepared from *A. cordifolia* leaves, flowers and stems induce cell rounding. **A.** HT-29 cells were either not-treated (NT) or treated with nocodazole, 150 µg/mL PP-1910B, or various concentrations of *A. cordifolia* leaf extract (LE), flower extract (FE), or stem extract (SE) for 18 h and observed by light microscopy. Scale bar represents 50 µm. **B.** The mean percentages of rounded cells from **A** were determined. The standard errors of the means are shown and treatments that were significantly different from not-treated cells are shown by letters ($p < 0.05$).

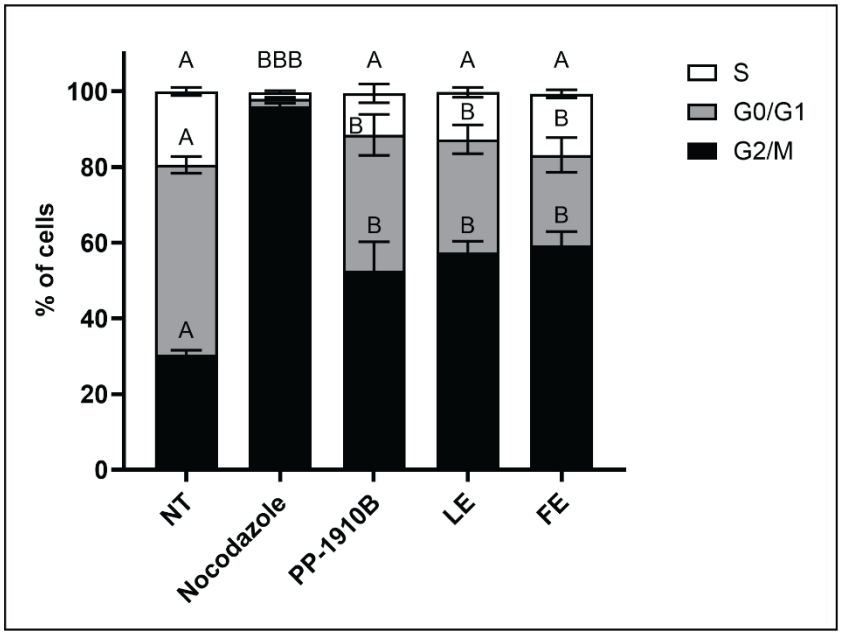

Figure 2.7. *A. cordifolia* extracts induce G2/M phase arrest. HT-29 cells were either not-treated (NT) or treated with nocodazole or 150 μg/mL PP-1910B, leaf extract (LE), or flower extract (FE) for 18 h and analyzed for DNA content by flow cytometry. G0/G1 represents the 2 N fraction and G2/M represents the 4 N fraction. The standard errors of the means are shown and fractions that were significantly different from not-treated cells are shown by letters ($p < 0.05$).

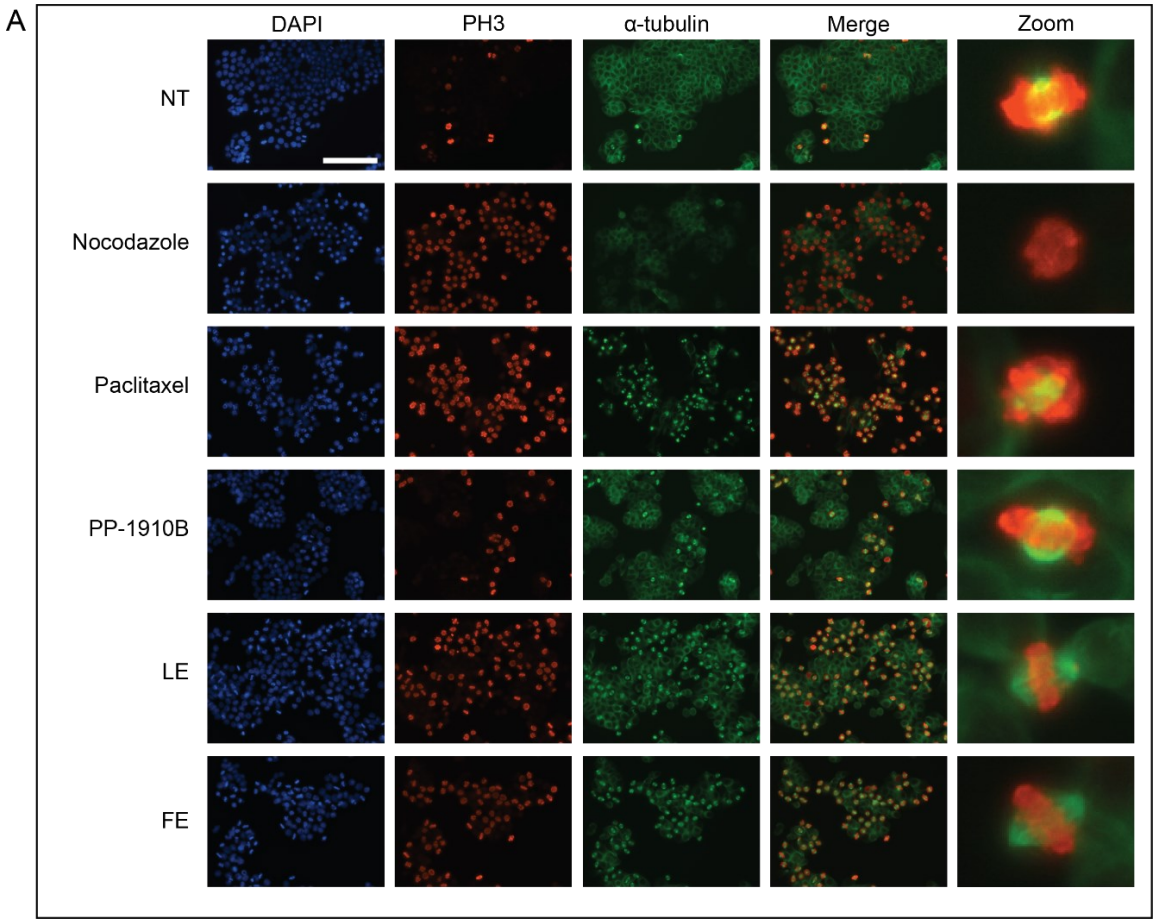
A
DAPI
PH3
α-tubulin
Merge
Zoom
NT
Nocodazole
Paclitaxel
PP-1910B
LE
FE

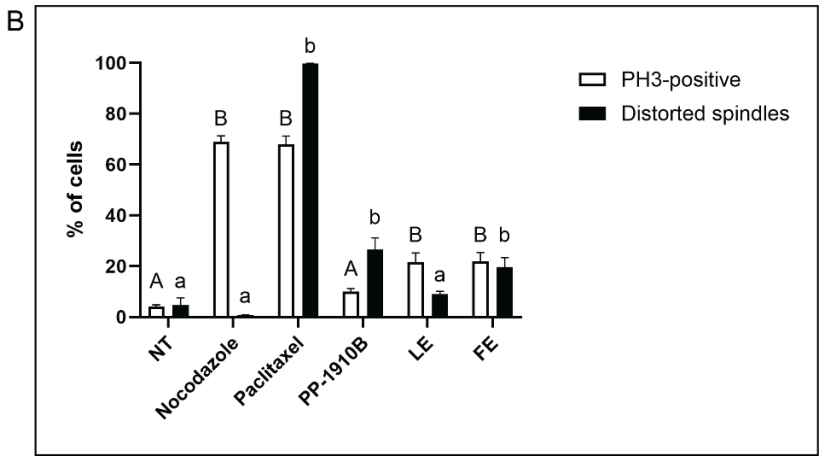
B
% of cells
100
80
60
40
20
0
PH3-positive
Distorted spindles
A a
B a
B b
A b
B a
B b
NT
Nocodazole
Paclitaxel
PP-1910B
LE
FE

Figure 2.8. Cells treated with *A. cordifolia* extracts contain phosphorylated histone H3, but these extracts have differing effects on the mitotic spindle. **A.** HT-29 cells were either not-treated (NT) or treated with nocodazole, paclitaxel, or 150 µg/mL PP-1910B, leaf extract (LE), or flower extract (FE) for 18 h and stained with DAPI (blue) to detect DNA, anti-phospho-histone H3 antibodies (PH3, red) and anti-α-tubulin antibodies (green). The merge column shows both PH3 and α-tubulin staining. Cells were observed by immunofluorescence microscopy. Scale bar represents 50 µm. **B.** The mean percentages of cells with PH3 staining and of mitotic spindles with distorted appearances after each treatment described in **A** were determined. Mitotic spindles of PH3-positive cells were manually scored for distorted mitotic spindle morphology in reference to NT cells. The standard errors of the means are shown and treatments that were significantly different from not-treated cells are shown by letters ($p < 0.05$).

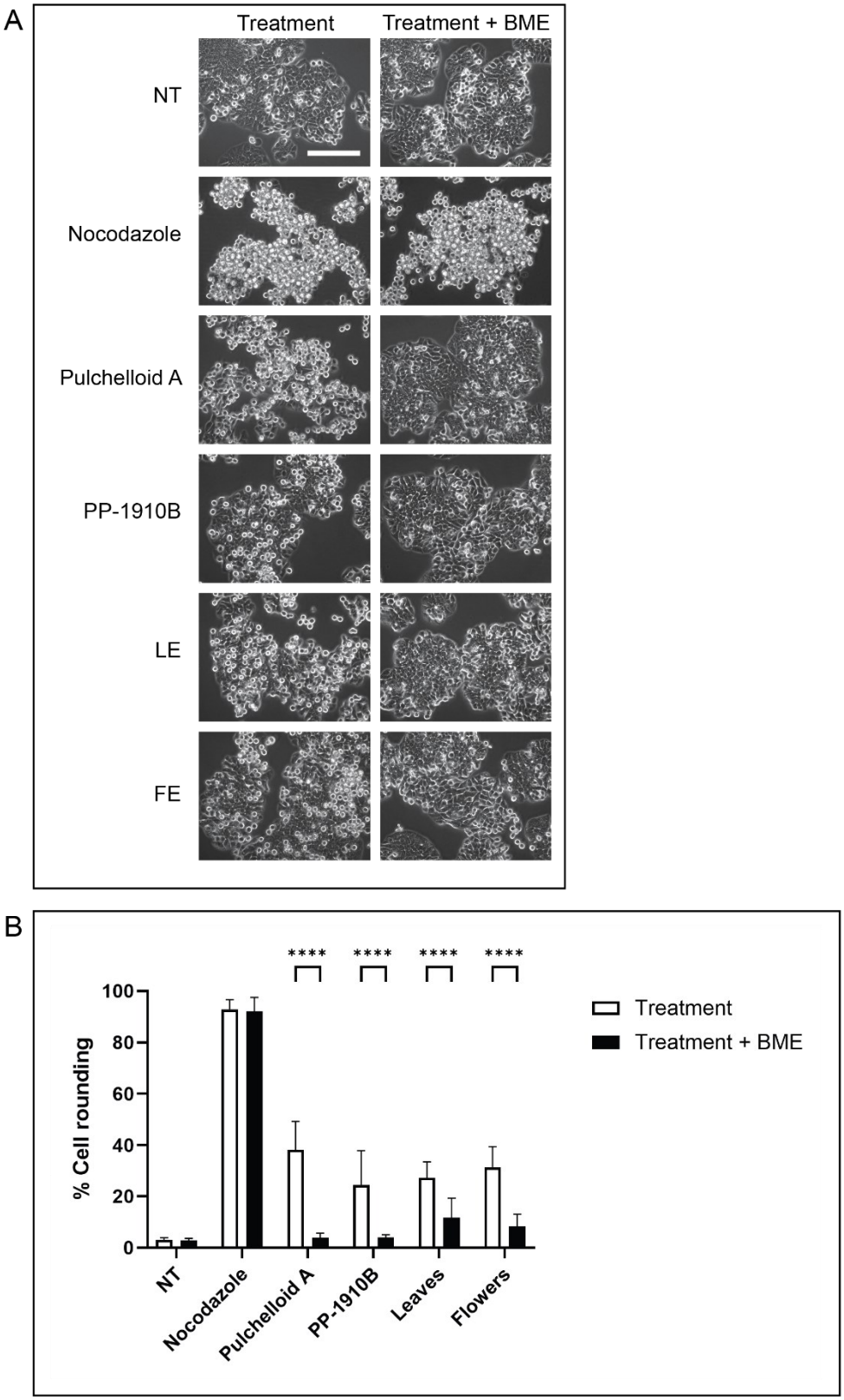
A
Treatment
Treatment + BME
NT
Nocodazole
Pulchelloid A
PP-1910B
LE
FE
B
****
****
****
****
100
80
60
40
20
0
% Cell rounding
Treatment
Treatment + BME
NT
Nocodazole
Pulchelloid A
PP-1910B
Leaves
Flowers

Figure 2.9. β-mercaptoethanol inhibits the anti-mitotic activity of *A. cordifolia* extracts. **A.** Treatments of vehicle control (not-treated, NT), nocodazole, pulchelloid A, and 150 μg/mL PP-1910B, leaf extract (LE), and flower extract (FE) were incubated at 37 °C for 2 h with or without 100 μM β-mercaptoethanol prior to addition to HT-29 cells. Cells were observed by light microscopy. Scale bar represents 50 μm. **B.** The mean percentages of rounded cells after each treatment described in **A** were determined. The standard errors of the means are shown and treatments that were significantly different from not-treated cells are shown by asterisks ($p < 0.05$).

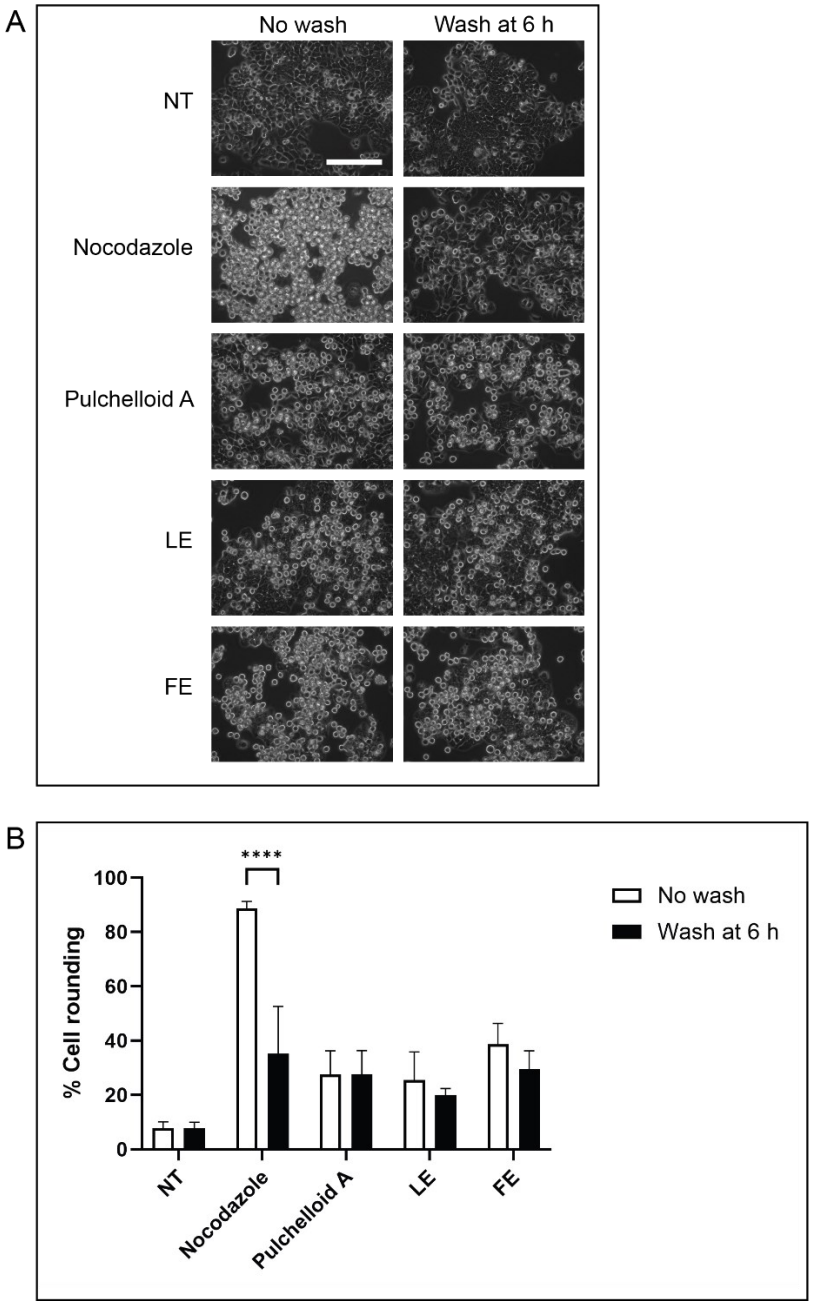

Figure 2.10. Anti-mitotic activity of *A. cordifolia* extracts is retained after treated cells are washed with untreated media. **A.** HT-29 cells were either not-treated (NT) or treated with nocodazole, pulchelloid A, or 150 µg/mL leaf extract (LE) or flower extract (FE) for 6 h, then were either not washed or washed with untreated media and observed by light microscopy after a further 12 h. Scale bar represents 50 µm. **B.** The mean percentages of rounded cells after each treatment described in **A** were determined. The standard errors of the means are shown and treatments that were significantly different from not-treated cells are shown by asterisks ($p < 0.05$).

2.3.2. Isolation and anti-mitotic activity of five sesquiterpene lactones from Arnica cordifolia

We used the cell rounding assay to guide the chemical fractionation and identification of the anti-mitotic compound(s) present in *A. cordifolia* leaf extract (bioassay-guided fractionation) (Figure 2.11, supplemental data). Four rounds of purification were undertaken and five different compounds were identified, of which three were novel structures (Table 2.1). Three compounds were separated completely (RA-312, RA-313, RA-315), and two were copurified in one fraction as an approximately 1:1 mixture (RA-314-1 and RA-314-2, referred to collectively as RA-314). All five compounds were sesquiterpene lactones: RA-315 was a germacranolide, whereas the other four compounds were pseudoguaianolides. The two known sesquiterpene lactones were identified as aromaticin (RA-312) (Romo et al., 1964) and pulchellin-2α-*O*-isovalerate (RA-314-1) (Wu et al., 2012). RA-313 differed from RA-314-1 solely by the arrangement of the ester functionality. RA-314-2 was identical to RA-313 apart from the stereochemistry of the α-methylene-γ-lactone, which was a uniquely different stereochemistry from any of the isolated compounds. RA-315 possessed the same ester functionality as RA-313 and RA-314-2, but contained both a germacranolide ring system and epoxide group that was not present in the pseudoguaianolide ring system of the other four compounds. The identification of five sesquiterpene lactones validated our supposition that the active compounds of *A. cordifolia* would be chemically similar to pulchelloid A, a pseudoguaianolide sesquiterpene lactone with an α-methylene-γ-lactone moiety.

The cytotoxicity of each isolated compound was tested on HT-29 cells by MTT assay (Figure 2.12). Camptothecin was used as a positive control and had an IC_{50} value of 37 ± 9 nM (not shown). Unlike the earlier *A. cordifolia* extracts, cell viability results from compound-treated cells were all readily fit to curves to allow for the determination of each compound's IC_{50} value. These IC_{50} values were similar for all isolated compounds (Table 2.2).

The cell rounding activity of each isolated compound was tested by the cell rounding assay (Figure 2.13A). HT-29 cells were either not-treated, or treated with nocodazole or varying concentrations of each compound. After 18 h, the percentage of rounded cells was determined (Figure 2.13B). Not-treated cells exhibited little rounding, whereas nearly all nocodazole-treated cells were rounded. RA-312 induced 24 ± 2% cell rounding at 5 μM and was toxic at 15 μM. RA-313 induced 48 ± 4% cell rounding at 5 μM and 46 ± 2% cell rounding at 15 μM. RA-314 induced 35 ± 2% cell rounding at 5 μM and 40 ± 1% cell rounding at 15 μM. RA-315 induced 29 ± 1% cell rounding at 5 μM and was toxic at 15 μM. None of the compounds induced cell rounding at 1.5 μM and all were toxic at 50 μM.

We had demonstrated that the cell rounding activity of the *A. cordifolia* extracts could be inhibited by β-mercaptoethanol. The discovery of these five chemical structures, all which contained an α-methylene-γ-lactone moiety, suggested that these compounds could be reduced by BME. Therefore, we performed a BME reduction assay to determine whether the isolated active compounds would be inhibited (Figure 2.14). Media containing either vehicle control, nocodazole or each isolated compound were incubated for 2 h with

or without 100 μM BME before their addition to HT-29 cells. Cells were examined for rounded morphology after 18 h of treatment. Both not-treated cells and nocodazole-treated cells showed no significant difference in cell rounding in the presence or absence of BME as expected. All isolated compounds induced significantly less cell rounding after BME incubation, thus agreeing with the earlier results of the *A. cordifolia* extracts.

To confirm that the rounded cells induced by isolated compound treatments were arrested in mitosis, we used immunofluorescence microscopy to examine PH3 and α-tubulin staining (Figure 2.15A). Cells were either not-treated or treated with nocodazole, pulchelloid A, or each compound for 18 h prior to fixation. The mean percentages of PH3-positive cells were 6 ± 0.4% for not-treated cells, 82 ± 1% for nocodazole-treated cells and 20 ± 1% for pulchelloid A-treated cells (Figure 2.15B). In comparison, 28 ± 2% of cells treated with RA-312, 33 ± 2% of cells treated with RA-313, 27 ± 1% of cells treated with RA-314, and 23 ± 2% of cells treated with RA-315 were PH3-positive. These data indicate that all isolated compounds resulted in the accumulation of mitotic cells, agreeing with the cell rounding assay results.

To determine the relationship of the isolated compounds to the distinct mitotic spindle effects seen earlier in *A. cordifolia* extract-treated cells, the α-tubulin organizations of compound-treated cells were observed (Figure 2.15B). Not-treated mitotic cells contained the normal range of mitotic figures including metaphasic bipolar shaped spindles, whereas nocodazole-treated mitotic cells lacked a mitotic spindle, and 68 ± 4% of pulchelloid A-treated cells contained a distorted mitotic spindle, as expected. Strikingly, significant mitotic spindle distortion was observed in cells treated with RA-313 (63 ± 3%)

and RA-314 (65 ± 5%), but not in cells treated with RA-312 (10 ± 2%) or RA-315 (12 ± 3%). The division of the isolated compounds into two distinct anti-mitotic activities (mitotic arrest without spindle distortion from RA-312 and RA-315, and mitotic arrest with distorted spindles from RA-313 and RA-314) paralleled the observations of similar effects in LE- and FE-treated cells, respectively. From these data we conclude that *A. cordifolia* contains multiple anti-mitotic compounds that induce mitotic arrest by at least two distinct mechanisms. For RA-313 and RA-314, this mitotic arrest resembled that of pulchelloid A-treated cells.

As with the *A. cordifolia* extract-treated cells, compound-treated cells with bipolar spindle structures showed the majority of chromosomes aligned at the metaphase plate, though a subset of cells also contained unaligned chromosomes. This metaphasic chromosome arrangement was seen after treatment with RA-312 or RA-315, as well as in the subpopulation of RA-313 and RA-314-treated cells without distorted spindles. In the remainder of RA-313 and RA-314-treated cells that had distorted spindles, chromosomes were disordered along the distorted spindle structure.

The observation of numerous metaphase-like cells after treatment with the isolated compounds prompted comparisons to other compounds known to induce metaphase arrest. Since the inhibition of protein degradation by proteasome inhibitors can arrest mitotic cells at metaphase (Wójcik et al., 1996), we postulated that the isolated compounds may target the ubiquitin-proteasome system. To investigate this, we used immunofluorescence microscopy to observe ubiquitin, a key regulatory protein for protein degradation, within treated cells (Figure 2.16). HT-29 cells were either not-treated or treated with the

proteasome inhibitor MG132, pulchelloid A, or each compound for 18 h, then fixed and stained with anti-ubiquitin antibodies. Not-treated cells displayed faint and diffuse ubiquitin signals throughout the cells, whereas MG132-treated cells contained numerous conspicuous ubiquitin foci. Strikingly, ubiquitin foci were also present in cells treated with RA-312. By contrast, cells treated with pulchelloid A, RA-313, RA-314, or RA-315 were devoid of ubiquitin foci and instead had diffuse signals similar to those of not-treated cells. We conclude that unlike the other anti-mitotic sesquiterpene lactones investigated in this study, RA-312 uniquely affects the ubiquitin-proteasome system. This activity distinguished it from RA-315, which was otherwise biologically similar by inducing mitotic arrest without mitotic spindle distortion.

In conclusion, five anti-mitotic compounds were isolated from *A. cordifolia* leaf material by bioassay-guided fractionation. These five compounds were sesquiterpene lactones, mirroring the anti-inflammatory sesquiterpene lactones of the taxonomically related medicinal plant *A. montana*. The biological effects of each isolated compound are summarized in Table 2.2. They induced mitotic arrest either with significant mitotic spindle distortion resembling that of pulchelloid A (RA-313, RA-314), or without spindle distortion (RA-312, RA-315). Additionally, the differences in RA-312 and RA-315's structures and effects on ubiquitin despite their similar effects on the mitotic spindle indicate that these sesquiterpene lactones are biologically and chemically distinct both from one another and from previously characterized anti-mitotic compounds.

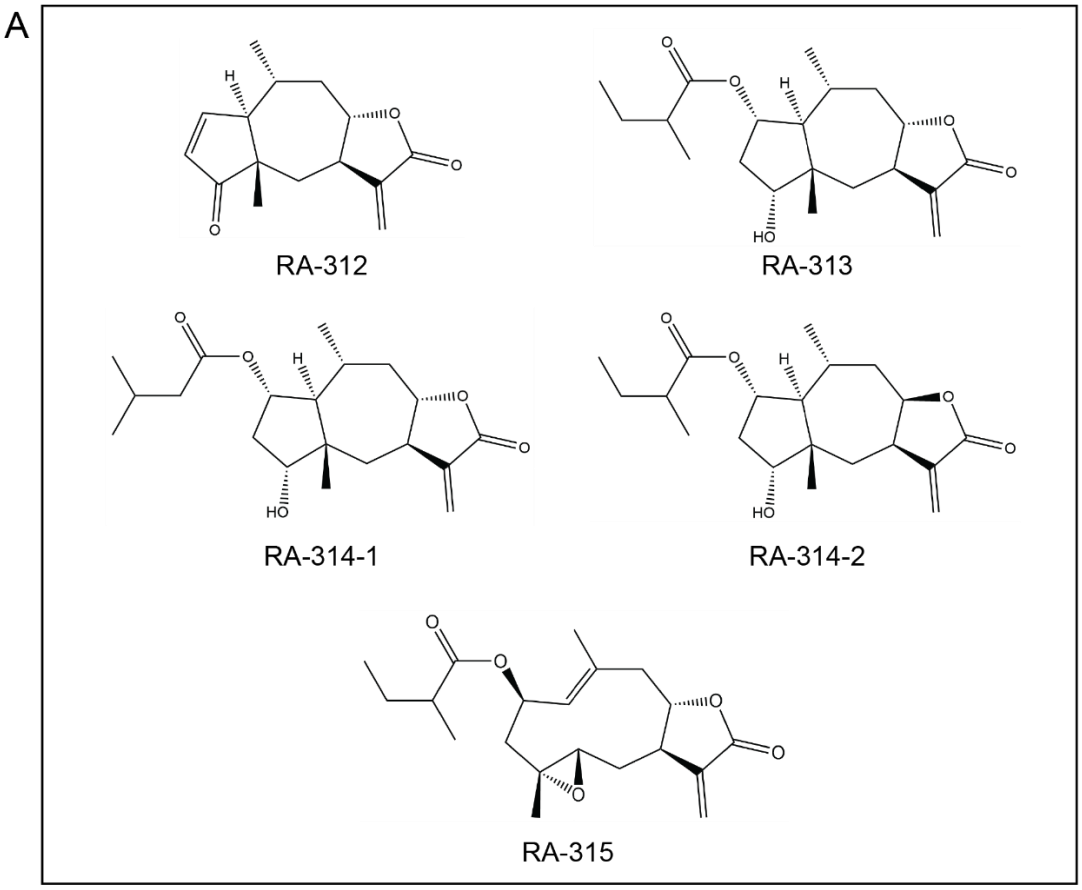

Figure 2.11. Chemical structures of five sesquiterpene lactones isolated from *A. cordifolia* leaf material.

Table 2.1. Comparison of the structural features and cytotoxicity of anti-mitotic sesquiterpene lactones isolated from *A. cordifolia*. IC_{50} values were determined by the MTT assay on HT-29 cells.

Feature	RA-312	RA-313	RA-314-1	RA-314-2	RA-315
Novel structure	Aromaticin	+	Pulchellin-2α-*O*-isovalerate	+	+
Molecular mass (Da)	246.31	350.46	350.46	350.46	348.44
Class	Pseudo-guaianolide	Pseudo-guaianolide	Pseudo-guaianolide	Pseudo-guaianolide	Germa-cranolide

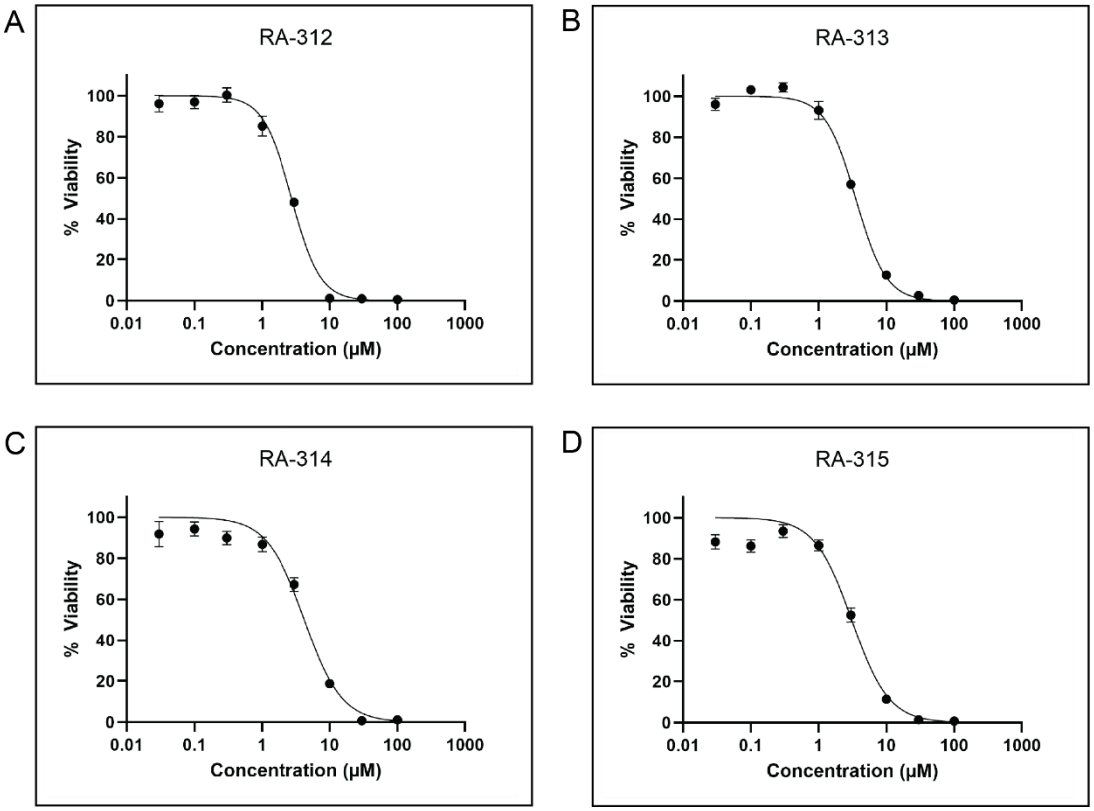

Figure 2.12. Isolated sesquiterpene lactones are cytotoxic to HT-29 cells. HT-29 cells were treated with varying concentrations of RA-312 (**A**), RA-313 (**B**), RA-314 (**C**), or RA-315 (**D**) for 72 h, then cell viability was determined by MTT assay. Standard errors of the means are shown.

Table 2.2. Comparison of the biological activities of sesquiterpene lactones isolated from *A. cordifolia* on HT-29 cells. IC_{50} values were determined by the MTT assay. All other features reflect a treatment concentration of 5 μM.

Feature	**RA-312**	**RA-313**	**RA-314-1**	**RA-314-2**	**RA-315**
IC_{50} (μM)	2.7 ± 0.3	3.5 ± 0.3	4.2 ± 0.7		3.1 ± 0.4
Percent cell rounding	24 ± 2%	48 ± 4%	35 ± 2%		29 ± 1%
Reduction by BME	+	+	+		+
Mitotic spindle distortion	-	+	+		-
Altered ubiquitin staining	+	-	-		-

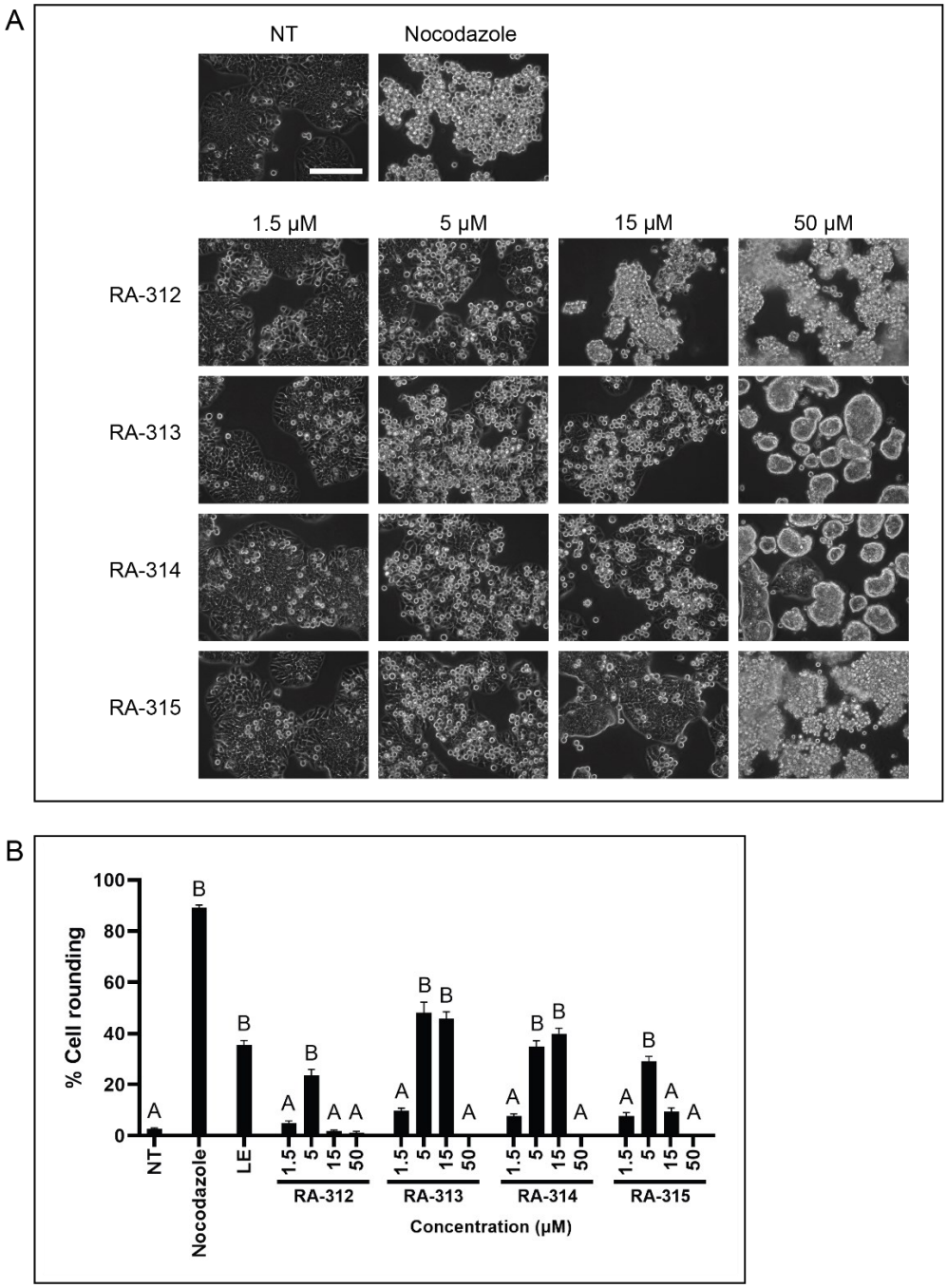

Figure 2.13. Isolated sesquiterpene lactones induce a rounded morphology in HT-29 cells. **A.** HT-29 cells were either not-treated (NT) or treated with nocodazole or various concentrations of RA-312, RA-313, RA-314, or RA-315 for 18 h and observed by light microscopy. Scale bar represents 50 µm. **B.** The mean percentages of rounded cells after each treatment described in **A** were determined. The standard errors of the means are shown and treatments that were significantly different from not-treated cells are shown by letters ($p < 0.05$).

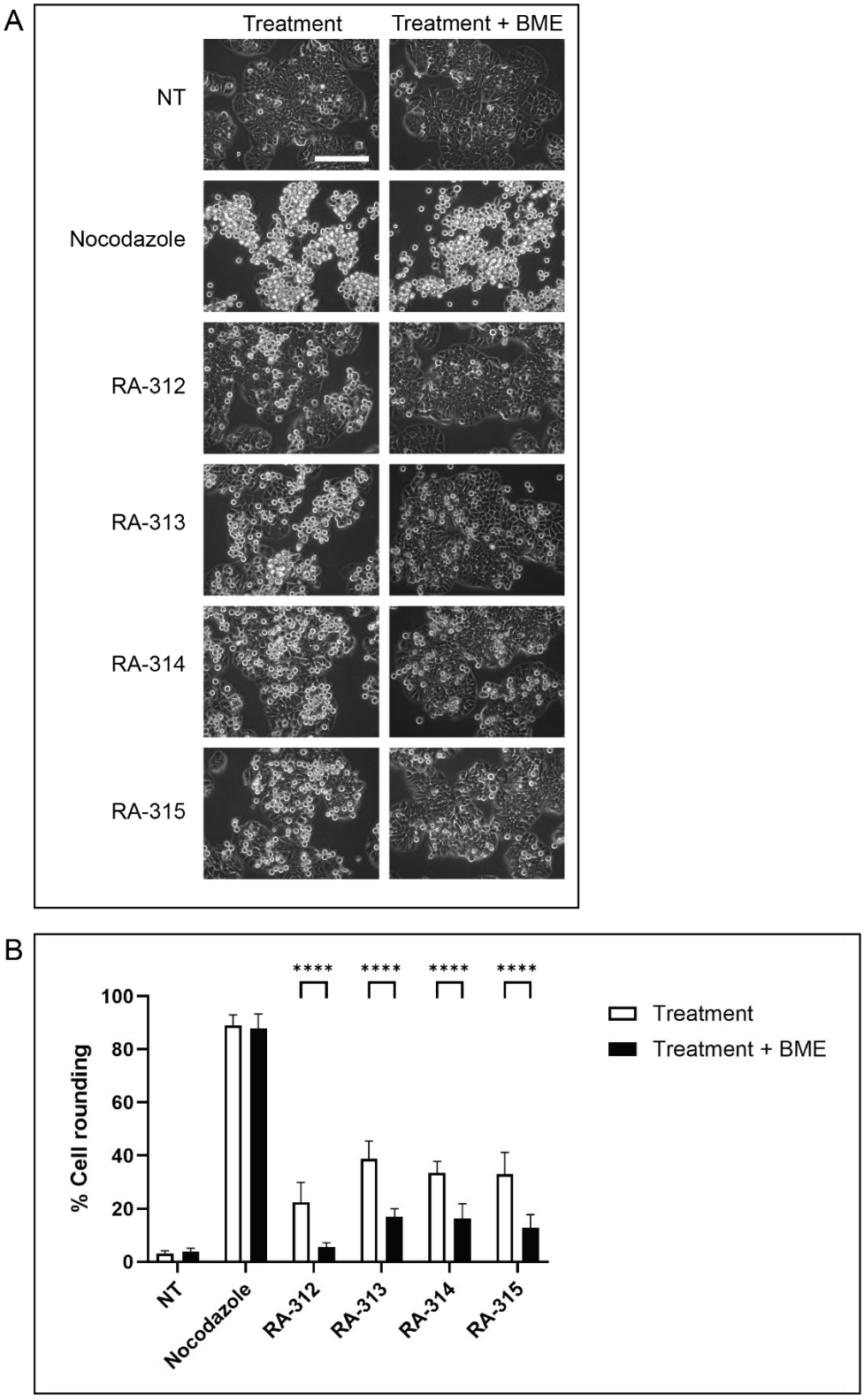
A
Treatment
Treatment + BME
NT
Nocodazole
RA-312
RA-313
RA-314
RA-315
B
% Cell rounding
100
80
60
40
20
0
****
****
****
****
Treatment
Treatment + BME
NT
Nocodazole
RA-312
RA-313
RA-314
RA-315

Figure 2.14. β-mercaptoethanol inhibits the anti-mitotic activity of isolated sesquiterpene lactones. **A.** Treatments of vehicle control (not-treated, NT), nocodazole, and 5 μM RA-312, RA-313, RA-314, and RA-315 were incubated at 37 °C for 2 h with or without 100 μM β-mercaptoethanol prior to addition to HT-29 cells. Cells were observed by light microscopy. Scale bar represents 50 μm. **B.** The mean percentages of rounded cells after each treatment described in **A** were determined. The standard errors of the means are shown and treatments that were significantly different from not-treated cells are shown by asterisks ($p < 0.05$).

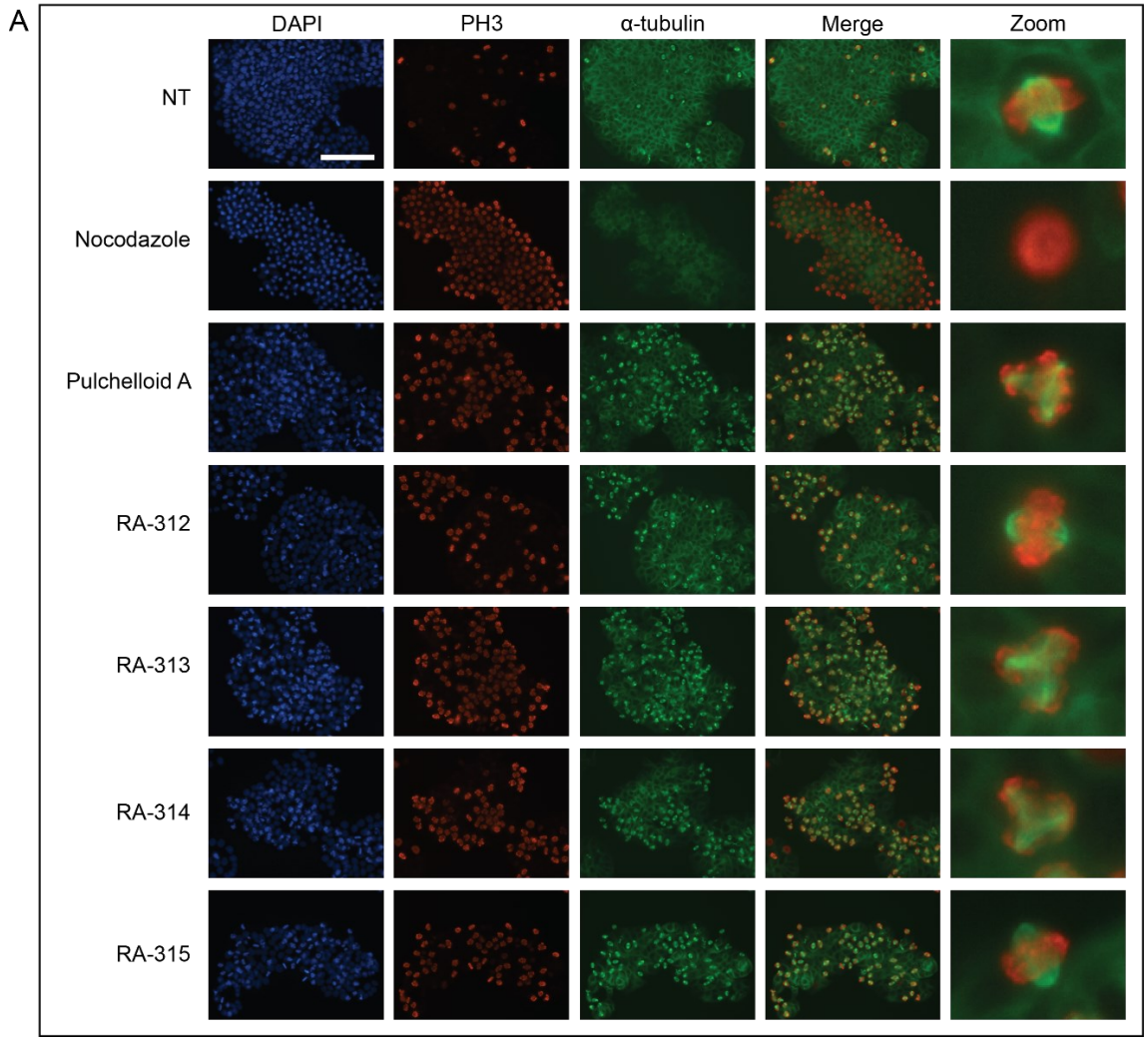
A
DAPI
PH3
α-tubulin
Merge
Zoom
NT
Nocodazole
Pulchelloid A
RA-312
RA-313
RA-314
RA-315

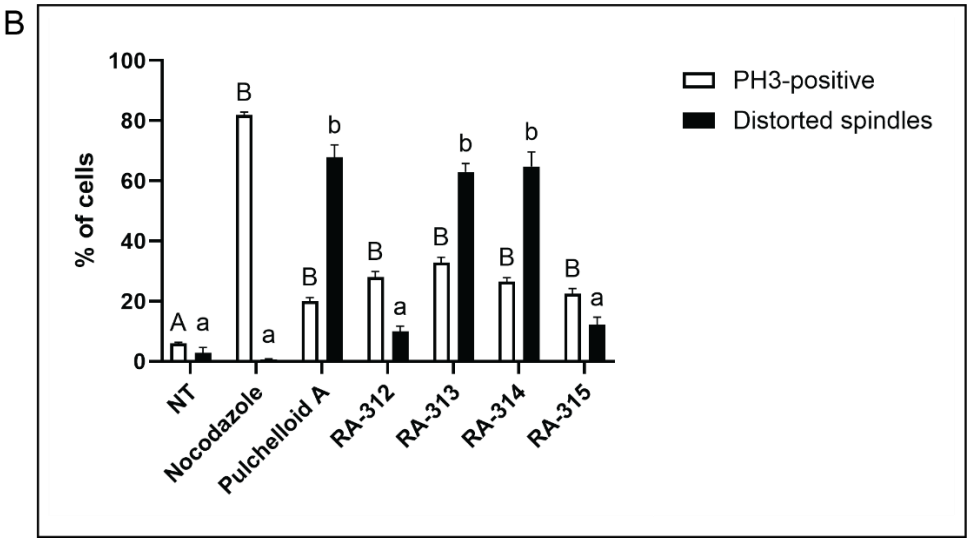
B
% of cells
100
80
60
40
20
0
PH3-positive
Distorted spindles
NT
Nocodazole
Pulchelloid A
RA-312
RA-313
RA-314
RA-315

Figure 2.15. Cells treated with isolated sesquiterpene lactones contain phosphorylated histone H3, but these compounds have differing effects on the mitotic spindle. **A.** HT-29 cells were either not-treated (NT) or treated with nocodazole, pulchelloid A, or 5 μM RA-312, RA-313, RA-314, or RA-315 for 18 h and stained with DAPI (blue) to detect DNA, anti-phospho-histone H3 antibodies (PH3, red) and anti-α-tubulin antibodies (green). The merge column shows both PH3 and α-tubulin staining. Cells were observed by immunofluorescence microscopy. Scale bar represents 50 μm. **B.** The mean percentages of cells with PH3 staining and of mitotic spindles with distorted appearances after each treatment described in **A** were determined. Mitotic spindles of PH3-positive cells were manually scored for distorted mitotic spindle morphology in reference to NT cells. The standard errors of the means are shown and treatments that were significantly different from not-treated cells are shown by letters ($p < 0.05$).

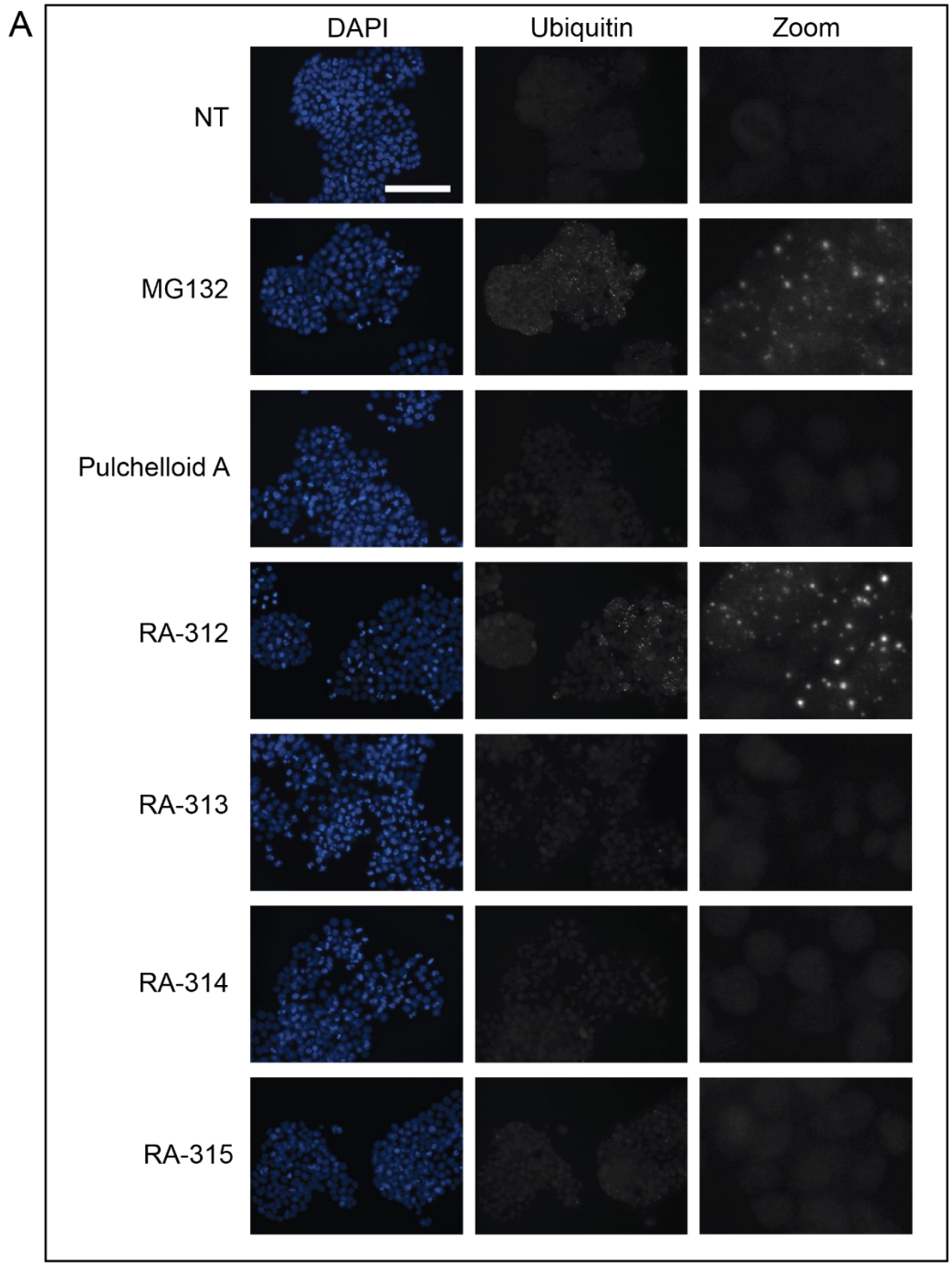

Figure 2.16. Cells treated with RA-312 show punctate ubiquitin staining. HT-29 cells were either not-treated (NT) or treated with MG132, pulchelloid A, or 5 μM RA-312, RA-313, RA-314, or RA-315 for 18 h and stained with DAPI (blue) to detect DNA and anti-ubiquitin antibodies (gray). The merge column shows both stains. Cells were observed by immunofluorescence microscopy. Scale bar represents 50 μm.

2.4. Discussion

Our preliminary studies of *Arnica cordifolia* extracts revealed they induced a mitotic arrest that was distinct from other extracts in our library and those reported in the literature. Based on this observation, we predicted that the chemicals that induced this arrest would be different from those isolated from other botanical species, including ones from the same taxonomic family. Paradoxically, we observed that some aspects of the cell rounding phenotype were reminiscent of those induced by natural products previously isolated by our laboratory. Therefore, it presented an interesting scientific question as to how both different and similar features would be reconciled at the chemical level. To solve this problem, we characterized the mitotic arrest phenotype induced by *A. cordifolia* extracts and isolated the chemicals that induced it. This phenotype-driven approach is in contrast to the taxonomy-driven approaches used in some natural product studies, including work by our own laboratory (Healy Knibb, 2024; Hoffman et al., 2018; Rønsted et al., 2012).

This is the first report of the anti-mitotic activities of five sesquiterpene lactones isolated from *A. cordifolia*, of which three of the compounds are novel. These compounds induced mitotic arrest with differing effects on the mitotic spindle. RA-313 and RA-314 induced mitotic spindle distortion in approximately two-thirds of arrested cells, an arrest reminiscent of other anti-mitotic sesquiterpene lactones isolated by our laboratory such as pulchelloid A (Bosco et al., 2021) and hymenoratin (Molina et al., 2021). By contrast, aromaticin (RA-312) and RA-315 induced mitotic arrest without distortion of the mitotic spindle. This unique mitotic arrest phenotype distinguished these compounds from other

anti-mitotic sesquiterpene lactones in this study and in the literature. Aromaticin further distinguished itself by affecting ubiquitin staining in HT-29 cells, an observation that has not been previously reported. These novel mitotic inhibitors reveal a diversity in chemical structures and mitotic arrest phenotypes that spans botanical diversity.

Arnica cordifolia, also known as heartleaf arnica, is one of 18 Arnica species native to Canada (Brouillet et al., 2024). Flower extracts of other *Arnica* species, particularly the European species *A. montana*, have been used in traditional medicine and clinical trials to treat inflammation and pain (Kriplani et al., 2017; Jeffrey and Belcher, 2002; Kneusel et al., 2002). The bioactivity of *A. montana* is due to the presence of pseudoguaianolide sesquiterpene lactones, predominantly helenalin and dihydrohelenalin esters (Lyss et al., 1998). In research settings, helenalin has been shown to inhibit the NF-κB pathway (Lyss et al., 1998) and induce apoptosis in cancer cells (Kriplani and Guarve, 2020). Despite this, little research has been done on the related North American species *A. cordifolia* and its constituents. Our laboratory previously found that *A. cordifolia* extracts induced a mitotic arrest distinct from that of other anti-mitotics in our laboratory (Molina, 2018), prompting further investigation into this species. This study reports the isolation of the compounds responsible for the anti-mitotic activity of *A. cordifolia* and the first characterization of the mitotic arrest phenotypes they induce.

2.4.1. Multiple anti-mitotic compounds isolated from Arnica cordifolia

The isolation of multiple anti-mitotic compounds with differing effects on mitotic spindle organization agreed with our earlier results involving *A. cordifolia* whole plant, leaf, and flower extract-treated cells. The lack of mitotic spindle distortion in leaf extract-treated cells corresponded to the activities of RA-312 and RA-315, with RA-315 being the active compound purified in greatest quantity from leaves. By contrast, the distortion of some but not all spindles in whole plant and flower extract-treated cells may be explained by a greater proportion of the spindle-distorting RA-313 and RA-314 being present in these organs. The composition of sesquiterpene lactones in *A. montana* has been found to differ between leaves and flowers (Parafiniuk et al., 2023), so a similar pattern existing in *A. cordifolia* aerial parts is plausible.

The β-mercaptoethanol reduction assay revealed a chemical similarity between the active compounds of *A. cordifolia* despite their distinct biological activities. This was first seen by the reduction of *A. cordifolia* whole plant, leaf, and flower extracts' cell rounding activities after BME treatment. These findings then matched the reduction of cell rounding activity by each compound after BME treatment. By contrasting against the two distinct mitotic arrest phenotypes (distorted and undistorted spindles), these results suggest that though the electrophilic lactone functionality is likely responsible for each compound's activity, the unique structure and features of each compound provides a different range of targets. Differences in targets between the isolated compounds could then explain the two distinct mitotic arrest phenotypes.

When compared to previously described anti-mitotic sesquiterpene lactones, the structures and mitotic arrest phenotypes of RA-313 and RA-314 were similar to those of pulchelloid A and hymenoratin (Bosco et al., 2021; Molina et al., 2021). These are pseudoguaianolide sesquiterpene lactones with α-methylene-γ-lactone functionalities that induce approximately 40% mitotic arrest with 60 to 80% mitotic spindle distortion, and these anti-mitotic activities are inhibited by incubation with BME (Bosco et al., 2021; Molina et al., 2021; Healy Knibb, 2024). The similarities in the structure and function of these compounds suggest that they induce mitotic arrest by a common mechanism. However, the precise targets and mechanisms of action of pulchelloid A, hymenoratin, and the compounds isolated in this study are not yet known.

Interestingly, RA-313 and RA-314 treatments also induced more cell rounding than RA-312 or RA-315 treatments, further separating these compounds into distinct groups. Our laboratory has recently found that other anti-mitotic compounds that induced mitotic arrest in only a fraction of asynchronous cells, including pulchelloid A, induced mitotic arrest in nearly all cells of synchronized cultures (Healy Knibb, 2024). These effects were found to be indicative of mitotic delay. It may be possible that RA-313 and RA-314 treatments induce mitotic delays of longer duration than RA-312 and RA-315 treatments, resulting in a greater observed proportion of rounded cells in unsynchronized cultures. Further investigation of the compounds isolated in this study in synchronized cultures may aid in understanding the mechanisms by which they induce mitotic arrest and better position them with other anti-mitotic compounds.

Aromaticin (RA-312) is a pseudoguaianolide sesquiterpene lactone first isolated from *Helenium aromaticum* (Romo et al., 1964) in 1964. Aromaticin has also been found in other members of the Asteraceae family, including *Helenium amarum* (Lucas et al., 1964) and *Inula* species *I. hookeri* (Cheng et al., 2011), *I. hupehensis* (Qin et al., 2011), and *I. japonica* (Yu et al., 2019). This is the first report of aromaticin in *Arnica cordifolia*. Interestingly, a previous study reported that *A. cordifolia* contains graveolide, a compound that differs from aromaticin solely by possessing a cyclopentanone ring instead of a cyclopentenone ring, and its stereoisomer 2,3-dihydroaromaticin, but did not report aromaticin as a constituent (Figure 2.17) (Merfort and Wendisch, 1993). Since the cyclopentenone ring of aromaticin contains an α,β-unsaturated carbonyl, it may serve as an active site in addition to the α-methylene-γ-lactone (Schmidt, 2006). This cyclopentenone ring likely has different reactivity than the α-methylene-γ-lactone, which may confer additional targets (Heilmann et al., 2001). In addition to its unique cyclopentenone ring, aromaticin was also the only active compound in this study to lack a C2 ester functionality, which may further affect its ability to interact with different targets. Aromaticin has been previously demonstrated to have anti-inflammatory (Qin et al., 2011) and anti-mycobacterial (Cantrell et al., 2001) activities, and is cytotoxic to multiple cancer cell lines (Fernandes et al., 2008; Cheng et al., 2011; Yu et al., 2019). Despite previous reports of aromaticin cytotoxicity to cancer cells, this is the first study to demonstrate that aromaticin induces mitotic arrest.

Pulchellin-2α-*O*-isovalerate (RA-314-1) is a pseudoguaianolide sesquiterpene lactone first isolated from *Loxothysanus sinatus* (Bohlmann et al., 1985) in 1985.

Interestingly, pulchellin-2α-*O*-isovalerate has also been isolated from *Centipeda minima* (Wu et al., 2012), which contains the anti-mitotic sesquiterpene lactones 6-*O*-angeloylplenolin (Liu et al., 2011) and arnicolide D (Liu et al., 2019; Zhu et al., 2019). These two compounds have been reported to induce G2/M phase arrest in multiple cell lines at low micromolar doses, similar to pulchellin-2α-*O*-isovalerate (RA-314-1) in this study. However, previous research on pulchellin-2α-*O*-isovalerate has only reported anti-angiogenic activity (Huang et al., 2016). This study is the first to report the anti-mitotic activity of a fraction containing pulchellin-2α-*O*-isovalerate, as well as the compound's presence in *A. cordifolia*.

This is also the first report of the chemical structures and biological activities of RA-313, RA-314-2, and RA-315. RA-313 and pulchellin-2α-*O*-isovalerate (RA-314-1) differ solely by the arrangement of the ester functionality. RA-314-2 was a stereoisomer of RA-313, differing at the α-methylene-γ-lactone. Since RA-314-1 and RA-314-2 were not purified from each other, it remains unclear whether one or both compounds were responsible for the observed biological activities of RA-314. Further investigation of these compounds may clarify if the stereochemistry of the α-methylene-γ-lactone ring is related to the compounds' anti-mitotic activities.

RA-315 was the most structurally distinct compound isolated, being a germacranolide sesquiterpene lactone and possessing an C4-C5 epoxide group in contrast to the four pseudoguaianolides. Epoxide groups are a feature of some biologically active sesquiterpene lactones, such as the C4-C5 epoxide in parthenolide (Figure 2.18). Like the cyclopentenone ring of aromaticin, this epoxide group can serve as a second active site for

interacting with nucleophiles (Schmidt, 2006). However, as a hard electrophile, the epoxide group could be expected to preferentially interact with hard nucleophiles such as hydroxide and amino groups. This is in contrast to the α,β-unsaturated carbonyls of the cyclopentenone ring and α-methylene-γ-lactone, which are soft electrophiles that preferentially interact with thiol groups and other soft nucleophiles (Schmidt, 2006). Additionally, this interaction would be expected to occur on C2 in RA-315, as opposed to C4 in aromaticin. These chemical similarities and differences between aromaticin and RA-315 paralleled their biological effects. Both compounds induced mitotic arrest without distortion of the mitotic spindle, which may be due to the presence and position of a second active site when compared with the other monofunctional isolated compounds. However, RA-315 did not affect ubiquitin as aromaticin had done. This may indicate that the compounds induce a similar mitotic arrest phenotype by interacting with different targets on account of their differences in structure and the characteristics of their second potential active sites, or that the effects of aromaticin on ubiquitin are unrelated to its anti-mitotic activity.

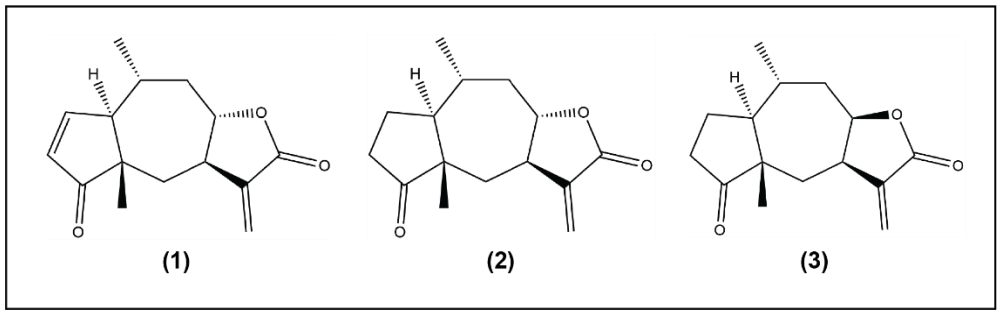

Figure 2.17. Chemical structures of aromaticin (RA-312) **(1)** and two sesquiterpene lactones previously isolated from *A. cordifolia*, graveolide **(2)** and 2,3-dihydroaromaticin **(3)**.

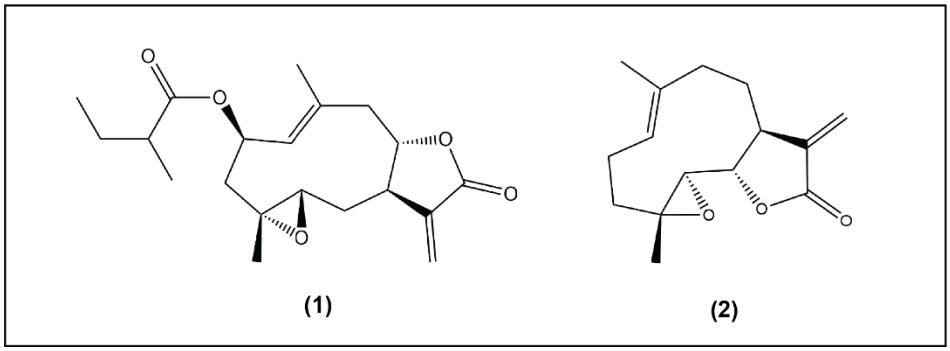

Figure 2.18. Chemical structures of the epoxide-containing sesquiterpene lactones RA-315 **(1)** and parthenolide **(2)**.

2.4.2. Aromaticin treatment affects ubiquitin staining in cancer cells

The observation of some cells with chromosomes aligned at the metaphase plate after RA-312 and RA-315 treatment suggested that these cells may be arrested in metaphase, prompting comparisons to MG132. As a proteasome inhibitor, MG132 prevents the degradation of ubiquitinated proteins which arrests mitotic cells at metaphase (Wójcik et al., 1996). The accumulation of ubiquitinated proteins appears as punctate staining when visualized with anti-ubiquitin antibodies. Furthermore, prolonged metaphase

arrest with MG132 can lead to chromosome misalignment by cohesion fatigue (Daum et al., 2011), which resembled the unaligned chromosomes sometimes seen after RA-312 and RA-315 treatment. Strikingly, the accumulation of punctate ubiquitin signals in cells after RA-312 treatment resembled the effects of MG132 treatment, suggesting that RA-312 may inhibit the ubiquitin-proteasome pathway. This is the first study to report the effects of aromaticin (RA-312) on ubiquitin. However, this change in ubiquitin staining was not seen after RA-315 treatment, despite both compounds possessing two potential active sites and inducing mitotic arrest without mitotic spindle distortion. The structural differences and different reactivity of the second active site in aromaticin may explain this unique effect on ubiquitin.

The ubiquitin-proteasome pathway is essential to regulate the cell cycle, including mitosis. Ubiquitination is required for the temporal regulation of cyclins, cyclin-dependent kinases (Cdks), Cdk inhibitors (CKIs), and mitotic proteins such as securin and Aurora kinases (Zou and Lin, 2021). Cell cycle regulation is primarily governed by two E3 ubiquitin ligase complexes: the Skp, Cullin, F-box containing (SCF) complex for the G1 to S-phase transition, and the anaphase promoting complex/cyclosome (APC/C) for the spindle assembly checkpoint (SAC) and mitotic exit. Numerous deubiquitinases are also involved in the regulation of the cell cycle, including mitosis (Fournane et al., 2012; Darling et al., 2017). Several sesquiterpene lactones have been reported to affect the ubiquitin-proteasome pathway by binding to ubiquitin ligases, ubiquitin conjugating enzymes, and deubiquitinases, with many of these enzymes containing catalytic cysteine residues. The α-methylene-γ-butyrolactone moieties of parthenolide and costunolide been

demonstrated to bind to numerous cysteine residues in the deubiquitinase USP7, leading to G2/M phase arrest (Li et al., 2020). The E2 ubiquitin conjugating enzyme UbcH5, which interacts with the APC/C, is selectively inhibited by the α-methylene-γ-butyrolactone moieties of multiple sesquiterpene lactones including arteannuin B (Chen et al., 2024), 1β-hydroxyalantolactone (Liu et al., 2014; Xu and Meng, 2020), and 2α,6α-diacetoxy-4β-hydroxy-11(13)-pseudoguaien-12,8α-olide (DHPO) (Qi et al., 2022). The anti-mitotic sesquiterpene lactone 6-*O*-angeloylplenolin has been proposed to inhibit NIPA, Skp2, and β-TRCP E3 ubiquitin ligases by binding to Skp1, an essential adaptor protein of the SCF complex, though this interaction does not rely on an α-methylene-γ-butyrolactone moiety (Liu et al., 2015). Further investigation into which ubiquitinated proteins accumulate after aromaticin treatment and the mechanism by which this occurs is required to understand this biological activity and its relationship to the anti-mitotic effects of aromaticin.

2.4.3. Conclusions

The isolation and characterization of these active compounds contributes to a growing body of research on anti-mitotic sesquiterpene lactones. Of the over 6000 sesquiterpene lactones described (Adekenov, 2017), only a small number have been reported to have anti-mitotic activity (Bosco and Golsteyn, 2017). Mitotic spindle distortion has been reported to occur after treatment with several anti-mitotic sesquiterpene lactones, including pulchelloid A (Bosco et al., 2021), hymenoratin (Molina et al., 2021), 6-*O*-angeloylplenolin (Liu et al., 2011), and psilostachyins A and C (Sturgeon et al., 2005).

RA-313, RA-314-1, and RA-314-2 from this study induce a similar mitotic arrest phenotype as these compounds, which may indicate that they share similar cellular targets. By contrast, RA-312 and RA-315 may represent a different group of anti-mitotic sesquiterpene lactones in that they induce mitotic arrest without distortion of the mitotic spindle. Further research into the cellular targets of anti-mitotic sesquiterpene lactones is required to better understand these distinct mitotic arrest phenotypes.

This is the first report of five anti-mitotic sesquiterpene lactones with distinct biological activities isolated from *Arnica cordifolia*, a Canadian plant. The pursuit of a novel mitotic arrest phenotype led to the discovery of three new and two known structures, all without previously-reported anti-mitotic activity. The discovery of novel mitotic inhibitors, including the ones described in this study, is crucial for advancing our understanding of mitosis. Further investigation is required to determine the cellular targets and mechanisms of action by which these compounds induce mitotic arrest. Once determined, these compounds may have valuable applications as research tools or as lead compounds in precision medicine.

CHAPTER 3

Partial separation of *Arnica cordifolia* leaf extract by column chromatography

3.1. Introduction

The observation of multiple distinct mitotic arrest phenotypes in cells treated with *Arnica cordifolia* whole plant, leaf, and flower extracts suggested that more than one anti-mitotic compound may be present. To test this hypothesis, we used two fractionation schemes concurrently to identify the active compounds in *A. cordifolia* leaf material. Firstly, we chromatographed *A. cordifolia* leaf material independently in our laboratory. Secondly, we conducted bioassay-guided fractionation in collaboration with Dr. Raymond Andersen at the University of British Columbia. This chapter details the first fractionation scheme. Subjecting *A. cordifolia* leaf extract to Sephadex LH-20 column chromatography yielded thirty spectrophotometrically-distinct fractions, of which a small number showed anti-mitotic activity on human cancer cells. The observation of anti-mitotic activity in multiple spectrophotometrically-distinct fractions suggested the presence of more than one active compound. Of the four most potent anti-mitotic fractions, the first and last were selected for further investigation. Cells treated with either fraction were positive for the mitotic indicator protein phospho-histone H3 and arrested in mitosis without distortion of the mitotic spindle. At the time, we concluded that all active compounds from *A. cordifolia* leaves were likely to induce mitotic arrest without spindle distortion. However, the biology-guided fractionation of *A. cordifolia* leaves described in Chapter 2 later revealed that leaves contain compounds that induce arrest both with and without spindle distortion.

3.2. Materials and Methods

3.2.1. Collection of plant material

Aerial parts of flowering *A. cordifolia* plants were collected sustainably in the Porcupine Hills, Alberta, Canada at 49° 58' 15" N and 114° 5' 13" W, elevation approximately 1700 m during 2022 and 2023. Permits from the local and provincial governments were obtained prior to collection. *A. cordifolia* taxonomy was confirmed to species level, and voucher specimens were submitted to the University of Lethbridge Herbarium as Golsteyn #420. After collection, plants were dried at 40 °C then stored at room temperature and protected from light.

3.2.2. Preparation of plant extracts

Extracts were prepared from either total or separated plant parts (leaves, flowers, stems) ground into a fine powder. The powdered material was suspended to 10% (w/v) in either 75% (v/v) ethanol (Greenfield Global; P016EAAN) in water or 100% dichloromethane (Fisher Chemical; D37-4). Suspensions were placed on a shaker overnight at room temperature and protected from light. Suspensions were then filtered by Grade 1 Whatman paper and the solvent was evaporated at room temperature. Extracts were dissolved in methanol (Fisher Chemical; A452-4) to 50 mg/mL and stored at -20 °C for use in subsequent experiments.

3.2.3. Fractionation of plant extracts

Sephadex LH-20 column chromatography of *A. cordifolia* leaf extract PP-1912B was carried out using a Bio-Rad Econo-Column (20 cm length × 1.5 cm internal diameter). Sephadex LH-20 beads were equilibrated in methanol, then used to pack the column to a bed volume of 15 mL. The column was washed and equilibrated with 2 column volumes of methanol prior to sample loading. 10 mg of *A. cordifolia* leaf extract (PP-1912B) were dissolved in methanol to an initial concentration of 50 mg/mL. This solution (200 µL) was loaded onto the LH-20 column for fractionation. Fractions were eluted with methanol and collected every 1 mL, for a total of 30 fractions. Fractions were evaporated under vacuum, then the dried material was resuspended in 200 µL of methanol. By assuming that the 10 mg of PP-1912B were distributed equally between the 30 fractions, the concentration of each fraction after resuspension was estimated to be 1.7 mg/mL.

3.2.4. UV-visible spectroscopy

From each fraction, 75 µL were loaded into separate wells of a 96-well plate. A control well was loaded with 75 µL of methanol. The absorbance of each sample was measured from 300 to 700 nm using a Biotek Epoch microplate spectrophotometer using Gen5 software (Agilent Technologies), with a step of 2 nm between reads. Absorbance data were blanked to the methanol control.

3.2.5. Cell culture

The human cell line HT-29 (ATCC HTB-38) was obtained from the American Type Culture Collection (ATCC). Cells were cultured in RPMI 1640 media (Gibco; 21870-092) supplemented with 10% (v/v) FBS (Gibco; 12484-028) and 1% (v/v) GlutaMAX (Gibco; 35050-061), and incubated at 37 °C in 5% CO_2. Cells were split and the media were changed every three to four days. HT-29 cells were plated at a density of 2.0 x 10^5 cells/well in 6-well culture plates or 2.0 x 10^4 cells/well in 12-well culture plates and incubated at 37 °C for 48-72 h prior to treatment.

The compounds nocodazole (Sigma-Aldrich; M1404) and paclitaxel (Sigma-Aldrich; T7402), were dissolved in DMSO (Sigma-Aldrich; D2438), stored at -20 °C, and used at concentrations of 500 nM and 100 nM respectively. In not-treated cells, 0.4% (v/v) methanol or DMSO was added as a solvent vehicle control.

3.2.6. Light microscopy

Images were captured with an Infinity 1 camera with Infinity Capture imaging software (Lumenera Corporation) on an Olympus CKX41 inverted microscope. Images were processed using Adobe Photoshop (CC 25.6.0). Cells were manually scored for rounded or flat morphology.

3.2.7. Immunofluorescence microscopy

HT-29 cells were plated at a density of 2.0 x 10^5 cells/well in 6-well culture plates and incubated at 37 °C for 48-72 h prior to treatment. After 18 h treatment, the media were aspirated and cells were fixed with 3% (v/v) paraformaldehyde (Ted Pella; 18505) in PBS for 20 minutes at room temperature. Fixation was then quenched with 50 mM NH_4Cl (Sigma-Aldrich; A4514) in PBS for 10 minutes. Cells were permeabilized with 0.2% (v/v) Triton X-100 (Millipore; EM-9410) in PBS for 5 minutes, followed by blocking with 3% (w/v) BSA (MP Biomedicals; 810551) in PBS-T (0.1% (v/v) Tween-20 (VWR Life Science; EM-9480) in PBS) for 30 minutes. Cells were then incubated overnight at 4 °C with anti-phospho-Ser10 histone H3 (Millipore; 06-570; 1:1000) and anti-α-tubulin (Santa Cruz Biotechnology; sc-53030; 1:300) primary antibodies. The following day, cells were washed with PBS-T, then incubated at room temperature for 45 minutes with secondary antibodies Alexa Fluor™ 594 AffiniPure™ goat anti-rabbit IgG (Jackson ImmunoResearch; 111-585-003; 1:400) and Alexa Fluor™ 488 goat anti-rat IgG (Invitrogen; A11006; 1:200). DNA was stained with 300 nM DAPI (4′,6-diamidino-2-phenylindole) (Invitrogen; D1306) in PBS-T for 15 minutes at room temperature. Cells were then imaged with a Cytation™ 5 Cell Imaging Multi-Mode Reader using Gen5 software (Agilent Technologies). Three independent experiments were conducted.

3.3. Results and Discussion

Due to the distinguishable anti-mitotic activities of *Arnica cordifolia* leaf and flower extracts, we suspected that this species contained more than one active compound, each with distinct effects on the mitotic spindle. To test this hypothesis, we utilized two fractionation schemes concurrently to identify the active compounds in *A. cordifolia* leaf material: bioassay-guided fractionation in collaboration with Dr. Raymond Andersen at the University of British Columbia, and column chromatography that we conducted independently in our laboratory.

LE was fractionated by Sephadex LH-20 column chromatography, yielding thirty fractions. To compare the composition of each fraction to that of the complete leaf extract, the fractions were analyzed by UV-visible spectrophotometry from 300 nm to 700 nm (data not shown). All fractions were spectrophotometrically distinct, with fractions 11 through 16 bearing the closest resemblance to the spectrum of LE with strong absorbance from 380-480 nm and slight absorbance at 665 nm. These distinct spectra indicated that the compounds present in LE had been successfully fractionated by column chromatography.

Each fraction was then tested for cell rounding activity on HT-29 cells by the phenotypic assay. Cells were either not-treated, treated with the tubulin depolymerizing agent nocodazole as a positive control, or treated with 50 μg/mL of each fraction. After 18 h, the cells were examined for rounded morphology (Figure 3.1). Few of the not-treated cells exhibited a rounded morphology, whereas nearly all nocodazole-treated cells were rounded, as expected. Cells treated with fractions 1 through 9 and 17 through 30 did not

appear different from the not-treated control. Fractions 10, 15, and 16 induced the accumulation of rounded cells, with fraction 16 being the least potent. Fractions 11 through 14 were toxic at the tested concentrations. These data showed that the cell rounding activity of *A. cordifolia* leaf extract was likely induced by more than one active compound because this activity was observed in several different fractions.

As LE was previously shown to be toxic at high concentrations, we suspected that the toxic fractions 11 through 14 contained the highest concentrations of the anti-mitotic compounds. To test this, we repeated the cell rounding assay using a range of concentrations of these fractions (Figure 3.2). HT-29 cells were either not-treated, treated with nocodazole, or treated with varied concentrations of fractions 11 through 14 for 18 h. Not-treated cells exhibited little rounding, whereas nearly all nocodazole-treated cells were rounded. Fractions 11 and 14 both induced cell rounding at 5 and 15 μg/mL. Fractions 12 and 13 were more potent, with both being toxic at 15 μg/mL and inducing cell rounding at 5 μg/mL; rounded cells were also seen after treatment with 1.5 μg/mL of Fraction 12. All four fractions were toxic at 50 μg/mL, and all but fraction 12 were indistinguishable from the not-treated control at 1.5 μg/mL. These results indicated that the majority of the active compounds from *A. cordifolia* leaf extract had been concentrated in fractions 11 through 14. The similar outcomes of these fractions at each tested concentration mirrored our later results with RA-312 through RA-315, which all had similar IC_{50} values and performed similarly in the cell rounding assay.

To confirm that the rounded cells induced by treatment with these fractions were arrested in mitosis, we used immunofluorescence microscopy to examine PH3 and α-

tubulin staining (Figure 3.3). Cells were either not-treated or treated with nocodazole, paclitaxel, LE, or fractions 11 or 14 for 18 h prior to fixation. Fractions 11 and 14 were selected for investigation as they represented the first and last fractions to induce cell rounding at 5 μg/mL and were thus considered the most likely fractions to contain different active compounds. Few not-treated cells were PH3-positive, whereas nearly all nocodazole- and paclitaxel-treated cells were PH3-positive, as expected. Many cells treated with LE were PH3-positive, matching earlier results. The proportion of fraction 11- and fraction 14-treated cells that were PH3-positive appeared similar to that of LE-treated cells, with no obvious difference between the fractions. These data confirmed that treatment with either fraction caused a similar accumulation of mitotic cells as did unfractionated LE; however, due to their different elution characteristics, we anticipated that these would be different chemicals.

To determine the relationship of these fractions to the distinct mitotic arrest phenotype of *A. cordifolia* leaf extract-treated cells, the α-tubulin organizations of fraction-treated cells were observed (Figure 3.3). Not-treated mitotic cells contained the normal range of mitotic figures including metaphasic bipolar shaped spindles. Nocodazole-treated cells lacked a mitotic spindle, whereas paclitaxel-treated cells contained intensely stained and distorted spindle structures. As before, LE-treated mitotic cells contained undistorted bipolar spindles. Strikingly, mitotic cells treated with either fraction 11 or fraction 14 also contained undistorted bipolar spindles. At the time, we concluded that all active compounds present in *A. cordifolia* leaf extract induced mitotic arrest without distortion of

the mitotic spindle, which suggested that the mitotic spindle distortion seen in whole plant- and flower extract-treated cells was due to active compounds not found in leaves.

In contrast to this conclusion, the bioassay-guided fractionation described in Chapter 2 later revealed that *A. cordifolia* leaves contain both compounds that induce mitotic arrest without spindle distortion (RA-312, RA-315) and compounds that arrest with spindle distortion (RA-313, RA-314). It is possible that fractions 12 and 13 contained the compounds later purified as RA-313 and RA-314, and would have induced mitotic arrest with spindle distortion if tested. The column chromatography fractions provided the critical evidence to continue bioassay-guided fractionation with a collaborating laboratory and to anticipate the presence of more than one active compound.

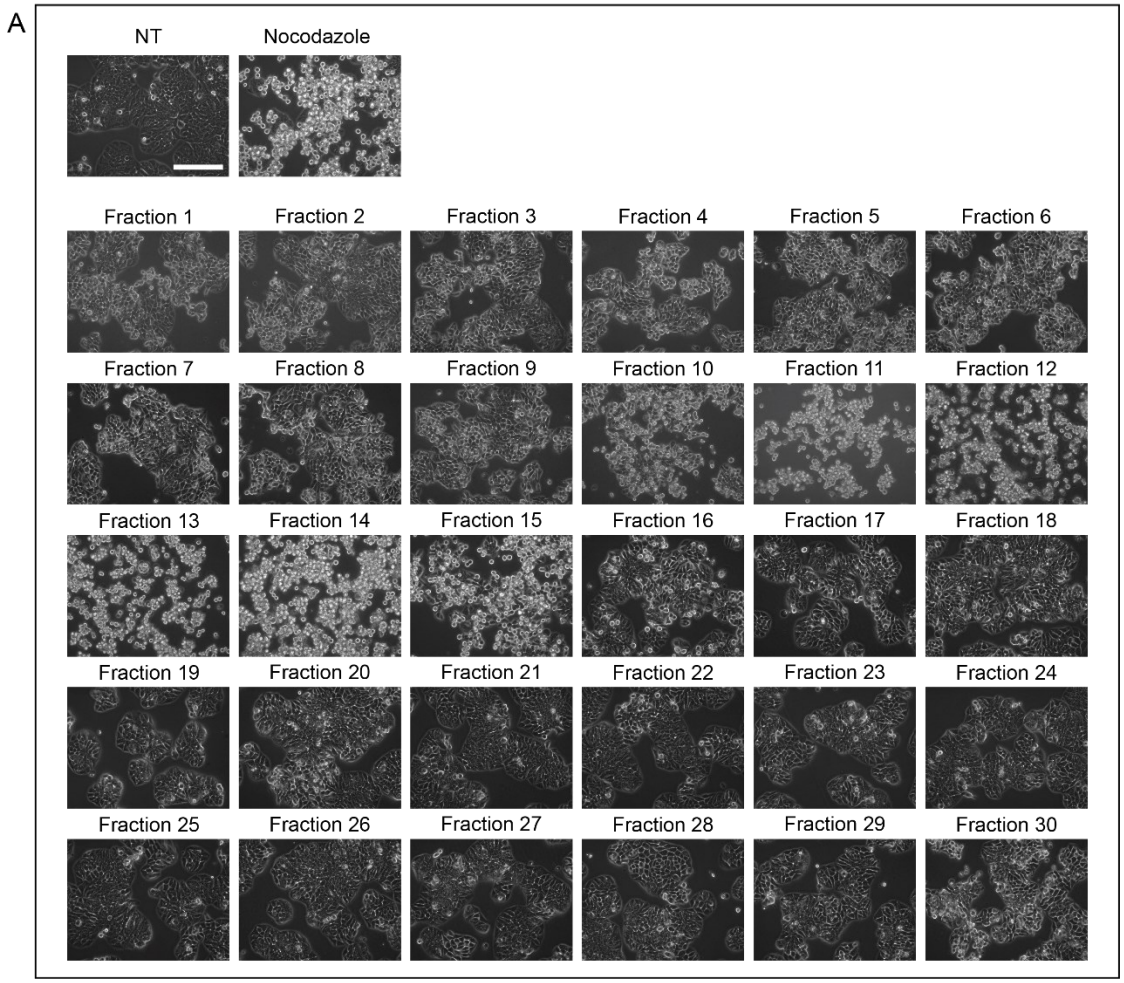

Figure 3.1. Anti-mitotic activity of *A. cordifolia* leaf extract is retained after column chromatography. HT-29 cells were either not-treated (NT) or treated with nocodazole or 50 µg/mL leaf extract fractions from LH-20 column chromatography for 18 h and observed by light microscopy. Scale bar represents 50 µm.

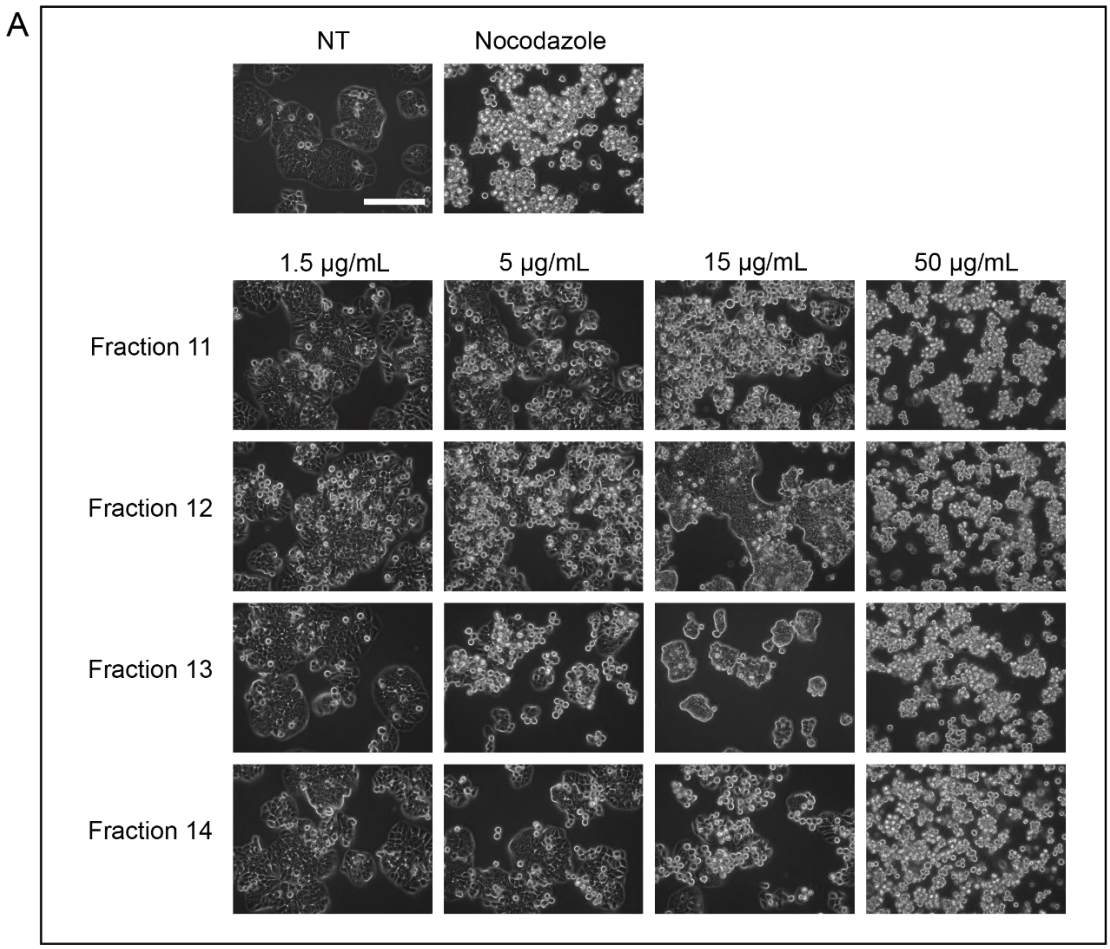

Figure 3.2. Cytotoxic *A. cordifolia* leaf extract fractions induce cell rounding at lower concentrations. HT-29 cells were either not-treated (NT) or treated with nocodazole or various concentrations of leaf extract fractions 11, 12, 13, or 14 for 18 h and observed by light microscopy. Scale bar represents 50 µm.

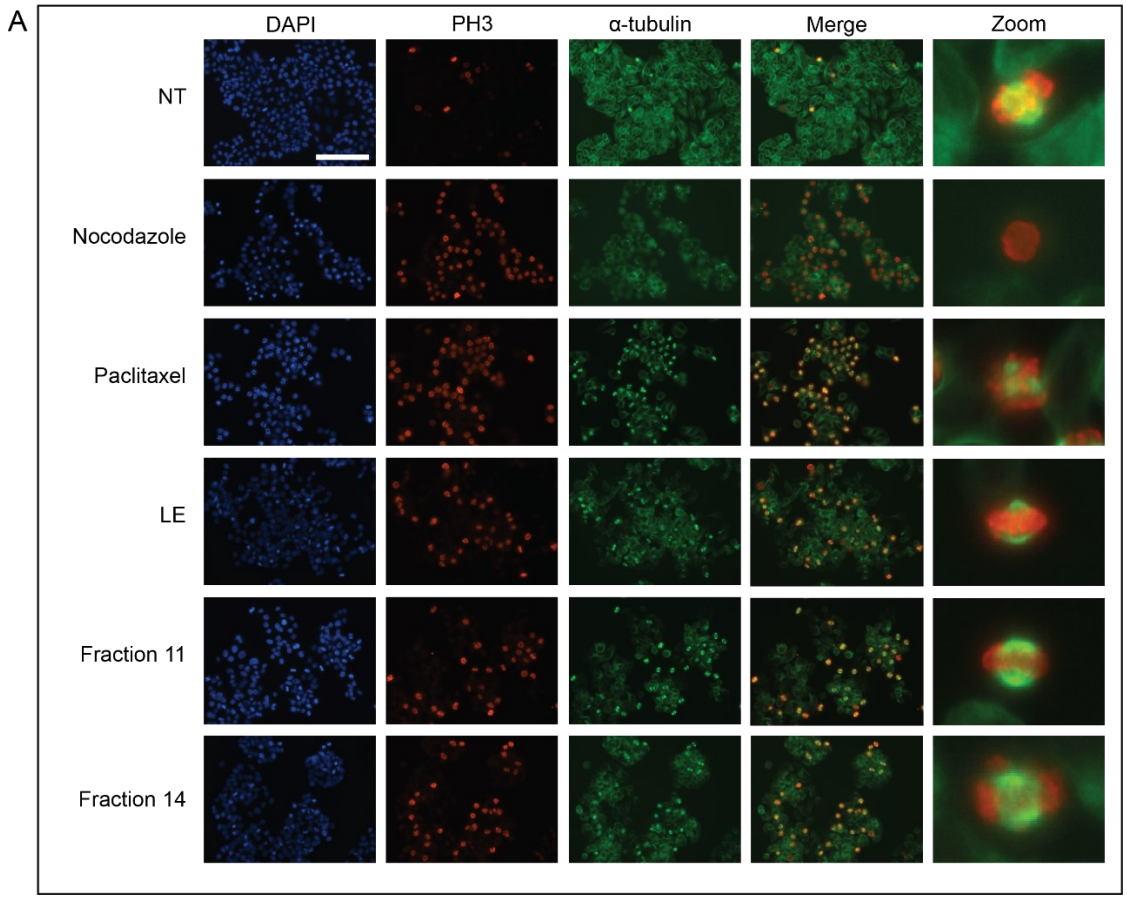

Figure 3.3. Cells treated with *A. cordifolia* leaf extract fractions contain phosphorylated histone H3 and undistorted mitotic spindles. HT-29 cells were either not-treated (NT) or treated with nocodazole, paclitaxel, 150 µg/mL leaf extract (LE), or 15 µg/mL LE fractions 11 or 14 for 18 h and stained with DAPI (blue) to detect DNA, anti-phospho-histone H3 antibodies (PH3, red) and anti-α-tubulin antibodies (green). The merge column shows both PH3 and α-tubulin staining. Cells were observed by immunofluorescence microscopy. Scale bar represents 50 µm.

CHAPTER 4

Investigation of potential cellular targets of *Arnica cordifolia* leaf extract

4.1. Introduction

Knowing that *A. cordifolia* leaf extract (LE) treatment induced mitotic arrest without distortion of the mitotic spindle, we explored potential cellular targets that can cause cells to delay in mitosis with bipolar spindles. We examined LE-treated cells for damaged DNA and observed the localization of CENP-E and BubR1, two proteins involved in the regulation of the spindle assembly checkpoint. As the active compounds of *A. cordifolia* were considered likely to be sesquiterpene lactones at this point, LE was compared with the anti-mitotic sesquiterpene lactone pulchelloid A in all tests. LE and pulchelloid A damaged DNA in a subset of mitotic cells that had unaligned chromosomes, but did not damage DNA in interphase cells or mitotic cells with aligned chromosomes. Neither LE nor pulchelloid A affected the localization of CENP-E or BubR1 to kinetochores. These results showed similarities between the active compounds of *A. cordifolia* leaves and pulchelloid A despite having different effects on the mitotic spindle.

4.2. Materials and Methods

4.2.1. Collection of plant material

Aerial parts of flowering *A. cordifolia* plants were collected sustainably in the Porcupine Hills, Alberta, Canada at 49° 58' 15" N and 114° 5' 13" W, elevation approximately 1700 m during 2022 and 2023. Permits from the local and provincial

governments were obtained prior to collection. *A. cordifolia* taxonomy was confirmed to species level, and voucher specimens were submitted to the University of Lethbridge Herbarium as Golsteyn #420. After collection, plants were dried at 40 °C then stored at room temperature and protected from light.

4.2.2. Preparation of plant extracts

Extracts were prepared from either total or separated plant parts (leaves, flowers, stems) ground into a fine powder. The powdered material was suspended to 10% (w/v) in either 75% (v/v) ethanol (Greenfield Global; P016EAAN) in water or 100% dichloromethane (Fisher Chemical; D37-4). Suspensions were placed on a shaker overnight at room temperature and protected from light. Suspensions were then filtered by Grade 1 Whatman paper and the solvent was evaporated at room temperature. Extracts were dissolved in methanol (Fisher Chemical; A452-4) to 50 mg/mL and stored at -20 °C for use in subsequent experiments.

4.2.3. Cell culture

The human cell line HT-29 (ATCC HTB-38) was obtained from the American Type Culture Collection (ATCC). Cells were cultured in RPMI 1640 media (Gibco; 21870-092) supplemented with 10% (v/v) FBS (Gibco; 12484-028) and 1% (v/v) GlutaMAX (Gibco; 35050-061), and incubated at 37 °C in 5% CO_2. Cells were split and the media were

changed every three to four days. HT-29 cells were plated at a density of 2.0 x 10^5 cells/well in 6-well culture plates or 2.0 x 10^4 cells/well in 12-well culture plates and incubated at 37 °C for 48-72 h prior to treatment.

The compounds nocodazole (Sigma-Aldrich; M1404), camptothecin (Supplier), and pulchelloid A were dissolved in DMSO (Sigma-Aldrich; D2438), stored at -20 °C, and used at concentrations of 500 nM, 100 nM, and 5 μM respectively. In not-treated cells, 0.4% (v/v) methanol or DMSO was added as a solvent vehicle control.

4.2.4. Immunofluorescence microscopy

HT-29 cells were plated at a density of 2.0 x 10^5 cells/well in 6-well culture plates on coverslips and incubated at 37 °C for 48-72 h prior to treatment. After 18 h treatment, the media were aspirated and cells were fixed with 3% (v/v) paraformaldehyde (Ted Pella; 18505) in PBS for 20 minutes at room temperature. Fixation was then quenched with 50 mM NH_4Cl (Sigma-Aldrich; A4514) in PBS for 10 minutes. Cells were permeabilized with 0.2% (v/v) Triton X-100 (Millipore; EM-9410) in PBS for 5 minutes, followed by blocking with 3% (w/v) BSA (MP Biomedicals; 810551) in PBS-T (0.1% (v/v) Tween-20 (VWR Life Science; EM-9480) in PBS) for 30 minutes. Cells were then incubated overnight at 4 °C with anti-phospho-histone γH2AX (Millipore; 05-363; 1:400), anti-CENP-E (Sigma-Aldrich; c7488; 1:400), or anti-BubR1 (Invitrogen; 720297; 1:250) primary antibodies. The following day, cells were washed with PBS-T, then incubated at room temperature for 45 minutes with secondary antibody Alexa Fluor™ 488 rabbit anti-mouse IgG (Invitrogen;

A11059; 1:400) or Alexa Fluor™ 488 goat anti-rabbit IgG (Invitrogen; A11008; 1:400). DNA was stained with 300 nM DAPI (4′,6-diamidino-2-phenylindole) (Invitrogen; D1306) in PBS-T for 15 minutes at room temperature. Once stained, the coverslips were mounted onto microscope slides with ProLong Gold Antifade Mountant (Thermo Fisher; P36934). Slides were imaged with a Cytation™ 5 Cell Imaging Multi-Mode Reader using Gen5 software (Agilent Technologies) and a ZEISS Axio Observer Z1 Motorized Inverted Fluorescence Microscope using AxioVision software (ZEISS). Three independent experiments were conducted.

4.3. Results

4.3.1. Arnica cordifolia leaf extract treatment damages DNA in some but not all mitotic cells

The observation that *A. cordifolia* leaf extract (LE) induced mitotic arrest without affecting mitotic spindle morphology led us to consider if these cells contained damaged DNA. We used immunofluorescence microscopy with anti-γ-histone H2AX (γH2AX) antibodies to examine cells for DNA double strand breaks (Figure 4.1). HT-29 cells were either not-treated or treated with the genotoxic agent camptothecin (CPT) as a positive control, pulchelloid A, or LE. After 18 h, cells were fixed and stained with anti-γ-histone H2AX antibodies to observe damaged DNA (Cahuzac et al., 2010). Not-treated cells had few γH2AX foci, whereas CPT treatment induced diffuse γH2AX signals in nearly all cells. Pulchelloid A-treated cells showed an accumulation of punctate γH2AX foci in mitotic

cells but not in interphase cells, agreeing with literature results (Bosco et al., 2021). LE-treated cells showed punctate γH2AX foci in mitotic cells but not interphase cells, which was similar to the results of pulchelloid A treatment. Interestingly, after treatment with either pulchelloid A or LE, several mitotic cells that had all chromosomes seemingly aligned at the metaphase plate lacked γH2AX foci. We conclude that *A. cordifolia* leaf extract treatment damages DNA in some but not all mitotic cells.

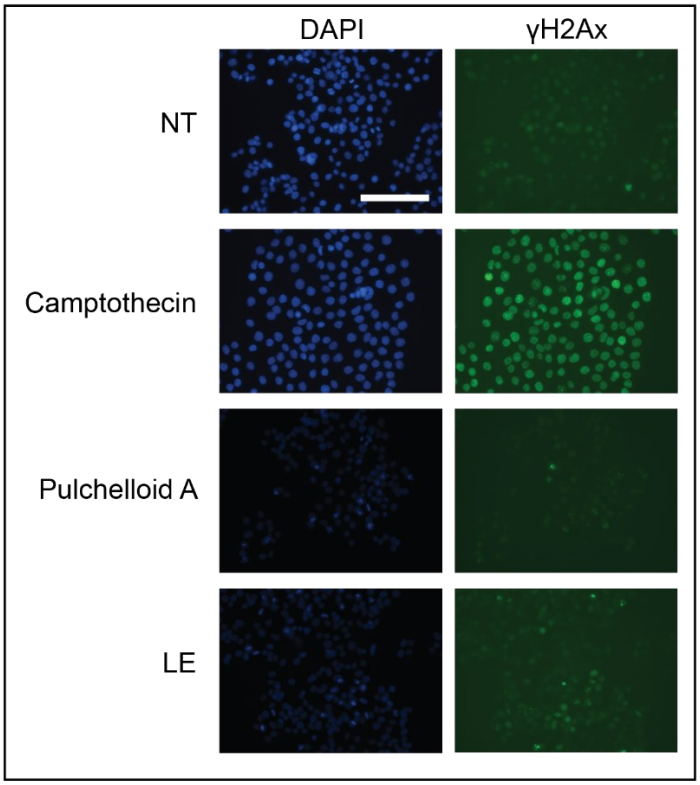

Figure 4.1. Treatment with *A. cordifolia* leaf extract damages DNA in some mitotic cells, but not in interphase cells. HT-29 cells were either not-treated (NT) or treated with camptothecin, pulchelloid A, or 150 μg/mL leaf extract (LE) for 18 h and stained with DAPI (blue) to detect DNA and anti-γ-histone H2AX antibodies (γH2AX, green) to detect DNA damage. Cells were observed by immunofluorescence microscopy. Scale bar represents 50 μm.

4.3.2. Arnica cordifolia leaf extract treatment does not impact CENP-E or BubR1 localization

Knowing that treatment of cells with *A. cordifolia* extracts could affect spindle organization, we investigated two proteins involved in the regulation of the metaphase to anaphase transition by the spindle assembly checkpoint. We first examined CENP-E, a kinesin-like motor protein that is required for chromosome alignment in prometaphase (Figure 4.2). We used immunofluorescence microscopy with anti-CENP-E antibodies to examine CENP-E localization in cells that were not-treated, or treated with nocodazole, pulchelloid A, or LE for 18 h. In not-treated cells, CENP-E was seen at the kinetochores of mitotic cells as expected. Punctate CENP-E signals were observed at the kinetochores of nocodazole-treated cells, which were distributed throughout the cells. CENP-E staining in pulchelloid A-treated cells with disorganized chromosomes was distinct from that of not-treated and nocodazole-treated cells, with signals distributed irregularly throughout these cells. In the portion of pulchelloid A-treated cells with aligned chromosomes, CENP-E staining was localized to the kinetochores and was reminiscent of not-treated cells. CENP-E staining in LE-treated cells was also reminiscent of not-treated cells, with CENP-E localized to the kinetochores of aligned chromosomes. CENP-E signals were also seen at the kinetochores of any unaligned chromosomes after LE treatment.

We next examined the localization of BubR1, a protein kinase whose interaction with CENP-E is essential for CENP-E's recruitment to kinetochores (Figure 4.3). We examined cells that were not-treated, or treated with nocodazole, pulchelloid A, or LE for

18 h for BubR1 using immunofluorescence microscopy with anti-BubR1 antibodies. BubR1 was localized to the kinetochores of not-treated cells in prophase through metaphase, with only weak signals in cells in anaphase. In nocodazole-treated cells, punctate BubR1 signals were seen at the kinetochores, distributed throughout the cells in a manner similar to that of the CENP-E staining. The BubR1 staining of pulchelloid A-treated cells was also reminiscent of the earlier CENP-E staining, seemingly distributed to the kinetochores. In LE-treated cells, punctate BubR1 signals were seen at the kinetochores of both aligned and unaligned chromosomes. From these data we conclude that *A. cordifolia* leaf extract does not affect the localization of BubR1, nor does it inhibit BubR1's ability to recruit CENP-E to kinetochores.

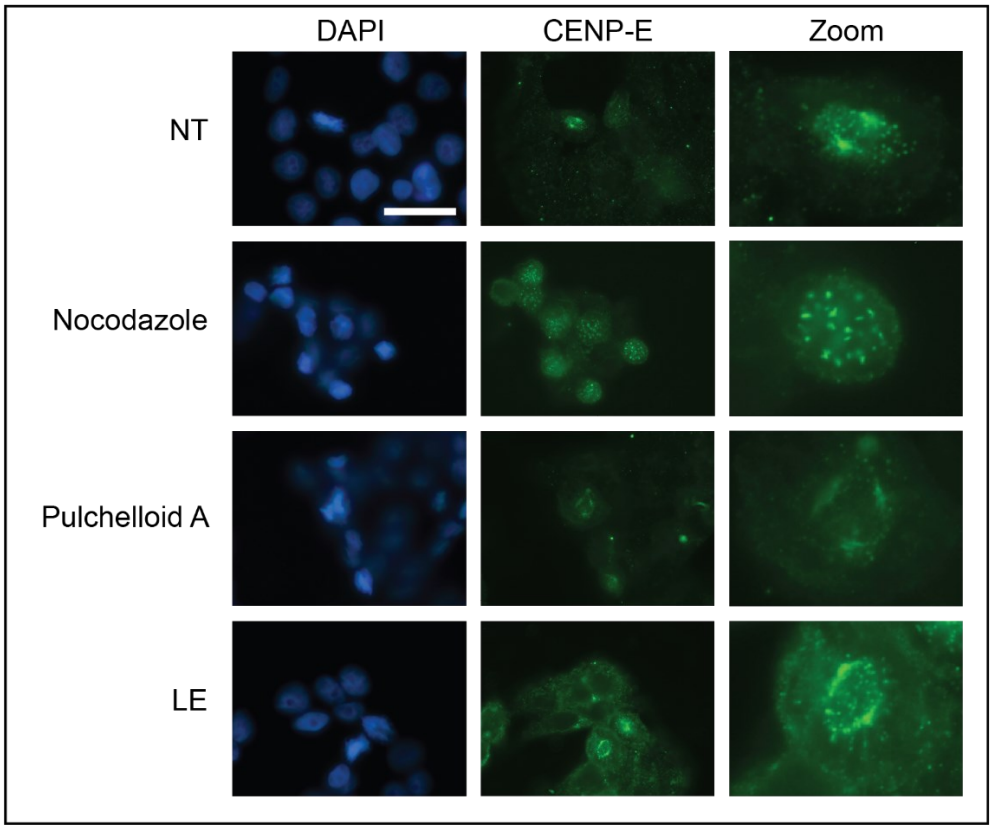

Figure 4.2. Treatment with *A. cordifolia* leaf extract does not affect CENP-E localization in mitotic cells. HT-29 cells were either not-treated (NT) or treated with nocodazole, pulchelloid A, or 150 μg/mL leaf extract (LE) for 18 h and stained with DAPI (blue) to detect DNA and anti-CENP-E antibodies (green). Cells were observed by immunofluorescence microscopy. Scale bar represents 15 μm.

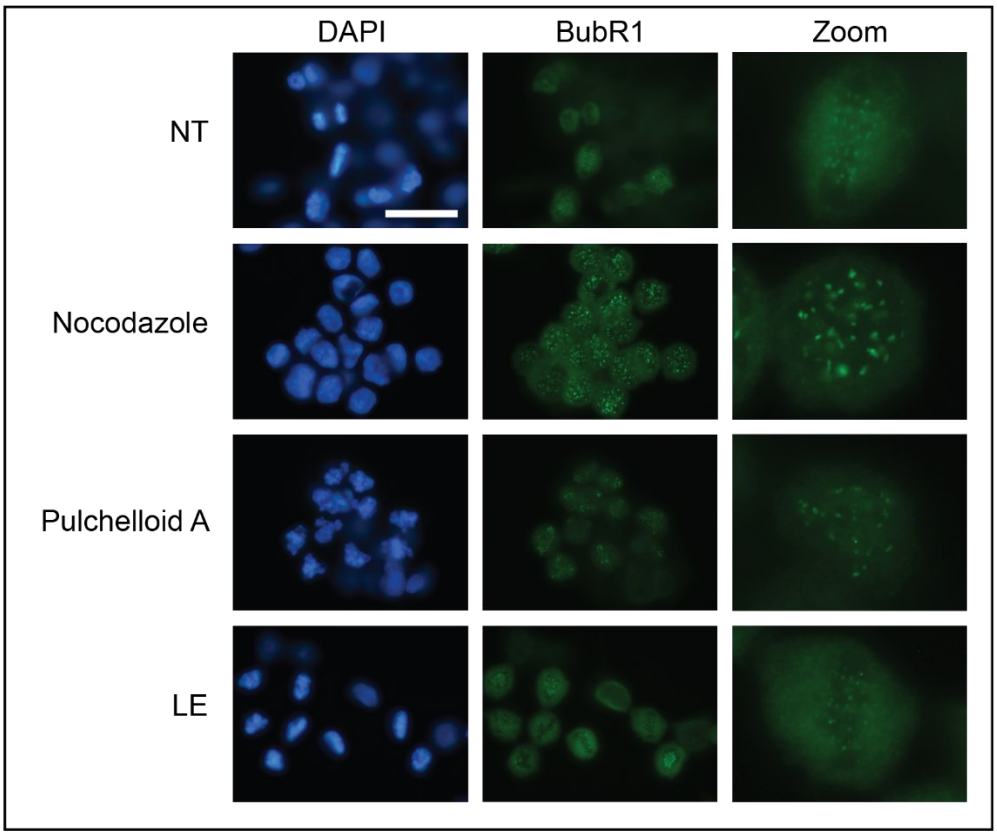

Figure 4.3. Treatment with *A. cordifolia* leaf extract does not affect BubR1 localization in mitotic cells. HT-29 cells were either not-treated (NT) or treated with nocodazole, pulchelloid A, or 150 μg/mL leaf extract (LE) for 18 h and stained with DAPI (blue) to detect DNA and anti-BubR1 antibodies (green). Cells were observed by immunofluorescence microscopy. Scale bar represents 15 μm.

4.4. Discussion

The mitotic arrest induced by *A. cordifolia* leaf extract (LE) was unlike those we had observed with other extracts in our library. Furthermore, the features of this arrest being approximately 40% of cells arrested in a metaphase-like arrangement made it unlikely that the active compound(s) targeted tubulin. We instead considered mechanisms by which cells can delay in mitosis with bipolar spindles. In each case, we compared LE to pulchelloid A, an anti-mitotic sesquiterpene lactone suspected–and later confirmed (Chapter 2)–to be chemically similar to the active compounds of LE, but which induces a different mitotic arrest phenotype with spindle distortion. Though the cellular targets of pulchelloid A are not yet known, this comparison permitted greater understanding of the distinct mitotic arrest phenotypes.

We first examined LE-treated cells for damaged DNA because activation of the DNA-damage checkpoint can cause cells to arrest in mitosis (Thompson et al., 2019). The phosphorylation of histone H2AX on serine 139 (γH2AX) is an indicator of damaged DNA in treated cells (Rogakou et al., 1998; Cahuzac et al., 2010). We observed similar effects after treatment with either LE or pulchelloid A where γH2AX signals appeared only in mitotic cells and not in interphase cells. It is possible that this DNA damage occurred after prolonged mitotic arrest. Prolonged mitotic arrest is known to damage DNA (Dalton et al., 2007; Ganem and Pellman, 2012). Furthermore, other studies have reported that the percentage of γH2AX-positive cells after pulchelloid A treatment increases over time (Bosco et al., 2021; Healy Knibb, 2024). A similar trend may exist in cells treated with *A. cordifolia* extracts, as the mitotic arrest phenotypes induced by isolated compounds RA-313 and RA-314 resembled those of pulchelloid A treatment. Further research into the

timings of mitotic arrest and DNA damage induced by the active compounds of *A. cordifolia* may clarify the relationship between the mitotic arrest phenotypes and damaged DNA.

We then examined CENP-E and BubR1, two proteins required for spindle organization. CENP-E is a kinesin-like motor protein that binds to kinetochores and is required to align chromosomes in prometaphase (Craske and Welburn, 2020). The inhibition or depletion of CENP-E results in defective chromosome alignment, with some chromosomes failing to align at the metaphase plate and instead remaining near the spindle poles (Schaar et al, 1997; McEwen et al., 2001). These defects do not affect spindle morphology (Tanudji et al., 2004). Punctate CENP-E signals were observed at the kinetochores of both aligned and unaligned chromosomes after LE treatment. This result indicated that the localization of CENP-E to kinetochores was not affected by LE treatment, though it remains unclear if CENP-E is functioning while present in the correct location. The observation of kinetochore-localized CENP-E signals in pulchelloid A-treated cells suggested similar conclusions, and agreed with previous work done by our laboratory (Healy Knibb, 2024).

We next investigated BubR1 localization within the cells. BubR1 is a protein kinase involved in the spindle assembly checkpoint and the initial recruitment of CENP-E to kinetochores (Chan et al., 1998). The inhibition or depletion of BubR1 results in chromosome alignment defects without affecting spindle morphology, similar to the effects of CENP-E inhibition or depletion (Lampson and Kapoor, 2005). This is seen after treatment with the BubR1 inhibitors bubristatin and pharicin A, both of which are ent-kaurenes which inhibit chromosome congression and delay mitotic progression (Huang et

al., 2019; Xu et al., 2010). These ent-kaurenes contain an α,β-unsaturated carbonyl moiety, similar to the α-methylene-γ-butyrolactones of pulchelloid A and RA-312 through RA-315. Although LE treatment did not inhibit CENP-E recruitment to kinetochores, CENP-E recruitment also occurs by a second, slower pathway independent of BubR1 (Legal et al., 2020). This pathway is instead suspected to involve kinetochore corona proteins and dyneins (Cmentowski et al., 2023; Weber et al., 2024). As such, we explored the possibility that BubR1 may be inhibited by LE. Since punctate BubR1 signals were seen at the kinetochores of both aligned and unaligned chromosomes in LE-treated cells, the localization of BubR1 had not been affected by LE. The observation of kinetochore-localized BubR1 signals in pulchelloid A-treated cells agreed with our laboratory's previous findings and indicated successful localization (Healy Knibb, 2024).

We conclude that despite the distinct mitotic arrest phenotypes induced by *A. cordifolia* leaf extract and pulchelloid A treatments, the treatments have several commonalities. Firstly, damaged DNA was observed in mitotic cells after either treatment, but was not present in interphase cells. Secondly, the localization of CENP-E and BubR1 to kinetochores was not inhibited by either treatment. Further study is necessary to determine if CENP-E and BubR1 are functionally inhibited by the active compounds of *A. cordifolia*. It is possible that the targets of these compounds are instead other proteins involved in mitotic progression, supported by the effect of aromaticin (RA-312) on ubiquitin described previously (Chapter 2). Identification of the targets of these anti-mitotic natural products will allow us to understand better the mechanisms by which they induce mitotic arrest, and whether these targets have therapeutic value.

CHAPTER 5

Future Directions

We have described the discovery of novel anti-mitotic natural products and distinguished between their biological activities, suggesting that these compounds act upon different cellular targets. Future research should focus on elucidating the precise cellular targets and mechanisms of action of these compounds. One method to identify the protein targets would be to use chemical-genetic interaction (CGI) profiling. By identifying mutants that are sensitized or resistant to the compound's phenotypic effect, CGI screening could identify proteins or pathways of interest (Cacace et al., 2017). Another possible method would be to use click chemistry. Click chemistry involves linking an easily identifiable probe to the compound of interest via simple and high-yield reactions that require minimal purification (Hein et al., 2008). The tagged compound is allowed to covalently bind to its biological target in a live-cell system, then the target protein is pulled down and identified by mass spectrometry. We are currently utilizing both of these approaches to identify the targets of pulchelloid A, conducting click chemistry in collaboration with Dr. Raymond Andersen at the University of British Columbia and CGI profiling in haploid human cells in collaboration with Dr. Charles Boone at the University of Toronto. Similar strategies could be employed to identify the targets of the compounds isolated in this study. Identification of the precise targets of each compound will contribute to our understanding of mitosis and its inhibitors, and these compounds and their targets may have potential for therapeutic exploration.

Regarding aromaticin, future studies should explore the ubiquitin foci formed after cell treatment in greater detail. Determination of which ubiquitinated proteins accumulate after aromaticin treatment would provide insight as to which part of the ubiquitin-proteasome pathway may be affected. The precise target could then be identified using click chemistry. These studies would determine if the activity of aromaticin on ubiquitin is related to its anti-mitotic activity. Comparison of the structure of aromaticin to that of the other isolated compounds which did not induce ubiquitin foci would then provide valuable information about the structure-function relationships of sesquiterpene lactones.

Natural products continue to serve as a primary source of mitotic inhibitors. Through the pursuit of a unique mitotic arrest phenotype, this thesis has contributed three novel mitotic inhibitors and attributed anti-mitotic activity to two previously known natural products. These compounds broaden our understanding of the structure-function relationships of anti-mitotic natural products, and may aid in the development of new precision medicines. Furthermore, their discovery underscores the value in investigating native Canadian plants and organisms from other underexplored regions as sources of bioactive natural products. This research demonstrates the ongoing importance of natural products in early drug discovery.

REFERENCES

Adekenov, S. 2017. Sesquiterpene lactones with unusual structure. Their biogenesis and biological activity. Fitoterapia, 121, 16-30.

Akbari, V. et al. 2011. Comparison of epothilone and taxol binding in yeast tubulin using molecular modeling. Avicenna J Med Biotechnol, 3, 167-175.

Akula, R. and Ravishankar, G. 2011. Influence of abiotic stress signals on secondary metabolites in plants. Plant Signal Behav, 6, 1720-1731.

Alokam, S. et al. 2002. Red/far-red light mediated stem elongation and anthocyanin accumulation in Stellaria longipes: differential response of alpine and prairie ecotypes. Can J Bot, 80, 72-81.

Amorim, M. et al. 2013. Sesquiterpene lactones: adverse health effects and toxicity mechanisms. Crit Rev Toxicol, 43, 559-579.

Atanasov, A. et al. 2021. Natural products in drug discovery: advances and opportunities. Nat Rev Drug Discov, 20, 200-216.

Bailon-Moscoso, N. et al. 2017. Natural compounds as modulators of cell cycle arrest: application for anticancer chemotherapies. Curr Genomics, 18, 106-131.

Barbero, M. and Prandi, C. 2018. Pseudoguaianolides: recent advances in synthesis and applications. Nat Prod Commun, 13, 241-248.

Bavetsias, V. and Linardopoulos, S. 2015. Aurora kinase inhibitors: Current status and outlook. Front Oncol, 5, 278.

Bennett, M. et al. 1994. The phytoalexin response of lettuce to challenge by Botrytis cinerea, Bremia lactucae and Pseudomonas syringae pv. Phaseolicola. Physiol Mol Plant Pathol, 44, 321-333.

Bhat, K. and Setaluri, V. 2007. Microtubule-associated proteins as targets in cancer chemotherapy. Clin Cancer Res, 13, 2849-2854.

Bocca, C., Gabriel, L., Bozzo, F., and Miglietta, A. 2004. A sesquiterpene lactone, costunolide, interacts with microtubule protein and inhibits the growth of MCF-7 cells. Chem Biol Interact, 147, 79-86.

Bode, C. et al. 2002. Epothilone and paclitaxel: unexpected differences in promoting the assembly and stabilization of yeast microtubules. Biochemistry, 41, 3870-3874.

Bohlmann, F. et al. 1985. Pseudoguaianolides carabrone derivatives from Loxothysanus sinuatus. Phytochemistry, 24, 1021-1026.

Bosco, A. and Golsteyn, R. 2017. Emerging anti-mitotic activities and other bioactivities of sesquiterpene compounds upon human cells. Molecules, 22, 459.

Bosco, A. et al. 2021. Pulchelloid A, a sesquiterpene lactone from the Canadian prairie plant Gaillardia aristata inhibits mitosis in human cells. Mol Biol Rep, 48, 5459-5471.

Brandeis, M. and Hunt, T. 1996. The proteolysis of mitotic cyclins in mammalian cells persists from the end of mitosis until the onset of S phase. EMBO J, 15, 5280-5289.

Brouillet, L. et al. 2024. VASCAN, the Database of Vascular Plants of Canada. http://data.canadensys.net/vascan/ (consulted on 2024-05-08).

Cacace, E. et al. 2017. Chemical genetics in drug discovery. Curr Opin Syst Biol, 4, 35-42.

Cahuzac, N. et al. 2010. An unusual DNA binding compound, S23906, induces mitotic catastrophe in cultured human cells. Cancer Lett, 289, 178-187.

Callaway, R. and Ridenour, W. 2004. Novel weapons: invasive success and the evolution of increased competitive ability. Front Ecol Environ, 2, 436-443.

Canduri, F. et al. 2004. Molecular models of cyclin-dependent kinase 1 complexed with inhibitors. Biochem Biophys Res Commun, 324, 661-666.

Cantrell, C. et al. 2001. Antimycobacterial plant terpenoids. Planta Med, 67, 685-695.

Chadwick, M. et al. 2013. Sesquiterpenoids lactones: benefits to plants and people. Int J Mol Sci, 14, 12780-12805.

Chan, G. et al. 1998. Characterization of the kinetochore binding domain of CENP-E reveals interactions with the kinetochore proteins CENP-F and hBUBR1. J Cell Biol, 143, 49-63.

Chan, K. et al. 2012. Mitosis-targeted anti-cancer therapies: where they stand. Cell Death Dis, 3, e411.

Chen, H. et al. 2024. Arteannuin B, a sesquiterpene lactone from Artemisia annua, attenuates inflammatory response by inhibiting the ubiquitin-conjugating enzyme UBE2D3-mediated NF-κB activation. Phytomed, 123, 155263.

Cheng, X. et al. 2011. Sesquiterpene lactones from Inula hookeri. Planta Med, 78, 456-471.

Chiarle, M. et al. 2021. Relations between climate change and mass movement: perspectives from the Canadian Cordillera and the European Alps. Glob Planet Change, 202, 103499.

Clague, J. et al. 2011. Canadian Rockies and Coast Mountains of Canada. In: Singh, V., Singh, P., Haritashya, U., editors. Encyclopedia of Snow, Ice and Glaciers, 1st Edition. Springer-Verlag; Dordrecht, Netherlands. p. 106-111.

Cmentowski, V. et al. 2023. RZZ-Spindly and CENP-E form an integrated platform to recruit dynein to the kinetochore corona. EMBO J, 42, e114838.

Cotugno, R. et al. 2012. Effect of sesquiterpene lactone coronopilin on leukaemia cell population growth, cell type-specific induction of apoptosis and mitotic catastrophe. Cell Prolif, 45, 53-65.

Cragg, G. 1999. Paclitaxel (Taxol®): a success story with valuable lessons for natural product drug discovery and development. Med Res Rev, 18, 315-331.

Cragg, G. and Newman, D. 2005. Biodiversity: A continuing source of novel drug leads. Pure Appl Chem, 77, 7-24.

Craske, B. and Welburn, J. 2020. Leaving no-one behind: how CENP-E facilitates chromosome alignment. Essays Biochem, 64, 313-324.

Crncec, A. and Hochegger, H. 2019. Triggering mitosis. FEBS Letters, 593, 2868-2888.

Dalton W. et al. 2007. Human cancer cells commonly acquire DNA damage during mitotic arrest. Cancer Res, 67, 11487–11492.

Darling, S. et al. 2017. Regulation of the cell cycle and centrosome biology by deubiquitylases. Biochem Soc Trans, 45, 1125-1136.

Daum, J. et al. 2011. Cohesion Fatigue Induces Chromatid Separation in Cells Delayed at Metaphase. Curr Biol, 21, 1018-1024.

De Azevedo Jr., W. et al. 1996. Structural basis for specificity and potency of a flavonoid inhibitor of human CDK2, a cell cycle kinase. Proc Natl Acad Sci U S A, 93, 2735-2740.

Defossez, E. et al. 2021. Spatial and evolutionary predictability of phytochemical diversity. Proc Natl Acad Sci U S A, 118, e2013344118.

Dias, D. et al. 2012. A historical overview of natural products in drug discovery. Metabolites, 2, 303-336.

Dickson, M. and Schwartz, G. 2009. Development of cell-cycle inhibitors for cancer therapy. Curr Oncol, 16, 36-43.

Dimitrov, D. et al. 2023. Diversification of flowering plants in space and time. Nat Commun, 14, 7609.

Ekenäs, C. et al. 2009. Secondary chemistry and ribosomal DNA data congruencies in Arnica (Asteraceae). Cladistics, 25, 78-92.

Ekor, M. 2013. The growing use of herbal medicines: issues relating to adverse reactions and challenges in monitoring safety. Front Pharmacol, 4, 177.

Elshafie, H. et al. 2023. A comprehensive review on the biological, agricultural and pharmaceutical properties of secondary metabolites based-plant origin. Int J Mol Sci, 24, 3266.

Fabricant, D. and Farnsworth, N. 2001. The value of plants used in traditional medicine for drug discovery. Environ Health Perspect, 109, 69-75.

Fenteany, G. et al. 1995. Inhibition of proteasome activities and subunit-specific amino-terminal threonine modification by lactacystin. Science, 268, 726-731.

Fernandes, M. et al. 2008. Use of self-organizing maps and molecular descriptors to predict the cytotoxic activity of sesquiterpene lactones. Eur J Med Chem, 43, 2197-2205.

Fournane, S. et al. 2012. Decoding ubiquitin for mitosis. Genes Cancer, 3, 697-711.

Freund, R. et al. 2020. Advances in chemistry and bioactivity of parthenolide. Nat Prod Rep, 37, 541-565.

Ganem, N. and Pellman, D. 2012. Linking abnormal mitosis to the acquisition of DNA damage. J Cell Biol, 199, 871-881.

García-Piñeres, A. et al. 2001. Cysteine 38 in p65/NF-kappaB plays a crucial role in DNA binding inhibition by sesquiterpene lactones. J Biol Chem, 276, 39713-39720.

Gascoigne, K. and Taylor, S. 2008. Cancer cells display profound intra- and interline variation following prolonged exposure to antimitotic drugs. Cancer Cell, 14, 111-122.

Ghantous, A. et al. 2010. What made sesquiterpene lactones reach cancer clinical trials? Drug Discov Today 15, 668-678.

Golsteyn, R. et al. 1995. Cell cycle regulation of the activity and subcellular localization of Plk1, a human protein kinase implicated in mitotic spindle function. J Cell Biol, 129, 1617-1628.

Goodson, H. and Jonasson, E. 2018. Microtubules and microtubule-associated proteins. Cold Spring Harb Perspect Biol, 10, a022608.

Harmatha, J. and Nawrot, J. 1984. Comparison of the feeding deterrent activity of some sesquiterpene lactones and a lignan lactone towards selected insect storage pests. Biochem Syst Ecol, 12, 95-98.

Harmon, A. et al. 1979. The structure of rohitukine, the main alkaloid of Amoora rohituka (Syn. Aphanamixis polystachya) (meliaceae). Tetrahedron Lett, 20, 721-724.

Harris, S. 2007. Biodiversity of the alpine vascular flora of the N. W. North American cordillera: the evidence from phyto-geography. Erdkunde, 61, 344-357.

Hayashi, M.K. and Karlseder, J. 2013. DNA damage associated with mitosis and cytokinesis failure. Oncogene, 32, 4593-4601.

Healy Knibb, S. 2024. Investigating the structure-function relationship of anti-mitotic natural products in Canadian prairie plants. Master's thesis, University of Lethbridge, Dept. of Biological Sciences.

Heilmann, J. et al. 2001. The influence of glutathione and cysteine levels on the cytotoxicity of helenanolide type sesquiterpene lactones against KB cells. Bioorg Med Chem, 9, 2189-2194.

Hein, C. et al. 2008. Click chemistry, a powerful tool for pharmaceutical sciences. Pharm Res, 25, 2216-2230.

Himes, R. 1991. Interactions of the catharanthus (Vinca) alkaloids with tubulin and microtubules. Pharmacol Ther, 51, 257-267.

Hochegger, H. et al. 2008. Cyclin-dependent kinases and cell-cycle transitions: does one fit all? Nat Rev Mol Cell Biol, 9, 910-916.

Hoffman, T. et al. 2018. Correlating chemical diversity with taxonomic distance for discovery of natural products in myxobacteria. Nat Commun, 9, 803.

Hotta, T. et al. 2021. Parthenolide destabilizes microtubules by covalently modifying tubulin. Curr Biol, 31, 900-907.

Huang, W. et al. 2016. Anti-angiogenic activity and mechanism of sesquiterpene lactones from Centipeda minima. Nat Prod Commun, 11, 435-438.

Huang, Y. et al. 2019. BubR1 phosphorylates CENP-E as a switch enabling the transition from lateral association to end-on capture of spindle microtubules. Cell Res, 29, 562-578.

Hung, D. et al. 1996. Understanding and controlling the cell cycle with natural products. Chem Biol, 3, 623-639.

Ivie, G. et al. 1975. Hymenovin. Major toxic constituent of western bitterweed (Hymenoxys odorata DC) J Agric Food Chem, 23, 841-845.

Jackson, P. et al. 2017. Covalent modifiers: a chemical perspective on the reactivity of α,β-unsaturated carbonyls with thiols via hetero-Michael addition reactions. J Med Chem, 60, 839-885.

Jeffrey, S. and Belcher, H. 2002. Use of Arnica to relieve pain after carpal-tunnel release surgery. Altern Ther Health Med, 8, 66-68.

Joffe, S. and Thomas, R. 1989. Phytochemicals: a renewable global resource. AgBiotech News Info, 1, 697-700.

Jordan, M. and Wilson, L. 1998. Microtubules and actin filaments: dynamic targets for cancer chemotherapy. Curr Opin in Cell Biol, 10, 123-130.

Kernéis, S. et al. 2015. Natural product extracts of the Canadian prairie plant, Thermopsis rhombifolia, have anti-cancer activity in phenotypic cell-based assays. Nat Prod Res, 29, 1026-1034.

Kindscher, K. 1992. Medicinal Wild Plants of the Prairie: An Ethnobotanical Guide. University Press of Kansas.

Kitson, R. et al. 2009. The renaissance of α-methylene-γ-butyrolactones: new synthetic approaches. Angew Chem Int Ed Engl, 48, 9426-9451.

Kneusel, O. et al. 2002. Arnica montana gel in osteoarthritis of the knee: an open, multicenter clinical trial. Adv Ther, 19, 209-218.

Kowalski, R. et al. 1997. Activities of the microtubule-stabilizing agents epothilones A and B with purified tubulin and in cells resistant to paclitaxel (Taxol(R)). J Biol Chem, 272, 2534-2541.

Kreuger, O. et al. 2012. Sesquiterpene lactones as drugs with multiple targets in cancer treatment: focus on parthenolide. Anticancer Drugs 23, 883-896.

Kriplani, P. and Guave, K. 2020. Recent patents on anti-cancer potential of helenalin. Recent Pat Anticancer Drug Discov, 15, 132-142.

Kriplani, P. et al. 2017. Arnica montana L. – a plant of healing: review. J Pharm Pharmacol, 69, 925-945.

Kubara, P. et al. 2012. Human cells enter mitosis with damaged DNA after treatment with pharmacological concentrations of genotoxic agents. Biochem J, 446, 373-381.

Kupchan, S. et al. 1971. Tumor inhibitors. 69. Structure-cytotoxicity relationships among the sesquiterpene lactones. J Med Chem, 14, 1147-1152.

Lai, J. et al. 2022. A systemic review of taxanes and their side effects in metastatic breast cancer. Front Oncol, 12, 940239.

Lampson, M. and Kapoor, T. 2005. The human mitotic checkpoint protein BubR1 regulates chromosome–spindle attachments. Nat Cell Biol, 7, 93-98.

Lee, J. et al. 2002. Cytotoxic sesquiterpene lactones from Carpesium abrotanoides. Planta Med, 68, 745-747.

Legal, T. et al. 2020. The C-terminal helix of BubR1 is essential for CENP-E-dependent chromosome alignment. J Cell Sci, 133, jcs2466025.

Li, X. et al. 2020. Parthenolide inhibits ubiquitin-specific peptidase 7 (USP7), Wnt signaling, and colorectal cancer cell growth. Cell Biol, 295, 3576-3589.

Liu, C. et al. 2011. Costunolide causes mitotic arrest and enhances radiosensitivity in human hepatocellular carcinoma cells. Radiat Oncol, 6, 56.

Liu, L. et al. 2014. A sesquiterpene lactone from a medicinal herb inhibits proinflammatory activity of TNF-α by inhibiting ubiquitin-conjugating enzyme UbcH5. Chem Biol, 21, 1341-1350.

Liu, R. et al. 2019. Arnicolide D, from the herb Centipeda minima, is a therapeutic candidate against nasopharyngeal carcinoma. Molecules, 24, 1908.

Liu, Y. et al. 2011. Small compound 6-O-angeloylplenolin induces mitotic arrest and exhibits therapeutic potentials in multiple myeloma. PLoS One, 6, e21930.

Liu, Y. et al. 2015. Skp1 in lung cancer: clinical significance and therapeutic efficacy of its small molecule inhibitors. Oncotarget, 6, 34953-34967.

Lu, Y. et al. 2012. An overview of tubulin inhibitors that interact with the colchicine binding site. Pharm Res, 29, 2943-2971.

Lucas, R. et al. 1964. A new sesquiterpene lactone with analgesic activity from Helenium amarum (Raf.) H Rock J Org Chem, 29, 1549-1554.

Lyss, G. et al. 1998. The anti-inflammatory sesquiterpene lactone helenalin inhibits the transcription factor NF-κB by directly targeting p65. J Biol Chem, 273, 33508-33516.

Macías, F. et al. 1992. Potential allelopathic activity of several sesquiterpene lactone models. Phytochem, 31, 1969-1977.

Maguire, B. 1943. A monograph of the genus Arnica. Brittonia, 4, 386-510.

Marzo, I. and Naval, J. 2013. Antimitotic drugs in cancer chemotherapy: promises and pitfalls. Biochem Pharmacol, 86, 703-710.

Matson, D. and Stukenberg, P. 2011. Spindle poisons and cell fate: a tale of two pathways. Mol Interv, 11, 141-150.

McEwen, B. et al. 2001. CENP-E is essential for reliable bioriented spindle attachment, but chromosome alignment can be achieved via redundant mechanisms in mammalian cells. Mol Biol Cell, 12, 2776-2789.

McGinn, S. 2010. Weather and climate patterns in Canada's prairie grasslands. In: Shorthouse, J. and Floate, K., editors. Arthropods of Canadian Grasslands. Vol. 1: Ecology and Interactions in Grassland Habitats, Biological Survey of Canada; New Brunswick, Canada. p. 105-119.

Merfort, I. and Wendisch, D. 1993. Sesquiterpene lactones of Arnica cordifolia, subgenus Austromontana. Phytochem, 34, 1436-1437.

Miller, L. and Su, X. 2011. Artemisinin: discovery from the Chinese herbal garden. Cell, 146, 855-858.

Molina, L. 2018. Anti-mitotic activity of six Asteraceae plant extracts and identification of the sesquiterpene lactone hymenoratin from the Canadian plant Hymenoxys richardsonii. Master's thesis, University of Lethbridge, Dept. of Biological Sciences.

Molina, L. et al. 2021. Isolation of a natural product with anti-mitotic activity from a toxic Canadian prairie plant. Heliyon, 7, e07131.

Molina, L. et al. 2022. Connecting plant species and natural products from the Canadian prairie ecological zone to biomedical knowledge. Botany, 100, 231-245.

Newman, D. 2017. Screening and identification of novel biologically active natural compounds. F1000Res, 6, 783.

Newman, D. and Cragg, G. 2020. Natural products as sources of new drugs over the nearly four decades from 01/1981 to 09/2019. J Nat Prod, 83, 770-803.

Newman, E. 1994. Earth's vanishing medicine cabinet: rain forest destruction and its impact on the pharmaceutical industry. Am J Law Med, 20, 479-501.

Noble, R. 1990. The discovery of the vinca alkaloids—chemotherapeutic agents against cancer. Biochem Cell Biol, 68, 1344-1351.

Omura, S. and Crump, A. 2019. Lactacystin: first-in-class proteasome inhibitor still excelling and an exemplar for future antibiotic research. J Antiobiot (Tokyo), 72, 189-201.

Padilla-Gonzalez, G. et al. 2016. Sesquiterpene lactones: more than protective plant compounds with high toxicity. Crit Rev Plant Sci, 35, 18-37.

Parafiniuk, A. et al. 2023. Localization of sesquiterpene lactones biosynthesis in flowers of Arnica taxa. Molecules, 28, 4379.

Perez, E. 2009. Microtubule inhibitors: differentiating tubulin-inhibiting agents based on mechanisms of action, clinical activity, and resistance. Mol Cancer Ther, 8, 2086-2095.

Petrovska, B. 2012. Historical review of medicinal plants' usage. Pharmacogn Rev, 6, 1-5.

Poole, L. 2015. The basics of thiols and cysteines in redox biology and chemistry. Free Radic Biol Med. 80, 148-157.

Prigent, C. and Dimitrov, S. 2003. Phosphorylation of serine 10 in histone H3, what for? J Cell Sci, 116, 3677-3685.

Qi, S. et al. 2022. Targeting E2 ubiquitin-conjugating enzyme UbcH5c by small molecule inhibitor suppresses pancreatic cancer growth and metastasis. Mol Cancer, 21, 70.

Qin, J. et al. 2011. Pseudoguaianolides and guaianolides from Inula hupehensis as potential anti-inflammatory agents. J Nat Prod, 74, 1881-1887.

Ravelli, R. et al. 2004. Insight into tubulin regulation from a complex with colchicine and a stathmin-like domain. Nature, 428, 198-202.

Requejo, R. et al. 2010. Cysteine residues exposed on protein surfaces are the dominant intramitochondrial thiol and may protect against oxidative damage. FEBS J, 277, 1465-1480.

Robles, A. et al. 2015. Melampodium leucanthum, a source of cytotoxic sesquiterpenes with antimitotic activities. J Nat Prod, 78, 388-395.

Rogakou, E. et al. 1998. DNA double-stranded breaks induce histone H2AX phosphorylation on serine 139. J Biol Chem, 273, 5858–5868.

Romo, J. et al. 1964. The constituents of Helenium aromaticum (Hook) Bailey: the structures of aromatin and aromaticin. Tetrahedron, 20, 79-85.

Rønsted, N. et al. 2012. Can phylogeny predict chemical diversity and potential medicinal activity of plants? A case study of amaryllidaceae. BMC Evol Biol, 12, 182.

Sauchyn, D. et al. 2002. Aridity on the Canadian plains. Géogr Phys Quatern, 56, 247-259.

Schaar, B. et al. 1997. CENP-E function at kinetochores is essential for chromosome alignment. J Cell Biol, 139, 1373-1382.

Schmidt, T. 2006. Structure-activity relationships of sesquiterpene lactones. In: Atta-ur-Rahman, F., editor. Studies in Natural Products Chemistry. Vol. 33. Elsevier; Amsterdam, The Netherlands. p. 309-392.

Schmidt, T. et al. 2009. Quantitative structure − antiprotozoal activity relationships of sesquiterpene lactones. Molecules 14, 2062-2076.

Snyder, J. et al. 2001. The binding conformation of Taxol in β-tubulin: a model based on electron crystallographic density. Proc Natl Acad Sci U S A, 98, 5312-5316.

Sorokina, M. and Steinbeck, C. 2020. Review on natural products databases: where to find data in 2020. J Cheminform, 12, 20.

Sturgeon, C. et al. 2005. Modulation of the G2 cell cycle checkpoint by sesquiterpene lactones psilostachyins A and C isolated from the common ragweed Ambrosia artemisiifolia. Planta Med, 71, 938-943.

Su, X., and Miller, L. 2015. The discovery of artemisinin and Nobel Prize in Physiology or Medicine. Sci China Life Sci, 1070, 29-42.

Swift, L. and Golsteyn, R. 2014. Genotoxic anti-cancer agents and their relationship to DNA damage, mitosis, and checkpoint adaptation in proliferating cancer cells. Int J Mol Sci, 15, 3403-3431.

Swinney, D. and Anthony, J. 2011. How were new medicines discovered? Nat Rev Drug Discov, 10, 507-519.

Takahashi, M. et al. 2024. DrugMap: A quantitative pan-cancer analysis of cysteine ligandability. Cell, 187, 2536-2556.

Tanudji, M. et al. 2004. Gene silencing of CENP-E by small interfering RNA in HeLa cells leads to missegregation of chromosomes after a mitotic delay. Mol Biol Cell, 15, 3771-3781.

Thastrup, O. et al. 1990. Thapsigargin, a tumor promoter, discharges intracellular Ca2+ stores by specific inhibition of the endoplasmic reticulum Ca2(+)-ATPase. Proc Natl Acad Sci U S A, 87, 2466-2470.

Thompson, R. et al. 2019. How cells handle DNA breaks during mitosis: detection, signaling, repair, and fate choice. Cells, 8, 1049.

Thornburg, C. et al. 2018. NCI program for natural product discovery: a publicly-accessible library of natural product fractions for high-throughput screening. ACS Chem Biol, 13, 2484-2497.

Tietje, M. et al. 2022. Global variation in diversification rate and species richness are unlinked in plants. Proc Natl Acad Sci U S A, 119, e2120662119.

Tomoda, H. and Omura, S. 2000. Lactacystin, a proteasome inhibitor: discovery and its application in cell biology. Yakugaku Zasshi, 120, 935-949.

Tuescher, J. et al. 2020. The Canadian prairie plant Thermopsis rhombifolia contains luteolin, a flavone that inhibits cyclin dependent kinase 9 and arrest cells in the G1-phase of the cell cycle. J Nat Health Prod Res, 2, 1-14.

Tuescher, J. et al. 2021. Extracts prepared from a Canadian toxic plant induce light-dependent perinuclear vacuoles in human cells. Toxins, 13, 138.

Van Horn, R. et al. 2010. Cdk1 activity is required for mitotic activation of Aurora A during G2/M transition of human cells. J Biol Chem, 285, 21849-21857.

Verweij, J. et al. 1994. Paclitaxel (Taxol™) and docetaxel (Taxotere™): not simply two of a kind. Ann Oncol, 5, 495-505.

Vigneron, S. et al. 2004. Kinetochore localization of spindle checkpoint proteins: who controls whom? Mol Biol Cell, 15, 4584-4596.

Vincent, F. et al. 2022. Phenotypic drug discovery: recent successes, lessons learned and new directions. Nat Rev Drug Discov, 21, 899-814.

Weber, J. et al. 2024. A conserved CENP-E region mediates BubR1-independent recruitment to the outer corona at mitotic onset. Curr Biol, 34, 1133-1141.

Whipple, R. et al. 2013. Parthenolide and costunolide reduce microtentacles and tumor cell attachment by selectively targeting detyrosinated tubulin independent from NF-κB inhibition. Breast Cancer Res, 15, R83.

Willems, E. et al. 2018. The functional diversity of Aurora kinases: a comprehensive review. Cell Div, 13, 7.

Wilson, B. et al. 2020. Creating and screening natural product libraries. Nat Prod Rep, 37, 893-918.

Wójcik, C. et al. 1996. An inhibitor of the chymotrypsin-like activity of the multicatalytic proteinase complex (20S proteasome) induces arrest in G2-phase and metaphase in HeLa cells. Eur J Cell Biol, 70, 172-178.

Wolf, S. 1980. Cytogeographical Studies in the Genus Arnica (Compositae: Senecioneae). I. Am J Bot, 67, 300-308.

Wolf, S. and Denford, K. 1984. Taxonomy of Arnica (Compositae) subgenus Austromontana. Rhodora, 86, 239-309.

Wu, P. et al. 2012. Supercritical fluid extraction assisted isolation of sesquiterpene lactones with antiproliferative effects from Centipeda minima. Phytochem, 76, 133-140.

Xu, H. et al. 2010. Pharicin A, a novel natural ent-kaurene diterpenoid, induces mitotic arrest and mitotic catastrophe of cancer cells by interfering with BubR1 function. Cell Cycle, 9, 2897-2907.

Xu, Y. and Meng, X. 2020. Molecular simulation elaborating the mechanism of 1β-hydroxy alantolactone inhibiting ubiquitin-conjugating enzyme UbcH5s. Sci Rep, 10, 141.

Yu, Z. et al. 2019. Bioactive sesquiterpenoids and sesquiterpenoid glucosides from the flowers of Inula japonica. Fitoterapia, 138, 104292.

Zeidner, J. and Karp, J. 2015. Clinical activity of alvocidib (flavopiridol) in acute myeloid leukemia. Leuk Res, 39, 1312-1318.

Zhai, S. et al. 2002. Flavopiridol, a novel cyclin-dependent kinase inhibitor, in clinical development. Ann Pharmacother, 36, 905-911.

Zhang, M. et al. 2021. CDK inhibitors in cancer therapy, an overview of recent development. Am J Cancer Res, 11, 1913-1935.

Zhang, S. et al. 2005. Anti-cancer potential of sesquiterpene lactones: bioactivity and molecular mechanisms. Curr Med Chem Anticancer Agents, 5, 239-249.

Zheng, B. et al. 2013. Telekin induces apoptosis associated with the mitochondria-mediated pathway in human hepatocellular carcinoma cells. Biol Pharm Bull, 36, 1118-1125.

Zhu, P. et al. 2019. Arnicolide D exerts anti-melanoma effects and inhibits the NF-κB pathway. Phytomedicine, 64, 153065.

Zou, T. and Lin, Z. 2021. The involvement of ubiquitination machinery in cell cycle regulation and cancer progression. Int J Mol Sci, 22, 5754.

APPENDIX I: Supplementary Materials for Chapter 2:

Identification and characterization of five anti-mitotic sesquiterpene lactones from the Canadian plant species *Arnica cordifolia*

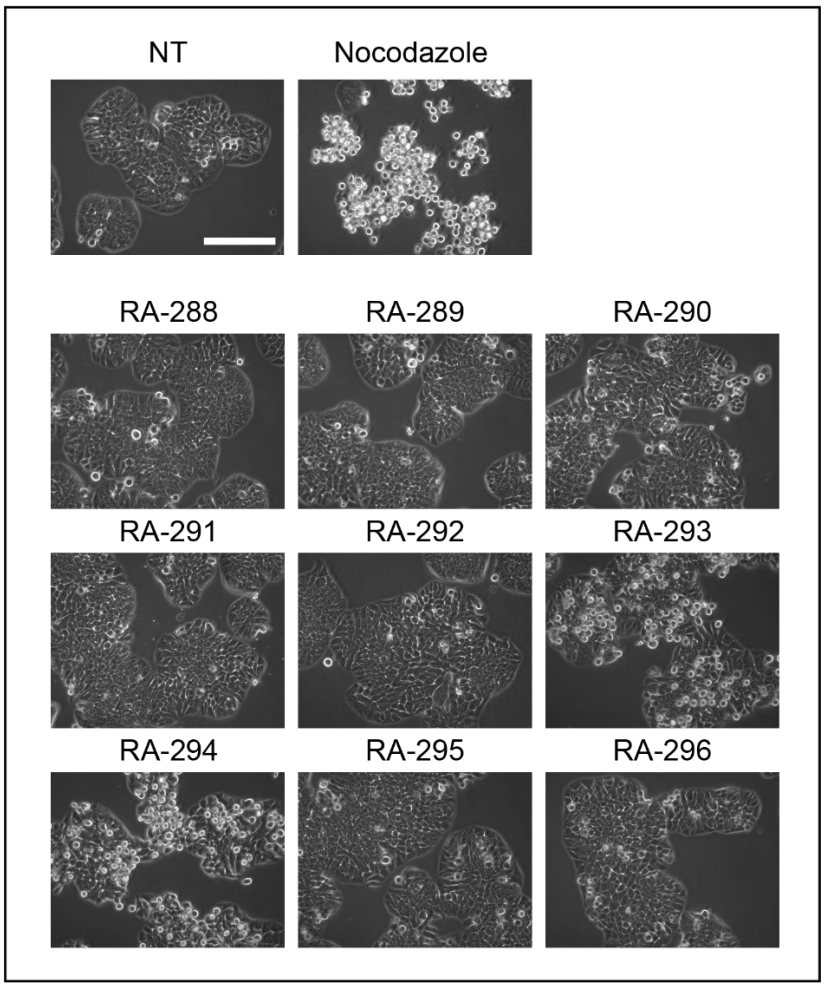

Supplemental Figure 2.1. Anti-mitotic activity of *A. cordifolia* leaf extract is retained after fractionation. HT-29 cells were either not-treated or treated with nocodazole or *A. cordifolia* extract fractions for 18 h and observed by light microscopy. Scale bar represents 50 μm.

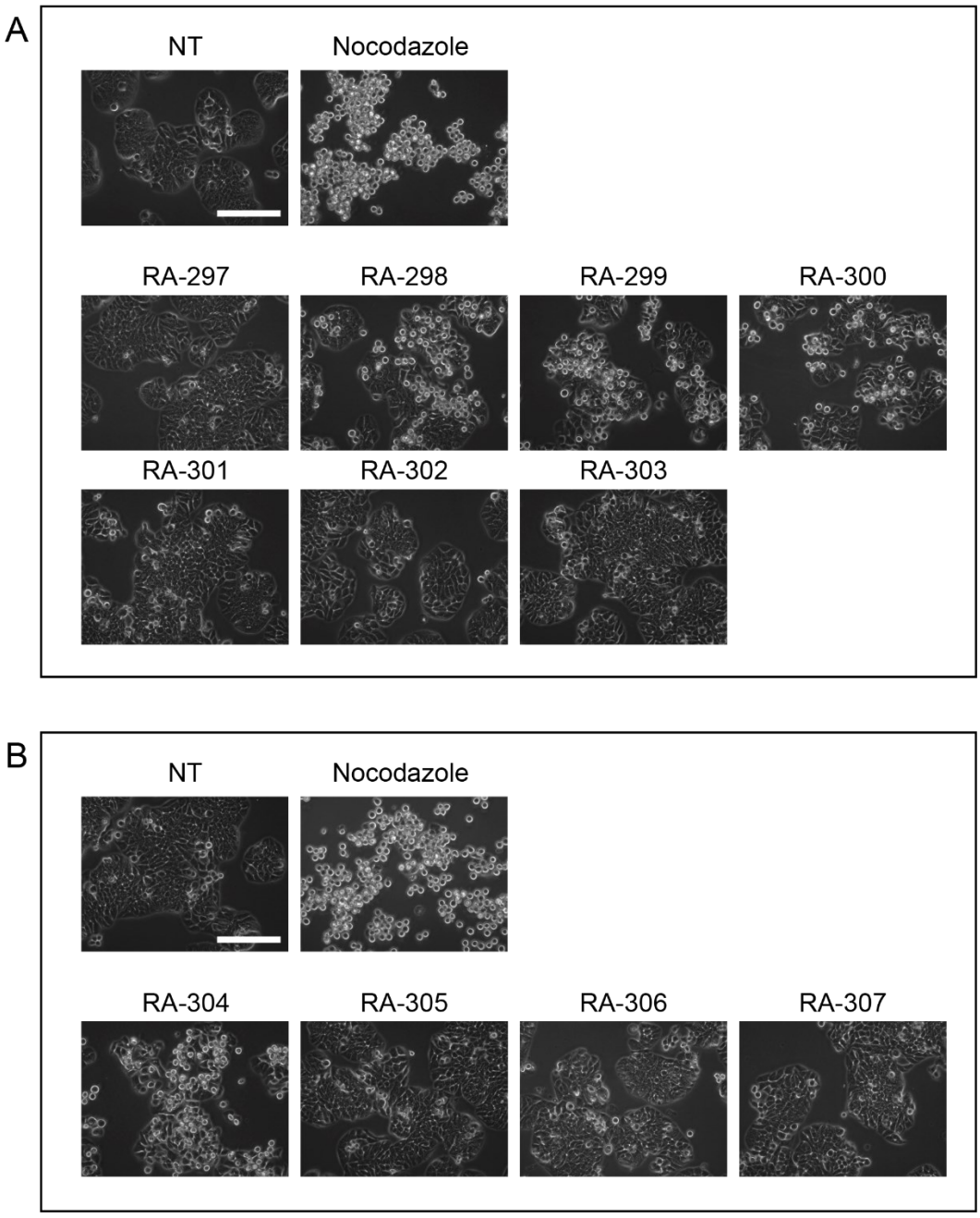

Supplemental Figure 2.2. Subfractions of *A. cordifolia* leaf extract fractions show anti-mitotic activity. **A.** HT-29 cells were either not-treated or treated with nocodazole or RA-293 subfractions for 18 h and observed by light microscopy. Scale bar represents 50 µm. **B.** HT-29 cells were either not-treated or treated with nocodazole or RA-294 subfractions for 18 h and observed by light microscopy. Scale bar represents 50 µm.

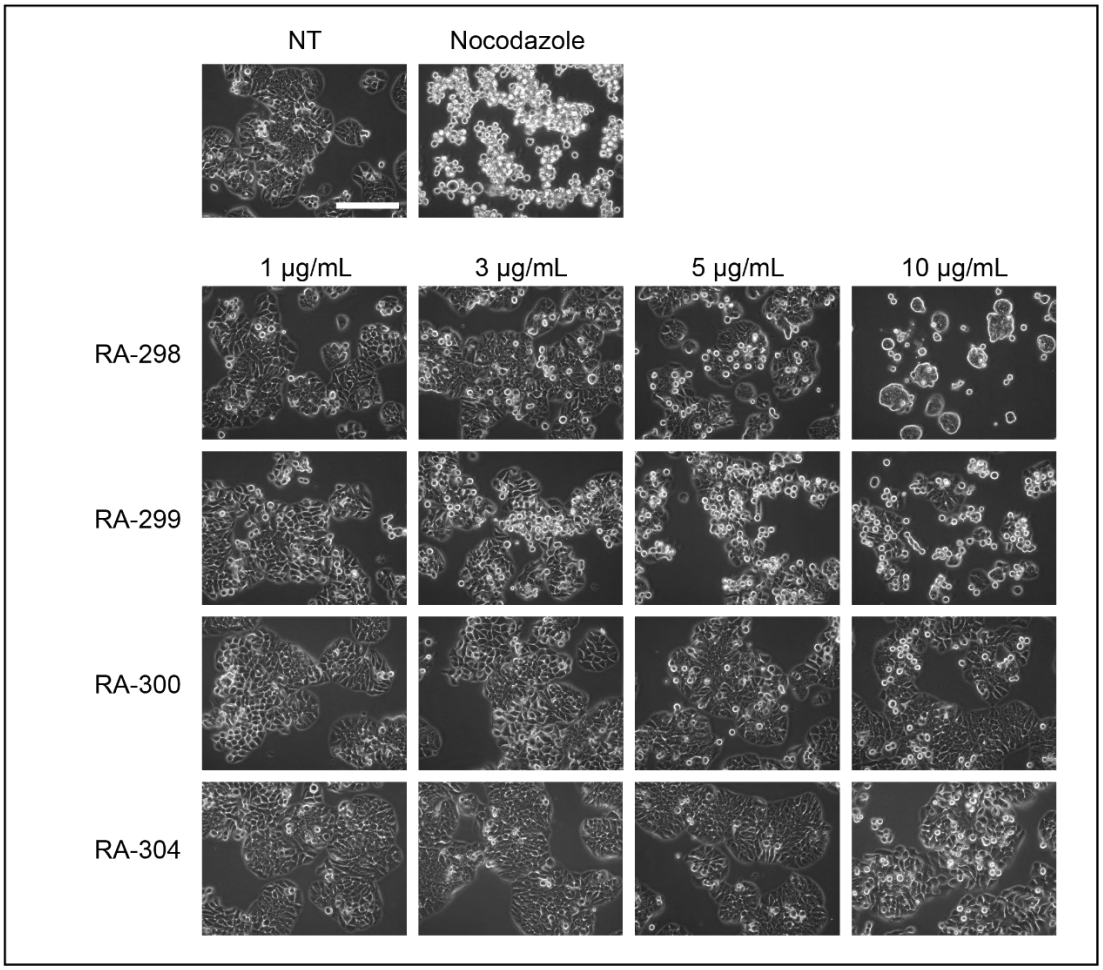

Supplemental Figure 2.3. RA-298 and RA-299 are the most potent anti-mitotic subfractions. HT-29 cells were either not-treated or treated with nocodazole or various concentrations of RA-298, RA-299, RA-300, or RA-304 for 18 h and observed by light microscopy. Scale bar represents 50 µm.